SLAC–Report–441
UC–413
UC–414
May 1994
(T/E)

HADRONIC WAVEFUNCTIONS IN LIGHT-CONE QUANTIZATION

A DISSERTATION

SUBMITTED TO THE DEPARTMENT OF PHYSICS

AND THE COMMITTEE ON GRADUATE STUDIES

OF STANFORD UNIVERSITY

IN PARTIAL FULFILLMENT OF THE REQUIREMENTS

FOR THE DEGREE OF

DOCTOR OF PHILOSOPHY

Thomas Hyer

Stanford Linear Accelerator Center

Stanford University, Stanford, CA 94309

⋆ Work supported by Department of Energy contract DE–AC03–76SF00515.

I certify that I have read this dissertation and that in my opinion it is fully adequate, in scope and in quality, as a dissertation for the degree of Doctor of Philosophy.

(Principal Adviser)

I certify that I have read this dissertation and that in my opinion it is fully adequate, in scope and in quality, as a dissertation for the degree of Doctor of Philosophy.

I certify that I have read this dissertation and that in my opinion it is fully adequate, in scope and in quality, as a dissertation for the degree of Doctor of Philosophy.

Approved for the University Committee on Graduate Studies:

Abstract

The analysis of light-cone wavefunctions seems the most promising theoretical approach to a detailed understanding of the structure of relativistic bound states, particularly hadrons. However, there are numerous complications in this approach.

Most importantly, the light-cone approach sacrifices manifest rotational invariance in exchange for the elimination of negative-energy states. The requirement of rotational invariance of the full theory places important constraints on proposed light-cone wavefunctions, whether they are modelled or extracted from some numerical procedure. A formulation of the consequences of the hidden rotational symmetry has been sought for some time; it is presented in Chapter 2.

In lattice gauge theory or heavy-quark effective theory, much of the focus is on the extraction of numerical values of operators which are related to the hadronic wavefunction. These operators are to some extent interdependent, with relations induced by fundamental constraints on the underlying wavefunction. The consequences of the requirement of unitarity are explored in Chapter 3, and are found to have startling phenomenological relevance.

To test model light-cone wavefunctions, experimental predictions must be made. The reliability of perturbative QCD as a tool for making such predictions has been questioned. In Chapter 4, we present a computation of the rates for nucleon-antinucleon annihilation, improving the reliability of the perturbative computation by taking into account the Sudakov suppression of exclusive processes at large transverse impact parameter.

The greatest experimental difficulty in probing hadronic wavefunctions is the tremendous suppression of the exclusive cross section with increasing energy. In Chapter 5, we develop the analysis of semiexclusive production, which minimizes

this difficulty by focusing on processes in which a single isolated meson is produced perturbatively and recoils against a wide hadronizing system. At energies above about 10 GeV, semiexclusive processes are shown to be the most sensitive experimental probes of hadronic structure.

Finally, we offer a survey of future directions in the application of light-cone quantization to hadronic problems.

Acknowledgements

Many thanks are due to Stan Brodsky, without whose unflagging enthusiasm and unstinting support much of this work could not have been completed. We have also profited from our interactions with Ratindranath Akhoury, Ted Allen, Giovanni Bonvicini, James Bjorken, David Burke, Phil Burrows, Lance Dixon, Jonathan Dorfan, JoAnne Hewett, Peter Kim, Alex Langnau, Amitabh Lath, Robert Laughlin, Peter Lepage, Hung Jung Lu, Vera Luth, Kirk McDonald, Joseph Milana, Al Mueller, Matthias Neubert, Martin Perl, Michael Peskin, Steve Pinsky, Helen Quinn, George Sterman, Leonard Susskind, Achim Weidemann, and Mike Witherell. Thanks are due to Margaret Helton, Sharon Jensen and Cindy Stevenson for their forbearance.

Every pestilence purifies.

Every plague has its day.

Every joy is the last.

Table of Contents

List of Tables

List of Illustrations

1. INTRODUCTION

The present state of phenomenological physics is one of frustration [1]. The continued success of the standard model in increasingly stringent quantitative tests [2], together with its myriad inconsistent or aesthetically undesirable features, has placed a high premium on the ability to isolate reliably even the most minor deviations from experiment.

This situation is further complicated in that the most promising searches for new physics generally involve the investigation of hadronic phenomena. Thus a detailed quantitative understanding of the structure of hadrons is imperative in order to maximize the prospects for advancing our understanding of truly elementary particles.

The current theoretical understanding of hadronic structure, however, is far from precise. This is largely due to the complexity arising from the underlying theory of strong interactions, Quantum Chromodynamics (QCD). The breakdown of QCD perturbation theory at small momentum transfer necessitates the development of reliable nonperturbative methods for modelling and investigating the structure of bound states.

The naive approach to this problem models hadrons as assemblages of uncorrelated partons, described by structure functions extracted from experiment. While this approach has proven tremendously valuable in the regime of very large momentum transfer, as in discovery channels at hadron colliders, it breaks down when confronted with the smaller momentum transfers involved in precision studies, such as B meson physics. Thus more sophisticated methods are required.

One such method is Lattice Gauge Theory [3], in which each dimension is discretized to allow numerical computation of observables. After great investment of computational resources [4], this discretized approach has recently begun to pay dividends. However, one limitation of Lattice Gauge Theory is its inevitable focus on individual operators, which must in general be evaluated in a single frame since the wavefunction information gained from lattice simulations is not boost-invariant. Thus it is difficult to envision a computationally feasible approach to high-energy observables through lattice analysis alone.

An alternative numerical approach to the systematic analysis of hadronic bound states, which offers the opportunity to extract boost-invariant wavefunctions in their entirety, lies within the framework of Light-Cone Quantization (LCQ) [5]. Here the quantization conditions are defined, and the initial conditions of a bound-state problem specified, on surfaces of constant *light-cone time*

$$\tau = x^+ \equiv x^0 + x^3.$$

With this definition, and the corresponding definition $x^- \equiv x^0 - x^3$, we have $x \cdot y = (x^+ y^- + x^- y^+)/2 - x_\perp \cdot y_\perp$. We will adhere to this convention throughout this work.

In the light-cone framework, translations in the τ-direction are generated by the light-cone Hamiltonian P^-. Light-cone perturbation theory (LCPTh) rules may be deduced, as usual, from the Hamiltonian [6]; each Feynman graph with n vertices corresponds to a sum of $n!$ τ-ordered LCPTh graphs. As in old-fashioned time-ordered perturbation theory, each internal particle propagates on its mass shell, while the energy P^- is not conserved in intermediate states.

LCPTh has several distinct advantages over ordinary time-ordered perturbation theory. Foremost is the fact that the light-cone momentum k^+ is conserved at each vertex, and is positive along each line. As a result, the contribution from any graph containing *vacuum-creation* vertices vanishes, greatly reducing the number of diagrams which must be computed in perturbation theory. For example, of the 516 time-orderings contributing to the electron anomalous magnetic moment at order α^2, all but 8 vanish. The additional feature that integrations over indeterminate momenta are three- rather than four-dimensional makes LCPTh a competitive tool for perturbative computations at high order [7].

In addition, the on-shell condition $k^2 = m^2$ implies

$$k^- \equiv \frac{k_\perp^2 + m^2}{k^+}.$$

This result leads to simple and rational denominators in each intermediate state, rendering LCPTh computations much more tractable analytically than their equal-time relatives.

The mathematics of LCPTh are identical to those of time-ordered perturbation theory in the infinite-momentum frame [8]. Thus many quantities inspired by the parton model, such as the structure functions of deep inelastic electron-hadron scattering, have a natural and intuitive interpretation in terms of the expansion of the hadron into Fock states on the light cone.

Thus it is natural to attempt a numerical solution of the bound-state Hamiltonian, discretizing momenta to render the basis space finite [9]. Since the total light-cone momentum P^+ of a system is conserved and each component has positive k^+, discretization of the light-cone momentum to multiples of P^+/K for some integer K immediately renders the number of particles in each basis state, and

the number of possible distributions of their momenta, finite. Hard contributions, which on the lattice come from excitations smaller than the lattice spacing, in this approach are due to large transverse momenta; soft contributions manifest themselves as excitations at small k^+. However, it is expected that in the analysis of bound states, the contribution from small but finite k^+ is naturally regulated by the finite size of the hadron, so that accurate results can be obtained without resorting to very large values of K [10].

However, there are several new problems which arise in the Discretized Light-Cone Quantization (DLCQ) approach. The most formidable is that of the vacuum structure of the theory itself, which in the light-cone approach is subsumed into the *zero modes* with $k^+ = 0$ [11]. Physically, these correspond to particles propagating parallel to the surface of quantization, which cannot be specified in initial conditions at fixed τ. Theories with nontrivial structure cannot be reliably analyzed until a thorough understanding of the effects of zero modes is obtained.

A further difficulty arises from the lack of rotational invariance of the quantization procedure and of most cutoffs. The surface of quantization $\tau = 0$ is invariant under seven of the ten continuous Lorentz transformations: the translations P^+, P^1, and P^2; the boost and rotation J^3 and K^3 along and about the $\hat{z}$-axis; and the combinations $G^i \equiv J^i + \epsilon^{ij} K^j$ for $i = 1, 2$, which unfortunately are customarily referred to as "transverse boosts." The generators J^1 and J^2, like the Hamiltonian P^- itself, are dynamical in nature; the symmetry of any theory under these operations is not manifest in the light-cone formulation.

Thus the most natural cutoff procedures, such as the imposition on transverse momenta of a lattice of finite size and finite spacing, and even the harmonic resolution K itself, violate rotational invariance [7,12]. This threatens the validity

of any numerical solution, since in renormalized theories such as QCD the short-distance physics of renormalization affects the parameters which determine the behavior of the discretized theory [13].

Also, to obtain numerical tractability, it is necessary to limit the number of basis states with some cutoff on the number of particles in a basis state or on the total light-cone kinetic energy. However, these cutoffs violate not only rotational invariance but also locality; in the computation of the two-loop ladder graph contribution to the electron anomalous moment, this combination leads to an incorrect result even when the cutoff is taken to infinity [7,14].

Since the rotational symmetry of QCD is not manifest on the light-cone, it has many nontrivial implications for light-cone wavefunctions. Some of these conditions can be extracted by carefully formulating rotationally invariant amplitudes, then computing them in terms of light-cone wavefunctions $\psi(x, k_\perp)$ and imposing rotational invariance as an *a posteriori* constraint, in a manner reminiscent of the derivation of the optical theorem from the imposition of unitarity. This is the subject of the first part of this thesis.

However, the derivation is complicated by the appearance in the amplitude of *instantaneous* interactions, which correspond to degenerate light-cone time-orderings in which two vertices have the same coordinate τ. Thus, before rotationally invariant quantities can be formulated, one must account for such instantaneous contributions. Fortunately, we are able to show that such terms are governed by simple effective wavefunctions, and thus can be treated on a par with the normal non-degenerate time-orderings. This result is important in itself, since without an understanding of the instantaneous effective wavefunctions, only the plus-components of hadronic transition elements between bound states can be

computed. It is crucial for our purposes, since a single wavefunction can be probed only in the transition from a bound to a free state.

The relations thus derived constitute a valuable consistency check on any numerically extracted model wavefunctions. If such wavefunctions are obtained in a well-controlled physical limit, they should exhibit the rotational invariance of the physical states they represent.

These relations have a simple and plausible form. However, they appear to conflict with known results about the asymptotic behavior of the distribution amplitude

$$\phi(x;Q) \equiv \left(\ln \frac{Q^2}{\Lambda^2}\right)^{-\gamma_F/\beta} \int^{Q} \frac{\mathrm{d}^2 k_\perp}{16\pi^3} \psi(x, k_\perp).$$

We discuss some mechanisms by which this apparent conflict might be reconciled.

Operators which depend on the structure of hadrons do not arise in isolation, but rather from the unique hadron wavefunction. Thus the relations between such operators, such as the decay constant f_h and moment $\left\langle k_\perp^2 \right\rangle$ of the transverse momentum in the valence state, are to some extent constrained by the requirement that the underlying wavefunction remain unitary. Chapter 3 is devoted to the derivation of such constraints, which have often been overlooked in the extraction of individual operators and which have surprising phenomenological relevance.

The second major part of this thesis deals with the prospects for experimentally constraining the distribution amplitudes of nucleons and mesons. At leading twist, exclusive amplitudes are dominated by these distributions in the valence Fock state; however, the simplifying assumptions which neglect higher-twist terms introduce a variety of spurious infinities into the computation. The most pernicious of these are

associated with the one-loop running coupling α_s, which diverges as the momentum transfer q approaches the QCD scale Λ.

Even hard exclusive processes are sensitive to such soft contributions from the *endpoint region* where one or more of the constituents carries an extremely small longitudinal momentum fraction x_i. It has been known for some time [15] that the endpoint contribution is controlled by Sudakov effects, which serve to nearly restore the dimensional-counting power-law behavior [16] even in the presence of Landshoff pinch singularities, which lead to apparent violations of the dimensional-counting behavior [17].

A heuristic appraisal of the importance of Sudakov suppression in this regime is as follows. The divergences of the running coupling at small x_i are predicated on the assumption that the exchanged gluon responsible for binding the quarks into a hadron can propagate for a distance on the order of Λ^{-1} in the transverse direction. However, in this case the qqq or $q\bar{q}$ system which is destined to form the hadron has a large color dipole moment; thus it is very likely to emit final-state radiation, in which case the final state is no longer exclusive. Since the coupling which determines the probability of final-state radiation is the same as that which determines the gluon exchange amplitude, the Sudakov factor vanishes as the naive amplitude diverges. Thus, in the computation of exclusive amplitudes, the infinities suggested by the naive use of the one-loop running coupling never materialize.

The treatment of Ref. [15] leaves a residual dependence on the infrared cutoff scale, which is determined by the finite size of hadrons. Botts and Sterman [18] took into account contributions to the Sudakov factor at next-to-leading logarithmic order in the hard momentum exchange, and derived a form whose only parametric dependence is on the QCD scale Λ. In Chapter 4, we apply their result to the

computation of the amplitudes for proton Compton scattering and the nucleon form factor, both in the timelike region. Our emphasis is on studying the perturbative result for indications of the breakdown of perturbation theory, and on forming experimentally measurable quantities which are sensitive to the choice of a model for the distribution amplitude but have small theoretical uncertainties.

The greatest hindrance to the experimental analysis of exclusive $p\bar{p}$ reactions at fixed angle is their tremendous suppression with increasing center-of-mass energy. The total cross sections for the processes analyzed in Chapter 4 are proportional to s^{-5}, so that the region in which perturbative calculations are reliable overlaps very little with that in which experimental measurements are currently available.

In an effort to minimize the degree of suppression with increasing energy, the penultimate chapter of this thesis considers *semiexclusive* processes. Here a meson formed in, *e.g.*, e^+e^- annihilation recoils against an inclusive state. There is thus only a single spectator, and the cross section is proportional to s^{-2}.

The author [19] is not the first to consider this process. It was pursued briefly several years ago by Grozin and Baier [20], who were the first to point out its advantages over the traditional analysis of exclusive scattering processes. However, the work in Refs. [19] and [20] failed to take into account the complications due to the hadronization of the recoil system, which we show are qualitatively crucial. The extensive development given in Chapter 5 takes into account the complications which invalidate the analyses of Refs. [19] and [20], and makes finite and quantitative predictions which can be used both to check the consistency of the pQCD approach with experimental results and to constrain models of the meson distribution amplitude. As before, we focus on the development of quantities which

are insensitive to the treatment of soft physics, and can be used unambiguously as probes of the mesonic structure.

Finally, Chapter 6 concludes our discussion with an appraisal of the results we have obtained, and with an outlook which identifies the most relevant areas to which future theoretical and experimental work may be directed.

Chapters 2–5 of this thesis have been either published or submitted for publication [21].

REFERENCES

[1] See, *e.g.*, J. L. Lopez *et al.*, *Phys. Rev.* **D48**, 3297 (1993); J. L. Lopez *et al.*, *Phys. Rev.* **D48**, 4029 (1993); D. V. Nanopoulos, in *College Station 1989, Proceedings, Strings 89* 261–281; J. L. Lopez, D. V. Nanopoulos, and K. Yuan, *Nucl. Phys.* **B399**, 654 (1993); J. L. Lopez and D. V. Nanopoulos, in *Johns Hopkins Workshop 1991* 277–297; I. Antoniadis *et al.*, *Phys. Lett.* **268B**, 188 (1991); J. L. Lopez and D. V. Nanopoulos, *Phys. Lett.* **268B**, 359 (1991); J. Ellis, J. L. Lopez, and D. V. Nanopoulos, *Phys. Lett.* **252B**, 53 (1990); I. Antoniadis *et al.*, *Phys. Lett.* **231B**, 65 (1989); A. E. Faraggi *et al.*, *Phys. Lett.* **221B**, 337 (1989); I. Antoniadis *et al.*, *Phys. Lett.* **208B**, 209 (1988); G. K. Leontaris and D. V. Nanopoulos, *Phys. Lett.* **212B**, 327 (1988); I. Antoniadis *et al.*, *Phys. Lett.* **213B**, 562 (1988); J. Ellis *et al.*, *Phys. Lett.* **207B**, 451 (1988); B. Campbell *et al.*, *Phys. Lett.* **200B**, 483 (1988); B. Campbell *et al.*, *Phys. Lett.* **198B**, 200 (1987); I. Antoniadis *et al.*, *Phys. Lett.* **194B**, 231 (1987).

[2] See, *e.g.*, OPAL Collaboration (C. P. Ward, *et al.*), in *Warsaw Symposium 1992*, 3–21.

[3] See, *e.g.*, J. Kogut and L. Susskind, *Phys. Rev.* **D11**, 395 (1975).

[4] G. P. Lepage has recently maintained (*e.g.*, in *TASI 93*) that intrinsically low-energy observables, such as masses and magnetic moments, can be computed cheaply and accurately on rather coarse lattices. This is in accord with the work of S. J. Brodsky and F. Schlumpf, who show (SLAC–PUB–6431, 1994) that low-energy properties of the proton are nearly independent of the shape of the light-cone wavefunction in the Tamm-Dancoff truncated theory containing only the valence qqq Fock state.

[5] P. A. M. Dirac, *Rev. Mod. Phys.* **21**, 392 (1949); for a recent overview see S. J. Brodsky *et al.*, *Part. World* **3**, 109 (1993), and references therein.

[6] The rules are tabulated in, *e.g.*, S. J. Brodsky and G. P. Lepage, *Phys. Rev.* **D22**, 2157 (1980).

[7] M. Burkardt and A. Langnau, *Phys. Rev.* **D47**, 3452 (1993).

[8] J. D. Bjorken, J. B. Kogut, and D. E. Soper, *Phys. Rev.* **D3**, 1382 (1971).

[9] S. J. Brodsky and H. C. Pauli, *Phys. Rev.* **D32**, 2001 (1985).

[10] K. J. Hornbostel, SLAC–0333 (1988).

[11] G. McCartor and D. Robertson, *Z. Phys.* **C53**, 679 (1992).

[12] M. Burkardt and A. Langnau, *Phys. Rev.* **D44**, 3857 (1991).

[13] Wilson and Perry (*Nucl. Phys.* **B403**, 587 (1992); OSU–NT–93–117) conjecture that physical symmetries may be regained through a natural construction of the effective Hamiltonian.

[14] This is not to say that correct results cannot be obtained in the framework of light-cone quantization with, *e.g.*, a Pauli-Villars regulator; see S. J. Brodsky, R. J. Roskies, and R. Suaya, *Phys. Rev.* **D8**, 4574 (1973). However, this is not a computationally feasible method for nonperturbative problems.

[15] V. V. Sudakov, *Zh. Eksp. Teor. Fiz.* **30**, 87 (1956) [*Sov. Phys. JETP* **3**, 65 (1956)]; A. H. Mueller, *Phys. Rept.* **73**, 237 (1981).

[16] S. J. Brodsky and G. R. Farrar, *Phys. Rev.* **D11**, 1309 (1975).

[17] P. V. Landshoff, *Phys. Rev.* **D10**, 1024 (1974).

[18] J. Botts and G. Sterman, *Nucl. Phys.* **B325**, 62 (1989).

[19] T. Hyer, *Phys. Rev.* **D48**, 147 (1993).

[20] V.N. Baier and A.G. Grozin, *Phys. Lett.* **96B**, 181 (1980); A.G. Grozin. *Sov. J. Nucl. Phys.* **37**, 255 (1983); V.N. Baier and A.G. Grozin, *Sov. J. Part. Nucl.* **16**, 1 (1985); see also A.G. Grozin, *Z. Phys.* **C34**, 531 (1987).

[21] Chapter 2 was submitted in two parts, SLAC–PUB–6279 (*Phys. Rev.* **D49**, 2074 (1992)) and SLAC–PUB–6424 (to appear in *Phys. Rev. Lett.* **72**). Chapter 3 (SLAC–PUB–6383) has been submitted to *Phys. Rev.* **D**. Chapter 4 (SLAC–PUB–5889) has been published (*Phys. Rev.* **D47**, 3875 (1993)). Chapter 5 was submitted in two parts, SLAC–PUB–6013 (*Phys. Rev.* **D48**, 147 (1993)) and SLAC–PUB–6359.

2. CONSTRAINTS FROM ROTATIONAL INVARIANCE

Amplitudes for exclusive hadronic reactions at large momentum transfer are dominated by the configuration in which each hadron is found in its "valence" state, the Fock state with $L_z = 0$ and with the minimal number of constituents. The reason is that each additional particle in an incoming hadron must be subjected to some large momentum transfer in order to emerge in approximate collinearity with an outgoing hadron. Thus the amplitude scales like $(\mu/Q)^n$ where μ is a typical hadronic scale, Q is the momentum scale of the hard process, and n is the number of "spectators" to the hard scattering.

The additional restriction $L_z = 0$ arises from the neglect of internal momenta relative to Q. Since the dependence of the hard-scattering amplitude T_H on the internal momentum $k_\perp$ is discarded, the wavefunction can be integrated over all values of $k_\perp$. Contributions to the wavefunction with $L_z \neq 0$, which contain the factor $\big(\arg(k_x + ik_y)\big)^{L_z}$, vanish under this integration.

We wish to reexamine these conclusions for another class of hard exclusive processes, involving scattering between bound and free states. An example is the photodissociation of a meson, $\gamma h \to Q\bar{q}$. While such amplitudes do not correspond directly to experimentally observable quantities in a confining theory, they may be considered as, *e.g.*, the leading contribution to the amplitude for $\gamma h \to 2$ jets in a specified angular configuration at asymptotically large energies. In theories without confinement, of course, they represent physically observable amplitudes; it seems to us that the constraints of rotational invariance should take the same form for confining and non-confining theories, so that we may consider amplitudes like this without further deliberation as to their physical meaning.

In this case, the conclusion that the leading-twist portion of the amplitude is contributed solely by the $Q\bar{q}$ Fock states of the meson still holds, for the same reasons given above in the case of purely hadronic exclusive reactions. However, the quantum numbers of the mesons, in particular their spin states, are now considered as observables; thus, when quark masses can be neglected, their spin states within the meson are specified. To leading twist, helicity is indeed conserved; thus we see that reactions like $\gamma h_s \to Q_\lambda \bar{q}_{\lambda'}$ probe the two-particle Fock wavefunction $\psi_{h_s \to Q_\lambda \bar{q}_{\lambda'}}$ in an arbitrary spin state. Here the subscripts s, λ, and λ' are used to denote particle helicity.

Just as a hadron is represented in the calculation of inclusive cross sections at leading twist as an assemblage of uncorrelated partons whose distribution is governed by the nonperturbative structure function $f_{p/h}(x)$, an incoming meson in an exclusive process can be represented by the factor

$$\int_0^1 \mathrm{d}x \int \frac{\mathrm{d}^2 k_\perp}{16\pi^3}\ \psi_{h\to\bar{Q}q}(x,k_\perp)\ \frac{u(\bar{x}p-k_\perp)}{\sqrt{\bar{x}p^+}}\ \frac{\bar{v}(xp+k_\perp)}{\sqrt{xp^+}}, \tag{2.1}$$

where we have introduced the notation $\bar{x} \equiv 1-x$. The nonperturbative wavefunction $\psi(x,k_\perp)$ is the Fourier transform of the covariant Bethe-Salpeter wavefunction evaluated at zero relative light-cone time; thus it represents an integral over all values of k^- of the Fourier transform of the Bethe-Salpeter wavefunction. As a result, the wavefunction is entirely parametrized by the variables x and $k_\perp$ given as its arguments. These process-independent wavefunctions are the projections onto the relevant Fock state of the eigenstates of the light-cone Hamiltonian, and can be used to extract physical amplitudes for any process.

In particular, amplitudes for exclusive dissociation processes have the invariance properties required of all physical observables. On the light cone, all of the

generators of Lorentz transformations except the rotations J_x and J_y are manifest. Since $J_x = i[J_z, J_y]$, whatever hidden consequences Lorentz invariance may hold for wavefunctions on the light cone are entirely contained in the operator J_y.

Of course, we are unable to write down the complete amplitude for a process like $\gamma h \to Q\bar{q}$. Instead, we can present only the contribution to leading order and to leading twist. Note that since the wavefunction mixes contributions from all orders of perturbation theory, the amplitudes we compute will not be order-by-order invariant. They will instead be Lorentz invariant only insofar as they approximate the true physical amplitude, *i.e.* up to corrections of order $\alpha_s(Q)$ and of order μ/Q [1].

To write down such a complete amplitude, we must understand the contribution from instantaneous exchange of one of the quarks. The treatment of this problem is the major achievement of this chapter. Once we have obtained a method for dealing with such contributions, we can extract the full consequences of Lorentz invariance by requiring that the amplitude we calculate remain invariant under rotations about the y-axis.

In Sections 2.1-2.4, we concern ourselves only with the case where h is a (pseudo)scalar meson. Subtleties arising from the effect of rotations on the spin state of h are postponed to Section 2.5.

2.1. Instantaneous Exchange Graphs

In the scattering of free particles, the form of the instantaneous propagator can be deduced from the Hamiltonian of the theory after integrating out dependent degrees of freedom. For fermions, the Dirac structure of these contributions is simply $\gamma^+ \equiv \gamma^0 + \gamma^3$ [2]. However, when a bound state scatters by exchange of an instantaneous particle, it is not immediately clear that a simple representation of the form of the interaction can be obtained.

For example, the simplest hadronic process imaginable is the photodissociation of a meson into a $q\bar{Q}$ pair. The standard methods of LCQ do not suffice to calculate the amplitude for this process, since the instantaneous interaction shown in Fig. 2.1 cannot be neglected. Thus, the applications of LCQ to wavefunction-controlled processes have largely been restricted to the computation of spacelike form factors, for which the evaluation of the +-component of the hadronic part of the amplitude is sufficient. Instantaneous terms do not affect such calculations, since $\gamma^+\gamma^+ = 0$.

We will now show that the instantaneous interaction does indeed have a simple form, and can be parametrized by a wavefunction analogous to those of Ref. [3].

An example of an instantaneous interaction contributing to the photodissociation $\gamma h \to q\bar{Q}$ is shown in Fig. 2.1; however, this diagram does not as yet represent anything. To describe such interactions in a simple form, we must take one step further into the 'muck' of the quark-meson vertex, as shown in Fig. 2.2. In Fig. 2.3, a non-instantaneous diagram contributing to the photodissociation process, the propagating internal quark line is represented by the factor $D_{\rm prop} = u_\lambda(q)/\sqrt{q^+}$, where $\lambda = \pm$ is the quark helicity.

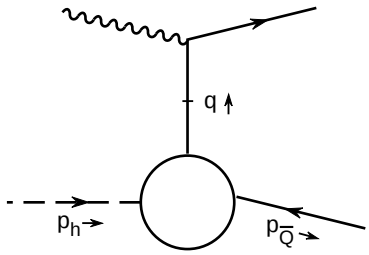

Fig. 2.1. Instantaneous interactions of a meson. Section 2.1 demonstrates that the interactions may indeed be written in the form suggested by this figure. Arrows indicate fermion flow; time flows from left to right.

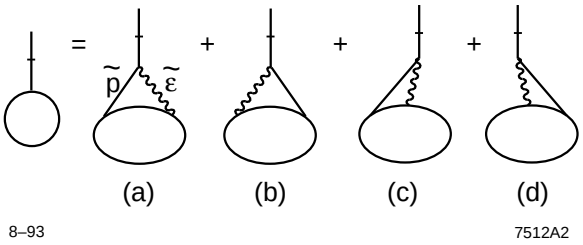

Fig. 2.2. Underlying processes which contribute to interactions like that shown in Fig. 1. We must account for the possibility of the 'invisible' internal quark and gluon being either forward- or backward-moving.

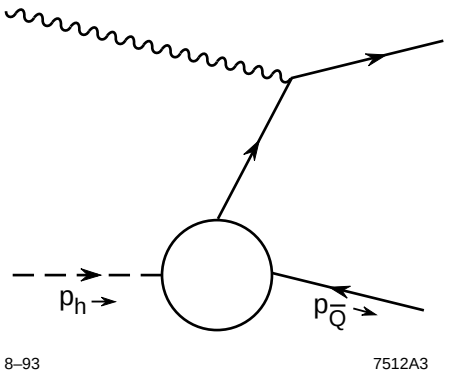

Fig. 2.3. Another diagram contributing to the photodissociation process, calculable using the methods of [2-3].

We first consider the time-ordering shown in Fig. 2.2(c). The instantaneous quark is now represented by

$$D_{\rm inst} = \frac{\gamma^+}{q^+}\ \tilde{\not{\epsilon}}\ \frac{u_\lambda(\tilde{p})}{\sqrt{\tilde{p}^+}}. \tag{2.2}$$

We will derive a more compact expression for eq. (2.2), depending only on the external momenta p_h, $p_{\bar{Q}}$, and q of Fig. 2.1. Once this is accomplished, the wavefunctions inside the muck of Fig. 2.2 may be integrated out, leaving a form similar to that of eq. (2.1). Fortuitously, the presence of the γ^+ acts as an 'information wall' which we now show serves to block out the dependence on the 'invisible' internal momentum $\tilde{p}$.

The wavefunctions are inevitably gauge-dependent; they possess the intuitively appealing correspondence with the parton model only in light-cone gauge $A^+ = 0$ [3]. Also, it is only in this gauge that our neglect of contributions from higher Fock states can be justified. Thus we lose no further generality by making the substitution $\gamma^+\tilde{\not{\epsilon}} \to -\gamma^+\tilde{\epsilon}_\perp \cdot \gamma_\perp$. Then we can explicitly evaluate eq. (2.2), obtaining

$$D_{\rm inst} = \frac{\tilde{\epsilon}_1 + i\lambda\tilde{\epsilon}_2}{q^+}\ \zeta_\lambda, \tag{2.3}$$

where (in the Dirac representation of γ^μ)

$$\zeta_+ \equiv \frac{1}{\sqrt{2}}\begin{pmatrix}0\\1\\0\\1\end{pmatrix} \qquad \text{and} \qquad \zeta_- \equiv \frac{1}{\sqrt{2}}\begin{pmatrix}-1\\0\\1\\0\end{pmatrix}; \tag{2.4}$$

the spinors $\zeta_\pm$ are related to the basis spinors χ of Ref. [3] by $\zeta_\pm = \gamma^0\gamma^1\chi_\pm = \pm\gamma^+\chi_\mp$.

We have almost accomplished our objective; the spinors $\zeta_\pm$ carry information about the spin of the invisible internal quark (as they must, since helicity is conserved for light quarks), but they do not depend on its momentum $\tilde{p}$ at all. The unwanted extra information has been blocked by the intervening γ^+.

It is worth noting that the form of ζ is unchanged if we substitute a scalar gluon into the internal vertex shown in Fig. 2.2 (except, of course, that the internal quark helicity is reversed). Thus the instantaneous effective wavefunction exists, and is associated with the spinors $\zeta_\pm$, for any theory of bound states of fermions.

The only remaining obstacle is the dependence on $\tilde{\epsilon}_\perp$. We use the light-cone gauge convention of Ref. [3], so that $\epsilon_\perp = (1, \pm i)/\sqrt{2}$. The gluon with spin $-\lambda$, opposite to the internal quark spin, contributes a factor $\sqrt{2}$; the gluon with spin $+\lambda$ does not contribute at all. Now we can write eq. (2.2) as

$$D_{\rm inst} = \sqrt{2}\ \frac{\zeta_\lambda}{q^+}, \tag{2.5}$$

with the implicit constraint that the internal gluon of Fig. 2.2 has helicity $-\lambda$. Though we have as yet discovered nothing about $\tilde{\psi}$, the form of eq. (2.5), into which no momenta other than q enter, is sufficient to demonstrate its existence.

The wavefunctions inside the muck of Fig. 2.2 carry an extra unit of orbital angular momentum, which is not present in the wavefunction of Fig. 2.3; the difference serves to balance the angular momentum carried by the gluon which we have explicitly extracted.

We can now define the instantaneous wavefunction $\tilde{\psi}_{h(q_\lambda)\bar{Q}}(x, k_\perp)$ required for the evaluation of the amplitude shown in Fig. 2.1. The parentheses in the subscript

denote the exchange of an instantaneous particle; the arguments x and $k_\perp$ are defined by

$$x \equiv \frac{p^+_{\bar{Q}}}{p^+_h} \qquad \text{and} \qquad k_\perp \equiv p_{\perp,\bar{Q}} - x p_{\perp,h}.$$

To ensure that the instantaneous wavefunction has the same spin properties as the propagating wavefunction $\psi_{h\to q\bar{Q}}$, we rewrite eq. (2.5) as

$$D_{\text{inst}} = \left[\frac{\sqrt{2}\; p^+_{\bar{Q}}}{q^+(k_1 + i\lambda k_2)}\right]\left(\frac{k_1 + i\lambda k_2}{p^+_{\bar{Q}}}\right)\zeta_\lambda, \tag{2.6}$$

and absorb the factor in square brackets into the definition of the wavefunction $\tilde{\psi}_{h(q_\lambda)\bar{Q}}$.

With this result, we can represent instantaneous interactions of the sort shown in Fig. 2.1 by replacing the incoming meson with the factor

$$\int_0^\infty \mathrm{d}x \int \frac{\mathrm{d}^2 k_\perp}{16\pi^3} \tilde{\psi}_{h(q_\lambda)\bar{Q}}(x, k_\perp) \left(\frac{k_1 + i\lambda k_2}{p^+_{\bar{Q}}}\right) \zeta_\lambda \; \frac{\bar{v}(xp + k_\perp)}{\sqrt{xp^+}}; \tag{2.7}$$

this should be compared to eq. (2.1), the standard expression, which appears in the evaluation of the propagating amplitude shown in Fig. 2.3. The new terms in eq. (2.7), $(k_1 + i\lambda k_2)\zeta_\lambda / p^+_{\bar{Q}}$, combine to mimic the properties under boosts and rotations about $\hat{z}$ of the corresponding term $u_\lambda / \sqrt{p^+_q}$ in eq. (2.1); thus the two wavefunctions behave identically under those transformations.

Though we have constructed this result for only one of the time-orderings of Fig. 2.2, the proof in the other cases proceeds in exactly the same manner except for the substitutions $u_\lambda \to v_{-\lambda}$ or $\tilde{\epsilon} \to \tilde{\epsilon}^*$, which do not affect the result.

For diagrams like that shown in Fig. 2.1, we must allow $x \in (0, \infty)$ since the momenta p^+_h and $p^+_{\bar{Q}}$ can take any positive value, and q^+ may have either sign.

Another class of diagrams, like that shown in Fig. 2.4, requires determination of the instantaneous fragmentation amplitude $\tilde{\psi}_{(Q)hq}$; we will return to this case in Section 2.3.

Figure 2.5 shows a configuration in which it is not clear which wavefunction we should use. This process may be considered either as an instantaneous process like those of Fig. 2.1, or as a higher-order correction to the tree-level diagram of Fig. 2.3. How do we avoid double-counting such contributions?

The answer depends on the choice of separation scale μ. Define the internal perpendicular momentum $k_\perp \equiv q_\perp - (q^+/p^+_{\bar{Q}})p_{\perp,\bar{Q}}$. If $|k_\perp| > \mu$, we must consider the process shown in Fig. 2.5 as a higher-order correction to the propagating amplitude of Fig. 2.3; for $|k_\perp| < \mu$, the same amplitude is already accounted for as part of the amplitude corresponding to Fig. 2.2(a). Thus the instantaneous wavefunctions, like the propagating ones, are dependent on the factorization scale; their μ-dependence is determined by diagrams like that of Fig. 2.5. Consideration of this evolution is outside the scope of the present work; we will fix the same factorization scale μ for the instantaneous and propagating wavefunctions, and compare the resulting quantities. The discussion, however, should highlight the fact that at small momentum transfer, the quark is not the simple object which enters into perturbative calculations, but has all the complexity usually associated with composite hadrons.

In sum, we have constructed a rule, eq. (2.7), for the calculation of instantaneous scattering from mesons; its use is exactly analogous to that of the familiar non-instantaneous wavefunctions of Ref. [3]. The power of this result is its independence of the internal dynamics of the muck, demonstrated by eq. (2.5); the internal momenta do not affect the form of the interaction.

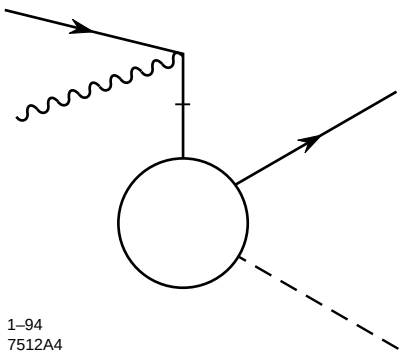

Fig. 2.4. A process involving the s-channel instantaneous fragmentation amplitude $\tilde{\psi}_{(Q)hq}$. Again, arrows indicate the direction of fermion flow.

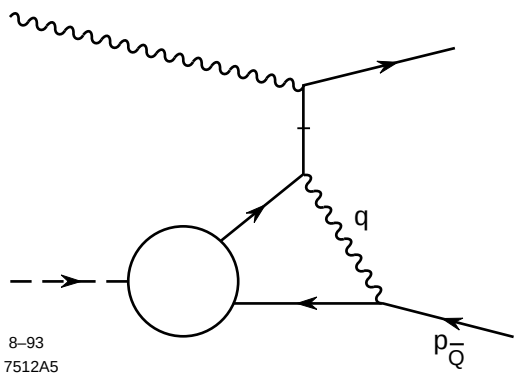

Fig. 2.5. A diagram which may or may not be considered instantaneous, depending on the momentum transfer $k_\perp$.

It must be pointed out that the theoretical stature of the instantaneous wavefunction is not on a par with that of the more familiar two-particle wavefunction. The latter is simply the projection onto a $q\bar{q}$ basis Fock state of an eigenstate of the light-cone Hamiltonian, while the former incorporates the sum and integration over more populous Fock states represented in Fig. 2.2. Thus the wavefunction entering into eq. 2.7 is, in terms of the expansion of the meson wavefunction over the Fock state basis, only an effective wavefunction entering into processes like that shown in Fig. 2.1.

Equation (2.7) ensures that the properties of the instantaneous wavefunction under rotations about $\hat{z}$ are the same as those of the propagating wavefunction with the same meson and parton helicities; thus the two contributions may readily be combined in the calculation of scattering amplitudes. Finally, we note that time-reversal invariance requires

$$\tilde{\psi}_{\bar{Q}(q)h}(x, k_\perp) = \tilde{\psi}^*_{h(q)\bar{Q}}(x^{-1}, x^{-1}k_\perp). \tag{2.8}$$

We next turn to the problem of relating the instantaneous contributions so defined to the conventional wavefunction.

2.2. Constraints From Rotational Invariance

With the introduction of the wavefunctions $\tilde{\psi}$, we are finally able to calculate entire hadronic amplitudes, rather than only their +-components. The simplest such process is the photodissociation of a meson; for definiteness, we will consider the process $\gamma K^0 \to \bar{d}_+ s_+$, where the subscripts denote particle helicities.

We neglect all quark mass terms in the following analysis; thus our results will suffer from corrections of order m/Q, where $Q^2 = -t$ is the momentum transfer in the scattering process. This enables us not only to probe the projections of the wavefunctions onto a state with definite helicities, but also to prepare the fermion spinors in the spin-projection eigenstates of Ref. [3] without spoiling the rotational invariance of the amplitude.

Armed with the result of eq. (2.7), we can now calculate all of the components of the hadronic part H^μ of the amplitude, rather than only H^+. Thus it is possible to circumvent the lack of gauge invariance of single Feynman diagrams by specializing immediately to Coulomb gauge and working only in center-of-momentum frames. While individual Feynman graphs lack the gauge invariance which is prerequisite to full Lorentz invariance, in this case they will be invariant (up to at most a phase) under rotations, though not under boosts.

For massless particles, the most general form for the initial- and final-state four-momenta $(k^+, k^-, k_\perp)$ satisfying $P_\perp = 0$ is

$$\begin{aligned} p_K &= (yP^+, \bar{y}P^-, l_\perp), \\ p_\gamma &= (\bar{y}P^+, yP^-, -l_\perp), \\ p_s &= (\bar{x}P^+, xP^-, -k_\perp), \text{ and} \\ p_{\bar{d}} &= (xP^+, \bar{x}P^-, k_\perp). \end{aligned} \tag{2.9}$$

Here we have introduced the notation $\bar{a} \equiv 1 - a$; the requirement that all particles be on mass shell means that $k_\perp^2 = x\bar{x}P^+P^-$ and $l_\perp^2 = y\bar{y}P^+P^-$.

In order to obtain rotationally invariant quantities, we must work in center-of-mass frames, where $P^+ = P^- = E_{\rm cm}$; since there is only one energy scale in the

problem, we set $E_{\rm cm} = 1$ for convenience. Then the three-momenta corresponding to the definitions of eq. (2.9) are

$$\begin{aligned} \vec{p}_K &= (l_\perp, y - \frac{1}{2}), \\ \vec{p}_\gamma &= (-l_\perp, \frac{1}{2} - y), \\ \vec{p}_s &= (k_\perp, x - \frac{1}{2}), \text{ and} \\ \vec{p}_{\bar{d}} &= (-k_\perp, \frac{1}{2} - x). \end{aligned} \tag{2.10}$$

We will use three-vectors, with the notation $\vec{v} = (v_\perp, v_z)$, in the remainder of this chapter.

In Coulomb gauge, $\epsilon^0 = 0$, and the photon polarization three-vectors are

$$\vec{\epsilon}_\uparrow = \vec{\epsilon}^{\,*}_\downarrow = \sqrt{2y\bar{y}}\Big(\frac{l_{_L}}{y}\hat{\epsilon}_{_R} - \frac{l_{_R}}{\bar{y}}\hat{\epsilon}_{_L}, 1\Big), \tag{2.11}$$

where for the sake of brevity we have introduced the notations

$$\hat{\epsilon}_{_R} \equiv \frac{1}{\sqrt{2}}(1, i), \qquad \hat{\epsilon}_{_L} \equiv \frac{1}{\sqrt{2}}(1, -i), \qquad \text{and} \qquad l_{_{R^{(L)}}} \equiv l_\perp \cdot \hat{\epsilon}_{R(L)}.$$

As a first example, we calculate the s-channel amplitude for Compton scattering $e\gamma \to e\gamma$, given these restrictions. When the electron helicity is positive, the only nonzero contribution is that in which both photon helicities are negative. If we let p_K and $p_{\bar{d}}$ above represent the incoming and outgoing electron momenta, the s-channel contribution to the full Compton amplitude is

$$e^2\Big[\sqrt{\bar{x}\bar{y}} + \frac{2l_{_L}k_{_R}}{\sqrt{\bar{x}\bar{y}}}\Big] = e^2 \cos\frac{\theta_{\rm cm}}{2} e^{i\phi},$$

where ϕ is a pure phase [5].

This is indeed rotationally invariant, except for a phase factor from our spinor conventions, due to the fact that the scattering plane is not parallel to the $\hat{z}$-axis. If we require $k_\perp \parallel \pm l_\perp$, the amplitude is purely real. We will impose this additional constraint in our later calculations by considering events which lie in the $\hat{x}\hat{z}$-plane. The kinematically allowed region of the xy-plane is shown (with and without this restriction) in Fig. 2.6.

Now we can implement the program of using the requirement of rotational invariance to constrain the meson wavefunction. The first step is to calculate the t-channel contribution, shown in Fig. 2.7, to the amplitude for $\gamma_\uparrow K^0 \to s_+ \bar{d}_+$ in the massless approximation:

$$\begin{aligned}\mathcal{F} = -eq_s\sqrt{p_s^+ p_{\bar{d}}^+}\Bigg\{ &\Big[\frac{\bar{u}_+(p_s)}{\sqrt{\bar{x}}}\vec{\gamma}\cdot\vec{\epsilon}\frac{u_+(p_s-p_\gamma)}{\sqrt{y-x}}\Big]\theta(y-x)\psi_{K^0\to\bar{d}_+ s_+}\big(\frac{x}{y},-\frac{x}{y}t\big) \\ &+\Big[\frac{\bar{u}_+(p_s)}{\sqrt{\bar{x}}}\vec{\gamma}\cdot\vec{\epsilon}\frac{v_-(p_\gamma-p_s)}{\sqrt{x-y}}\Big]\theta(x-y)\psi^*_{\bar{d}_+\to K^0\bar{s}_-}\big(\frac{y}{x},-\frac{y}{x}t\big) \\ &+\Big[\frac{\bar{u}_+(p_s)}{\sqrt{\bar{x}}}\vec{\gamma}\cdot\vec{\epsilon}\zeta_+\Big]\Big(\frac{p_{\bar{d}_R}}{x}-\frac{p_{K^0{}_R}}{y}\Big)\tilde{\psi}_{K^0(s_+)\bar{d}_+}\big(\frac{x}{y},-\frac{x}{y}t\big)\Bigg\};\end{aligned}$$

the three terms in braces give the contributions from the wavefunction, fragmentation amplitude, and instantaneous exchange amplitude, respectively. Our notation is conventional, except that we have used $k_\perp^2$ rather than $k_\perp$ as the argument for the wavefunctions, for the sake of brevity. Note that the definition of $k_\perp$ in the fragmentation amplitude differs from that used in the wavefunctions.

Inserting the explicit representations from eqs. (2.10)-(2.11) and the spinors of Ref. [3], we can evaluate this expression:

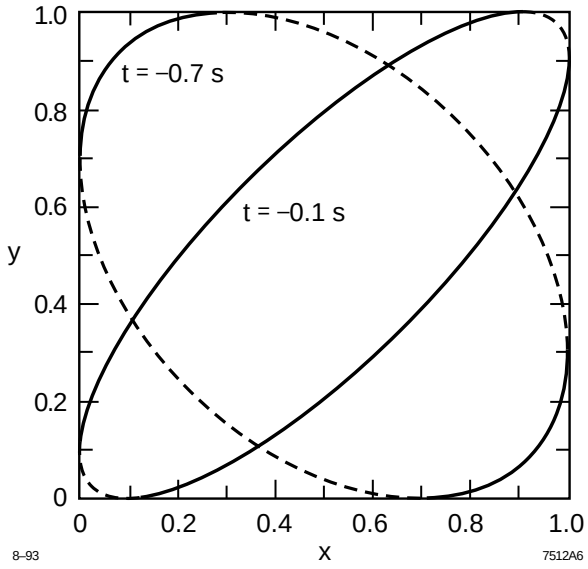

Fig. 2.6. The kinematically allowed region of the xy-plane for some values of t/s. In each case, the part of the boundary given by the heavy solid line is allowed when $k_\perp \parallel l_\perp$.

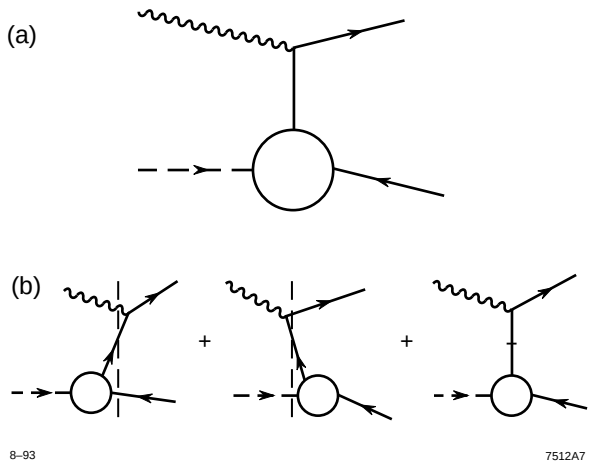

Fig. 2.7. Part of the K^0 photodissociation amplitude. (a) shows the Feynman diagram, (b) the associated LCPTh diagrams.

$$
\begin{aligned}
\mathcal{F} = -2eq_s\sqrt{2x\bar{x}y\bar{y}}\Big(&\frac{l_{_L}}{y}\hat{\epsilon}_{_R} - \frac{l_{_R}}{\bar{y}}\hat{\epsilon}_{_L}, 1\Big) \\
&\cdot\Bigg\{\Big(\frac{l_{_R}-k_{_R}}{y-x}\hat{\epsilon}_{_L} - \frac{k_{_L}}{\bar{x}}\hat{\epsilon}_{_R}, \frac{1}{2} + \frac{k_{_L}(l_{_R}-k_{_R})}{\bar{x}(y-x)}\Big)\theta(y-x)\psi_{K^0\to\bar{d}_+s_+}\big(\frac{x}{y}, -\frac{x}{y}t\big) \\
&\quad + \Big(\frac{k_{_R}-l_{_R}}{x-y}\hat{\epsilon}_{_L} - \frac{k_{_L}}{\bar{x}}\hat{\epsilon}_{_R}, \frac{1}{2} - \frac{k_{_L}(l_{_R}-k_{_R})}{\bar{x}(x-y)}\Big)\theta(x-y)\psi^*_{\bar{d}_+\to K^0\bar{s}_-}\big(\frac{y}{x}, -\frac{y}{x}t\big) \\
&\quad + \Big(\hat{\epsilon}_{_L}, \frac{k_{_L}}{\bar{x}}\Big)\Big(\frac{k_{_R}}{x} - \frac{l_{_R}}{y}\Big)\tilde{\psi}_{K^0(s_+)\bar{d}_+}\big(\frac{x}{y}, -\frac{x}{y}t\big)\Bigg\} \\
= -eq_s\sqrt{2}\Bigg\{&(x\bar{x}y + x^2\bar{y} - 2x\sqrt{x\bar{x}y\bar{y}})\frac{\theta(y-x)}{y-x}\psi_{K^0\to\bar{d}_+s_+}\big(\frac{x}{y}, -\frac{x}{y}t\big) \\
&\quad + (2x\sqrt{x\bar{x}y\bar{y}} - x\bar{x}y - x^2\bar{y})\frac{\theta(x-y)}{x-y}\psi^*_{\bar{d}_+\to K^0\bar{s}_-}\big(\frac{y}{x}, -\frac{y}{x}t\big) \\
&\quad + (2\sqrt{x\bar{x}y\bar{y}} - \bar{x}y - x\bar{y})\tilde{\psi}_{K^0(s_+)\bar{d}_+}\big(\frac{x}{y}, -\frac{x}{y}t\big)\Bigg\}.
\end{aligned}
\tag{2.12}
$$

In the last step, we have made explicit the assumption that $k_\perp \parallel l_\perp$. The requirement that the physics of this scattering process be rotationally invariant implies that $\mathcal{F}$ is a function of the Mandelstam invariants t and u only, for any x and y in the kinematically allowed region

$$(ys + \bar{x}t + xu)^2 \le 4utx\bar{x}.$$

The restriction $k_\perp \parallel l_\perp$ restricts us to the boundary of the allowed region; along this boundary, the phase and magnitude of $\mathcal{F}$ are constant.

The first step in extracting the consequences of this independence is to consider the two limits $x \to 1$ (which requires $y \to -u/s$) and $y \to 1$ (whence $x \to -u/s$). The equality of the amplitude in these two cases yields the requirement

$$
\begin{aligned}
-\hat{u}\psi_{K^0\to\bar{d}_+s_+}(\hat{u}, \hat{u}\hat{t}s) + \hat{t}\tilde{\psi}_{K^0(s_+)\bar{d}_+}(\hat{u}, \hat{u}\hat{t}s) \\
= \psi^*_{\bar{d}_+\to K^0\bar{s}_-}(\hat{u}, \hat{u}\hat{t}s) + \hat{t}\tilde{\psi}_{K^0(s_+)\bar{d}_+}(\hat{u}^{-1}, \hat{u}^{-1}\hat{t}s),
\end{aligned}
\tag{2.13}
$$

where we have defined $\hat{u} = -u/s$ and $\hat{t} = -t/s$.

To obtain another, similar constraint, we consider the process $\gamma_\downarrow K^0 \to s_+\bar{d}_+$. The calculation proceeds in identical manner, and we obtain the result

$$\hat{u}\psi_{K^0\to\bar{d}_+s_+}(\hat{u},\hat{u}\hat{t}s) = -\hat{t}\tilde{\psi}_{K^0(s_+)\bar{d}_+}(\hat{u}^{-1},\hat{u}^{-1}\hat{t}s). \tag{2.14}$$

Combined with eq. (2.13), this implies that

$$\hat{t}\tilde{\psi}_{K^0(s_+)\bar{d}_+}(\hat{u},\hat{u}\hat{t}s) = \psi^*_{\bar{d}_+\to K^0\bar{s}_-}(\hat{u},\hat{u}\hat{t}s). \tag{2.15}$$

We might hope to obtain an additional constraint by considering the process $K^0\phi \to s_-\bar{d}_+$ for a scalar 'photon' ϕ [6]. However, the constraint thus derived is merely eq. (2.15); the calculation provides a check of our results, but yields no new information.

We can now substitute eqs. (2.14)-(2.15) back into eq. (2.12) to eliminate the dependence of $\mathcal{F}$ on $\tilde{\psi}$. Ignoring an overall factor of $-eq_s\sqrt{2}$, we now have

$$\begin{aligned}\mathcal{F} = x\big(\sqrt{\bar{x}y}-\sqrt{x\bar{y}}\big)^2\,\frac{\theta(y-x)}{y-x}\Big[\psi_{K^0\to\bar{d}_+s_+}\big(\frac{x}{y},-\frac{x}{y}t\big) - \frac{y}{x}\psi^*_{\bar{d}_+\to K^0\bar{s}_-}\big(\frac{x}{y},-\frac{x}{y}t\big)\Big] \\ + (x\leftrightarrow y).\end{aligned} \tag{2.16}$$

Since this form is manifestly symmetric under $x \leftrightarrow y$, eqs. (2.13)–(2.15) encapsulate all of the consequences of the symmetry of $\mathcal{F}$ under $x \leftrightarrow y$. However, much more information is contained in eq. (2.12). To further clarify the meaning of eq. (2.16), we parametrize the momenta by $\hat{u}$, $k_\perp \equiv \sqrt{-t}$, and $z \equiv x/y$; for the moment we will assume $z < \hat{u}$. Then the constraint $k_\perp \parallel l_\perp$ requires

$$y = \frac{1-\hat{u}}{1+z-2\sqrt{\hat{u}z}} \qquad \Rightarrow \quad \frac{x}{y-x}\big(\sqrt{\bar{x}y}-\sqrt{x\bar{y}}\big)^2 = \frac{z}{1-z}(1-\hat{u}).$$

Inserting this result into eq. (2.16), we obtain a sum rule relating the wavefunction and fragmentation amplitude in the region $z < \hat{u}$. We can repeat the preceding

analysis with $k_\perp \parallel -l_\perp$ to probe the region $z > \hat{u}$. In either case, we obtain the same result:

$$\frac{z\psi_{K^0\to\bar{d}_+ s_+}(z,\sqrt{z}k_\perp) - \psi^*_{\bar{d}_+\to K^0\bar{s}_-}(z,\sqrt{z}k_\perp)}{1-z} = \frac{\mathcal{F}(s,t=-k_\perp^2,u)}{1-\hat{u}} = M_1(k_\perp^2), \tag{2.17}$$

where M_1 does not depend on z or $\hat{u}$ [7], and z can have any value in the allowed region $0 < z < 1$.

While our choice of the K^0 meson gave us a concrete example with which to work, our results in no way depend on the flavor of the meson in question. In addition, the above computation yields the same results regardless of the helicity of the struck quark. The only dependence on the spin properties of the particles arises from the fact that the argument of transverse momentum $k_\perp$ in the fragmentation amplitude $\psi^*_{\bar{q}}$ is antiparallel to that used in the wavefunctions. Taking this into account, we obtain the final result

$$\begin{aligned}\tilde{\psi}_{h(Q_s)\bar{q}_{s'}}(z,k_\perp) = \frac{\theta(1-z)}{1-z}(-1)^{\lambda-s-s'}\psi^*_{\bar{q}_{s'}\to h\bar{Q}_{-s}}(z,k_\perp) \\ - \frac{\theta(z-1)}{z-1}\psi_{h\to\bar{q}_{s'}Q_s}(z^{-1},z^{-1}k_\perp),\end{aligned} \tag{2.18}$$

valid for all $z > 0$, up to corrections of order $\alpha_s(k_\perp^2)$ and of order m_h/Q.

Thus the instantaneous wavefunction for any scalar meson is entirely determined in terms of the ordinary wavefunction and the fragmentation amplitude. This simplification should greatly advance the calculation of scattering processes which mix free and bound states, in which instantaneous contributions cannot be ignored. We have neglected some subtleties due to the fact that rotations mix the spin states of vector mesons; thus results for the vector case will be postponed to Section 2.5.

One noteworthy feature of eq. (2.18) is that the instantaneous contributions do not vanish as $z \to 1$. This is sensible, since the vanishing of the conventional wavefunction is due to the divergent energy denominator $k_\perp^2/z\bar{z}$; no such denominator appears in the instantaneous interaction.

The constraint (2.17) is equally general; we have the result

$$\frac{z\psi_{h\to\bar{q}_{s'}Q_s}(z,\sqrt{z}k_\perp) - (-1)^{s+s'}\psi^*_{\bar{q}_{s'}\to h\bar{Q}_{-s}}(z,\sqrt{z}k_\perp)}{1-z} = M_1(k_\perp). \tag{2.19}$$

One should keep in mind that eqs. (2.18) and (2.19) are subject to errors on the order of $\mu/|k_\perp|$, where μ is a typical mass for the particles in question; thus they are best applicable to light mesons at large momentum transfer. For example, the relationship between distribution amplitudes

$$\frac{z\phi_{h\to\bar{q}Q}(z) - \phi^*_{\bar{q}\to h\bar{Q}}(z)}{z(1-z)} = \text{constant} = 0, \tag{2.20}$$

obtained by integrating over $k_\perp$ in eq. (2.19) and considering the limit $z \to 0$, is subject to errors from the region in which $k_\perp$ is small.

2.3. The s-Channel Amplitude

We now examine the calculations of instantaneous exchange contributions to the s-channel graph shown in Fig. 2.4, which contributes to the amplitude $\mathcal{F}_{\phi Q\to hq}$ for a scalar probe ϕ coupling to the Q. For this purpose, a new instantaneous wavefunction $\psi_{(Q)hq}$ is required, as well as the fragmentation amplitude $\psi_{Q\to hq}$.

As before, the Dirac structure associated with the instantaneous Q line is given by the factor $\zeta_\pm$ of eq. (2.4). We may thus represent an insertion like that shown in Fig. 2.8 by the factor

$$\int \mathrm{d}x \, \frac{\mathrm{d}^2 k_\perp}{16\pi^3} \, \tilde{\psi}_{(Q)hq}(x, k_\perp) \, \left[\frac{k_1 \mp i k_2}{p_h^+} \bar{\zeta}_\pm \right] \, \frac{u(p_q)}{\sqrt{p_q^+}} \, , \tag{2.21}$$

where the hadron momentum $p_h = x p_Q + k_\perp$. The additional kinematic terms which have been extracted from $\tilde{\psi}$ and included in the square brackets again serve to give the quantity in brackets the same properties as $\bar{u}_\pm(p_Q)/\sqrt{p_Q^+}$ under boosts and under rotations about $\hat{z}$, so that the instantaneous effective fragmentation amplitude will in turn have the same transformation properties as the conventional fragmentation amplitude.

We again we set up the most general kinematics in the center-of-mass frame; in exact analogy to eq. (2.10), we have

$$\begin{aligned} \vec{p}_Q = -\vec{p}_\phi &= \big(k_\perp, x - \frac{1}{2}\big), \\ \vec{p}_h = -\vec{p}_q &= \big(l_\perp, y - \frac{1}{2}\big). \end{aligned}$$

The leading-twist contribution to the amplitude of the graph of Fig. 2.4 for negative external quark helicity is then

$$\begin{aligned} \mathcal{F}(s,t,u) &= -g\sqrt{y} l_\perp \Bigg\{ \bar{u}_+(P) \, \frac{u_-(p_Q)}{\sqrt{x}} \, \psi_{Q\to hq}(y, l_\perp) \\ &\qquad + \Big(\sqrt{2}\frac{l_{\scriptscriptstyle L}}{y}\Big) \bar{\zeta}_+ \frac{u_-(p_Q)}{\sqrt{x}} \, \tilde{\psi}_{(Q)hq}(y, l_\perp) \Bigg\} \\ &= -g\sqrt{2} \Bigg\{ \sqrt{\frac{\bar{y}}{x}} \, k_{\scriptscriptstyle L} \, \psi_{Q\to hq}(y, l_\perp) + \frac{\sqrt{x\bar{y}}}{y} \, l_{\scriptscriptstyle L} \, \tilde{\psi}_{(Q)hq}(y, l_\perp) \Bigg\} \, . \end{aligned} \tag{2.22}$$

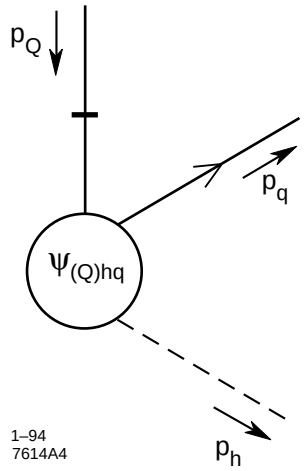

Fig. 2.8. Instantaneous insertions of the s-channel type, corresponding to the effective fragmentation amplitude $\tilde{\psi}_{(Q)hq}$.

The values of x and y are constrained by the values of the Mandelstam invariants s, t, u; also, $|l_\perp|$ is fixed by the relation $l_\perp^2 = y\bar{y}s$. We specialize to two particularly informative cases:

$$\begin{aligned}
&\textsc{Case 1}: \quad t=0,\ u=-s \qquad \Rightarrow \quad x=y,\ k_\perp = l_\perp, \text{ and} \\
&\qquad\qquad \mathcal{F} = M_2(s) = \bar{y}\psi(y,l_\perp) + \bar{y}\tilde{\psi}(y,l_\perp). \\
&\textsc{Case 2}: \quad u=0,\ t=-s \qquad \Rightarrow \quad x=\bar{y},\ k_\perp = -l_\perp, \text{ and} \\
&\qquad\qquad \mathcal{F} = M_3(s) = -\sqrt{y\bar{y}}\psi(y,l_\perp) + \bar{y}\sqrt{\frac{\bar{y}}{y}}\tilde{\psi}(y,l_\perp).
\end{aligned} \tag{2.23}$$

From these two equations, it is a simple matter to extract $\psi_{Q\to hq}(y,k_\perp)$ in terms of the two unknown amplitudes $M_{2,3}$; we obtain the general form

$$\begin{aligned}
\psi_{Q\to hq}(y,l_\perp) &= M_2\left(\frac{l_\perp^2}{y\bar{y}}\right) - \sqrt{\frac{y}{\bar{y}}}\ M_3\left(\frac{l_\perp^2}{y\bar{y}}\right) , \\
\tilde{\psi}_{(Q)hq}(y,l_\perp) &= \frac{y}{\bar{y}}\ M_2\left(\frac{l_\perp^2}{y\bar{y}}\right) + \sqrt{\frac{y}{\bar{y}}}\ M_3\left(\frac{l_\perp^2}{y\bar{y}}\right) .
\end{aligned} \tag{2.24}$$

Substituting these forms back into our expression for the amplitude, we obtain (modulo a phase arising from our spinor conventions, which vanishes when the $\hat{z}$ axis lies in the scattering plane)

$$\mathcal{F} = M_2\Big(\frac{l_\perp^2}{y\bar{y}}\Big)\sqrt{-u/s} + M_3\Big(\frac{l_\perp^2}{y\bar{y}}\Big)\sqrt{-t/s} = M_2(s)\cos(\theta_{\rm cm}/2) + M_3(s)\sin(\theta_{\rm cm}/2),$$

which is manifestly independent of x and y.

Thus in the region of large momentum transfer, where our neglect of higher-twist and higher-order contributions to the amplitude is an accurate approximation,

the fragmentation amplitude and its instantaneous counterpart have very simple few-parameter representations. Indeed, we will shortly demonstrate that $M_2 = 0$ for pointlike 'hadrons'.

We may also replace the scalar probe with a photon probe of arbitrary helicity quantized in the Coulomb gauge; the resulting constraints on ψ and $\tilde{\psi}$ are identical.

It must be emphasized here that the hadron h is considered to be in an eigenstate of helicity in the center-of-mass frame in question; the mixing of helicity states to form boost-invariant states can invalidate the above relations for vector mesons polarized along the z-axis. Thus the conclusions of eq. (2.24) hold only for fragmentation into scalars, where no such subtleties arise. We will return to the vector case in Sec. 2.5.

We have also ignored the possibility of higher-order corrections to the amplitude. Since the wavefunction mixes terms of all orders in the coupling constant, there is no good reason to suppose that diagrams involving wavefunction terms should be order-by-order invariant; the constraints we derive should thus be understood to be subject to corrections of order $\alpha_s(k_\perp^2)$ [1].

2.4. The Wavefunction

We now turn to the interesting question of the hadronic wavefunction. Equation (2.19) can be written in the form

$$\frac{y}{\bar{y}}\ \psi_{h\to Q\bar{q}}(y, \sqrt{y}\ k_\perp) = \frac{1}{\bar{y}}\ \psi_{Q\to hq}(y, \sqrt{y}\ k_\perp) + M_1(k_\perp^2)\ .$$

We make the further assumption that, in the region of large momentum transfer, the wavefunction scales as $|k_\perp|^{-2n}$. We thus obtain the constraint

$$y\bar{y}^{n-1}\ \psi_{h\to Q\bar{q}}(y,l_\perp)\ =\ \bar{y}^{n-1}\ \psi_{Q\to hq}(y,l_\perp)+M_1\left(\frac{l_\perp^2}{y\bar{y}}\right)\ . \tag{2.25}$$

Introducing the notation $\delta\mathcal{M}^2 = l_\perp^2/y\bar{y}$ to denote the light-cone virtuality, we substitute eq. (2.24) into (2.25) to obtain

$$\psi_{h\to Q\bar{q}}(y,l_\perp)\ =\ \frac{\bar{y}^{1-n}\,M_1(\delta\mathcal{M}^2)+M_2(\delta\mathcal{M}^2)}{y}+\frac{M_3(\delta\mathcal{M}^2)}{\sqrt{y\bar{y}}}\ .$$

For pointlike vertices, $n = 1/2$; thus ψ can only remain finite as $y \to 0$ if we also have $M_2 = -M_1$. It follows that rotationally invariant pointlike wavefunctions must have the form

$$\psi_{h\to Q\bar{q}}(y,l_\perp)\ =\ \frac{C_3+C_1(\bar{y}-\sqrt{\bar{y}})/\sqrt{y}}{|k_\perp|}\ , \tag{2.26}$$

where $C_i \equiv (\delta\mathcal{M}^2)^n\ M_i(\delta\mathcal{M}^2)$. However, we can repeat the above derivation with $Q\ \leftrightarrow\ \bar{q}$, so C_1 (whose corresponding term is not symmetric under $y\ \leftrightarrow\ \bar{y}$) must vanish as well. Thus in eq. (2.24), $M_2 = 0$ for pointlike scalars.

However, we are most interested in bound states, for which $n = 1$ [8]. For these states, we again expect $M_2 = -M_1$, so that the wavefunction $\psi(y, k_\perp)$ will vanish as $y \to 0, 1$ for fixed $k_\perp$. We thus derive the general form

$$\psi_{h\to Q\bar{q}}(y,k_\perp)\ =\ C_3\ \frac{\sqrt{y\bar{y}}}{k_\perp^2}\Big[1+\mathcal{O}\big(\alpha_s(k_\perp^2)\big)+\mathcal{O}\big(m_h/k_\perp^2\big)\Big] \tag{2.27}$$

for a scalar bound state.

This result is somewhat surprising, especially to an intuition shaped by the nonrelativistic expectation that ψ depends only on $\delta\mathcal{M}^2 = k_\perp^2/y\bar{y}$. The difference from the relativistic case lies in the spinor normalizations $u(p)/\sqrt{p^+}$ which are used in Ref. [3]. In the nonrelativistic case, p^+ is essentially determined by the mass, and can be treated as a constant. Here, however, we work in the opposite limit, where the masses are considered negligible.

2.5. The Vector Case

The results of eqs. (2.26)-(2.27) cannot be used to derive boost-invariant wavefunctions for vector mesons, since the amplitudes we consider have been prepared with meson polarizations that are not themselves aligned with the $\hat{z}$-axis. So far, we have obtained results which are valid only for mesons of definite helicity.

However, we note that in every amplitude we have computed (as shown in Figs. 2.4 and 2.7) the angle between the hadron and the boost axis is determined by either y or $\bar{y}$ [9]. Since the helicity eigenstates are formed from a superposition of boost-invariant eigenstates with coefficients y, $\bar{y}$, and $\sqrt{y\bar{y}}$, we have the general form for pointlike vector particles:

$$\psi_{h\to Q\bar{q}}(y, k_\perp) \;=\; \frac{C_+ y + C_0\sqrt{y\bar{y}} + C_-\bar{y}}{|k_\perp|}\;, \tag{2.28}$$

and for vector mesons:

$$\psi_{h\to Q\bar{q}}(y, k_\perp) \;=\; (C_+ y + C_0\sqrt{y\bar{y}} + C_-\bar{y})\;\frac{\sqrt{y\bar{y}}}{k_\perp^2}\;. \tag{2.29}$$

The coefficient C_0, which represents mixing with the helicity-zero state, vanishes for massless particles.

For transversely polarized mesons, one of the coefficients $C_\pm$ is expected to vanish when the Q and $\bar{q}$ helicities are opposite, since a quark which inherits nearly the entire momentum of a hadron should also share its helicity. Similarly, for longitudinally polarized mesons, symmetry under reflections in the xy-plane implies $C_+ = C_-$. Thus, we have obtained a two-parameter form for the wavefunctions of vector mesons.

2.6. Conclusions

The lack of manifest rotational invariance in the light-cone formulation of physical theories is a potentially serious drawback. However, it can be circumvented in part by extracting the hidden consequences of rotational invariance, which is what we have attempted here. We find that the wavefunction in the region of large momentum transfer must have the general form

$$\begin{aligned}
\psi_{h\to Q\bar{q}}(x,k_\perp) &= C\,\frac{\sqrt{x\bar{x}}}{k_\perp^2} && \text{for scalar mesons,}\\
\psi_{h\to Q\bar{q}}(x,k_\perp) &= \frac{C_+ x\sqrt{x\bar{x}} + C_0 x\bar{x}}{k_\perp^2} && \text{for some transverse vector mesons,}\\
\psi_{h\to Q\bar{q}}(x,k_\perp) &= \frac{C_\pm\sqrt{x\bar{x}} + C_0 x\bar{x}}{k_\perp^2} && \text{for other vector mesons}
\end{aligned} \tag{2.30}$$

The second form holds only for the 'asymmetric' helicity combination in which one quark shares the meson polarization, while the other does not; in all other cases, the symmetric form should be used.

The forms given in eq. (2.30) should serve as a guide to the formulation of realistic model wavefunctions and as a check on wavefunctions extracted numerically through some discretization procedure. We must reiterate, however, that the

relations we have derived are valid only at leading order and leading twist, so that the numerical precision with which they can be applied is limited.

Also, the wavefunctions are themselves gauge-dependent. All of the results derived here depend on the use of light-cone gauge $A^+ = 0$.

The derivation we have given depends on the assumption that $\psi \propto k_\perp^{-2}$ in the large-$k_\perp$ region; given this assumption, the corresponding x-dependence is almost entirely determined.

The coefficients $C_\pm$ and C_0 of eqs. (2.28)-(2.30) may be further constrained in a rotationally invariant theory. The extraction of such a relation, however, will require more subtlety than has been necessary to obtain the above results.

2.7. The Distribution Amplitude

As the factorization scale Q grows large, the integral $\int^Q \psi(x, k_\perp)$ which appears in the distribution amplitude diverges as $\ln Q$. Scale-dependent renormalization factors [3] balance this divergence, so that the distribution amplitude itself approaches the finite asymptotic limit

$$\phi_{\rm as} \propto x(1-x)$$

at very large Q.

However, the logarithmic divergence means that the distribution amplitude is dominated by the contribution from large values of $|k_\perp|$, where the form of eq. (2.27) is expected to accurately describe the wavefunction. Thus the requirement of rotational invariance leads to the expectation

$$\phi_{\rm as} \propto \sqrt{x(1-x)}.$$

The solution to this quandary is not immediately apparent. We conjecture that the apparent contradiction arises from the neglect in both Ref. [3] and the present work of the dependence of the wavefunction ψ itself on the factorization scale Q; what we probe here is $\psi(x, k_\perp; Q = |k_\perp|)$, while the distribution amplitude is dominated by $\psi(x, k_\perp; \mu \ll |k_\perp| \ll Q)$.

This comparison should serve to emphasize the deeply embedded dependence on rotationally non-invariant cutoffs which are characteristic of light-cone physics, and the importance of bearing constantly in mind the fact that in the analysis of bound states in renormalizable theories, one is inevitably working with a truncated approximation to the full theory.

References for Chapter 2

[1] This fact was pointed out to the author by G. P. Lepage.

[2] S. J. Brodsky, R. J. Roskies, and R. Suaya, *Phys. Rev.* **D8**, 4574 (1973).

[3] G. P. Lepage and S. J. Brodsky, *Phys. Rev.* **D22**, 2157 (1980).

[4] V.N. Gribov and L.N. Lipatov, *Sov. J. Nucl. Phys.* **15**, 675 (1972).

[5] This can be proved by identifying the square of the term in brackets as $-u/s$.

[6] The s helicity in the final state is now negative because the interaction with a scalar flips fermion spins. Thus this process again probes the wavefunction $\psi_{K^0 \to \bar{d}_+ s_+}$.

[7] Since the left-hand side of the equation does not depend on $\hat{u}$, F must be a function of $k_\perp$ only. Thus we obtain the additional result $\mathcal{F} = (-t/s)F(k_\perp) = f(t)/s$ at large momentum transfer t, which is the expected Regge behavior for an amplitude resulting from the exchange of a single spinor particle.

[8] Ref. [3], Appendix A.

[9] Due to the Regge behavior of the amplitude of Fig. 2.7, we can always obtain $x = 1$ by setting $s = -t/\bar{y}$. Thus the momentum fraction z probed in the scattering is the same as the momentum fraction y which determines the angle between p_h and $\hat{z}$.

3. CONSTRAINTS FROM UNITARITY

In this chapter, we show that nontrivial bounds from unitarity can be derived, relating meson decay constants to the transverse momentum distribution of the quark constituents.

A heuristic overview of our procedure is as follows. We form positive-definite integrals containing the two-particle wave function $\psi_{q\bar{q}}(x, k_\perp)$, whose integral corresponds to the meson decay constant f_h, and its square, whose integral is constrained by unitarity. We use the condition of positivity to derive constraints on the behavior of the wave function.

The decay constant is defined by

$$\frac{f_h}{2\sqrt{2N_c}} \;=\; \int_0^1 \mathrm{d}x \int^Q \frac{\mathrm{d}^2 k_\perp}{16\pi^3} \quad \psi_{q\bar{q}}(x, k_\perp; Q) + O(Q^{-2}) \quad . \tag{3.1}$$

The wave function $\psi_{q\bar{q}}$ is weakly dependent on the separation scale Q; we will ignore this dependence, and assume that Q is much larger than a typical intrinsic transverse momentum. We will always assume that the decay constant is real and positive, thus fixing the phase of $\psi_{q\bar{q}}$. For pseudoscalar mesons, the decay constant f_h is entirely independent of Q.

The light-cone wave function must also satisfy

$$\int_0^1 \mathrm{d}x \int^Q \frac{\mathrm{d}^2 k_\perp}{16\pi^3} \quad |\psi_{q\bar{q}}|^2 \;\leq\; P_v \;, \tag{3.2}$$

where $P_v \leq 1$ is the probability to find the meson in its valence state [1]. This is the unitarity constraint with which we will work.

Now, consider a region R of $(x, k_\perp)$–space. Define

$$A[R] \;=\; \int_R \frac{\mathrm{d}x\ \mathrm{d}^2k_\perp}{16\pi^3}\ ,$$

$$F[R] \;=\; 2\sqrt{2N_c}\quad \mathrm{Re}\left[\ \int_R \frac{\mathrm{d}x\ \mathrm{d}^2k_\perp}{16\pi^3}\quad \psi_{q\bar{q}}(x,k_\perp)\ \right]\quad .$$

Thus A is the "area" of the region R, and F is the part of the decay constant contributed by the region R. Then we have

$$0 \;\le\; \int_R \frac{\mathrm{d}x\ \mathrm{d}^2k_\perp}{16\pi^3}\ |\psi_{q\bar{q}}(x,k_\perp) - b|^2 \;\le\; P_v - \frac{bF[R]}{\sqrt{2N_c}} + b^2A[R]\quad , \tag{3.3}$$

so that

$$F[R] \;\le\; \sqrt{2N_c}\quad \frac{P_v + b^2A[R]}{b} \tag{3.4}$$

for all regions R and positive real b. This modest equation turns out to have significant consequences.

Setting $b = \big(P_v/A[R]\big)^{1/2}$, we obtain

$$F[R] \;\le\; 2\sqrt{2N_cP_vA[R]}\quad ; \tag{3.5}$$

if we set $P_v = 1$, the contribution to the decay constant from the region R cannot exceed this bound without violating unitarity. More realistic choices of P_v lead to more stringent bounds on $F[R]$.

For example, consider the π meson, whose decay constant is $f_\pi = 133$ MeV. Define

$$\delta\mathcal{M}^2 \;\equiv\; \frac{k_\perp^2}{x} + \frac{k_\perp^2}{1-x} - m_\pi^2 \;=\; \frac{k_\perp^2}{x\bar{x}} - m_\pi^2\quad ,$$

and let $R \equiv \{(x,k_\perp) : \delta\mathcal{M}^2 \leq \mathcal{M}^2_{\rm max}\}$. Then $A[R] = (\mathcal{M}^2_{\rm max} + m_\pi^2)/96\pi^2$, and (with $N_c = 3$) we have

$$F[R] \;\leq\; \frac{\sqrt{P_v\big(\mathcal{M}^2_{\rm max} + m_\pi^2\big)}}{2\pi} \quad . \tag{3.6}$$

Thus unitarity requires that half of the pion decay constant must arise from the region in which $\delta\mathcal{M}^2 > 0.15$ GeV^2, and at least 13% from the region where $\delta\mathcal{M}^2 > 0.5$ GeV^2. The contribution to the wave function from regions of sizable intrinsic transverse momentum is thus very substantial.

Brodsky *et al.* [2] have estimated that $P_v(\pi) \simeq 0.25$ [1]; using this estimate in eq. (5) leads to the conclusion that half of the pion decay constant arises from the region in which $\delta\mathcal{M}^2 > 0.66$ GeV^2, and 39% from $\delta\mathcal{M}^2 > 1$ GeV^2. The latter virtuality corresponds to $|k_\perp| = \sqrt{x(1-x)} \times 505$ MeV.

Alternatively, we may consider a region $R \equiv \big\{(x,k_\perp) : k_\perp^2 < Q^2\big\}$. Clearly then $A[R] = Q^2/16\pi^2$, and we have $F[R] < Q\sqrt{2N_cP_v}/2\pi$. If $P_v = 0.25$, we obtain $Q \geq 5.13\, F[R]$, so that for example 26% of the pion decay constant must be contributed by the region where $|k_\perp| > 500$ MeV.

Even more severe constraints can be derived for the B meson, due to the unexpectedly large decay constant $f_B \gtrsim 190$ MeV [3,4] and to the expectation that the heavy b quark should carry the bulk of the longitudinal momentum. In this case, we define

$$\delta\mathcal{M}^2 \;\equiv\; \frac{k_\perp^2}{1-x} + \frac{k_\perp^2 + m_b^2}{x} - m_B^2 \;=\; \frac{k_\perp^2}{x(1-x)} + \frac{m_b^2}{x} - m_B^2 \quad .$$

Defining R as above, we obtain the bound

$$F[R] \;\leq\; \frac{\sqrt{P_v}}{2\pi}\, \frac{\big(\mathcal{M}^2_{\rm max} + m_B^2 - m_b^2\big)^{3/2}}{(\mathcal{M}^2_{\rm max} + m_B^2)} \quad . \tag{3.7}$$

Using $m_B = 5.28$ GeV and $m_b = 4.94$ GeV [5], we find that the region $\delta\mathcal{M}^2 < 3.9$ GeV^2 can support only 100 MeV of the decay constant, and $\delta\mathcal{M}^2 < 6.7$ GeV^2 only 150 MeV. Current lattice estimates tend to cluster around $f_B = 190$ MeV [4], while calculations using heavy-quark symmetry suggest $f_B = 240$ MeV [3]. Thus even the most conservative estimates of the decay constant require the $b\bar{q}$ states to carry a very substantial light-cone virtuality.

A plausible upper bound for $P_v(B)$ is $P_v(B) \leq \sqrt{P_v(\pi)}$; this estimate arises from the assumption that gluons in the meson wavefunction are directly associated with one of the valence quarks, and that gluon radiation from the heavy quark is entirely suppressed. In actuality, we expect that this somewhat overestimates $P_v(B)$, and thus that $P_v(B) = 0.5$ will lead to fairly conservative conclusions.

Inserting $f_B = 190$ MeV and $P_v(B) = 0.5$ into eq. (3.7), we find that half of f_B must be contributed by the region $\delta\mathcal{M}^2 > 5.8$ GeV^2, and 22% by the region in which $\delta\mathcal{M}^2 > 10$ GeV^2.

The numerically large value of f_B can only be consistent with unitarity if the B wave function in the $q\bar{q}$ state is greatly spread out in momentum space. For example, at $x = 0.9$ the value $\delta\mathcal{M}^2 = 10$ GeV^2 corresponds to $|k_\perp| = 0.97$ GeV, and at $x = 0.8$ to $|k_\perp| = 1.09$ GeV; see Fig. 3.1. Such large transverse momenta, and sizable values of $1 - x$, must be typical of the B meson.

In place of the constant b of eq. (3.3), we can insert an arbitrary function $B(x, k_\perp)$. This allows us to obtain unitarity bounds on the contribution to the moment $\langle B \rangle$ from a region R.

The most interesting such constraints arise when we consider the contribution to $\left\langle Q^2 - k_\perp^2 \right\rangle$ from the region $k_\perp^2 < Q^2$. With $B \equiv b(Q^2 - k_\perp^2)$, we obtain the bound

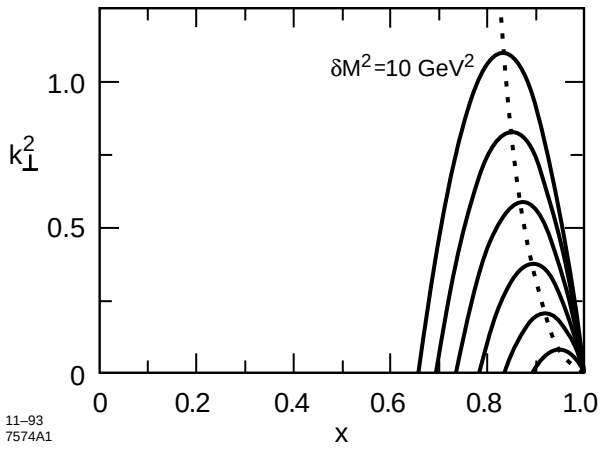

Fig. 3.1. Contours of constant light-cone virtuality $\delta\mathcal{M}^2$ for the B meson. As the transverse momentum increases, the light-cone momentum fraction x_b is pushed away from 1.

$$\mathrm{Re}\Big[\int\limits_{k_\perp^2<Q^2} \frac{\mathrm{d}^2k_\perp}{16\pi^2}(Q^2-k_\perp^2)\psi\Big] \leq \frac{Q^3}{4\pi}\sqrt{\frac{P_v}{3}}\ . \tag{3.8}$$

Thus the contribution to the integral representing $f_\pi \left\langle k_\perp^2 \right\rangle$ from the region $k_\perp^2 < Q^2$ is bounded below by the constraint of unitarity, while that from the region $k_\perp^2 > Q^2$ is greater than the corresponding integral with $k_\perp^2 \to Q^2$. Adding these two bounds, we obtain

$$\left\langle k_\perp^2 \right\rangle \geq Q^2 - \frac{Q^3}{2\pi f_\pi}\sqrt{\frac{2N_c P_v(\pi)}{3}};$$

since this holds for all Q, we obtain

$$\left\langle k_\perp^2 \right\rangle_\pi \geq \frac{8\pi^2}{9}\frac{f_\pi^2}{N_c P_v} \to \frac{32\pi^2}{27}f_\pi^2 = (455\ \mathrm{MeV})^2. \tag{3.9}$$

In the final step, we have inserted the favored value $P_v(\pi) = 0.25$.

We can repeat this process for the B, or any other, meson. With the assumption that $P_v(B) = 0.5$, we obtain $\left\langle k_\perp^2 \right\rangle_B \geq (2.4 f_B)^2$. Here the intimate connection between the decay constant and the spread in momentum space is made manifest. In every case, the moment is evaluated only in the valence Fock state.

Of course, the resulting restrictions on the B meson are rather weak, since the region R in this case includes all values of x. We can correct this deficiency by using the function $B = b\big(\mathcal{M}^2_{\mathrm{max}} - \delta\mathcal{M}^2\big)$ to constrain the moment of the virtuality. For nonzero masses, the resulting analytic formulae are quite inconvenient; however, in the phenomenologically interesting region $150\ \mathrm{MeV} < f_B/\sqrt{P_v(B)} < 400\ \mathrm{MeV}$, the lower bounds lie above the linear bound

$$\left\langle \delta\mathcal{M}^2 \right\rangle_B > (33\ \mathrm{GeV})\Big(\frac{f_B}{\sqrt{P_v(B)}} - 130\ \mathrm{MeV}\Big). \tag{3.10}$$

The latter is thus a rigorous bound on the moment associated with the light-cone virtuality. For example, if $f_B = 270\sqrt{P_v(B)}$ MeV, we obtain $\langle \delta\mathcal{M}^2 \rangle > 4.8$ GeV^2.

We can repeat the analysis with the π or any other meson; for example, for the pion we obtain

$$\langle \delta\mathcal{M}^2 \rangle_\pi \geq \Big(\frac{0.31 \text{ GeV}^2}{P_v(\pi)} - m_\pi^2 \Big) \simeq 1.2 \text{ GeV}^2.$$

Implicit in the above derivations is the assumption that the real part of the tail of the wavefunction has the same sign as the decay constant. At large values of the transverse momentum, this is a good assumption, since the one-gluon exchange kernel whose contribution dominates the wavefunction at large momentum transfer [1] is real and positive.

For example, in the derivation of the lower bound on $\langle k_\perp^2 \rangle$, the value of Q used is roughly $3f_h/\sqrt{P_v} \sim 800$ MeV. While not extremely large, this momentum transfer is sufficient to make the implicit assumption a quite plausible one.

If we make the further assumption that the wave function depends only on the virtuality of the intermediate state, $\psi(x, k_\perp) = \psi(\delta\mathcal{M}^2)$ and the measure of integration over the invariant phase space is

$$\int_{m_b^2 - m_B^2} \frac{(\delta\mathcal{M}^2 + m_B^2 - m_b^2)^2 \; (\delta\mathcal{M}^2 + m_B^2 + 2m_b^2) \; \mathrm{d}\delta\mathcal{M}^2}{96\pi^2 (\delta\mathcal{M}^2 + m_B^2)^3} \quad .$$

It is then a simple problem in the calculus of variations to maximize the functional

$$\langle x^1 \rangle \;\equiv\; \frac{\int x\psi(x, k_\perp)}{\int \psi(x, k_\perp)} \;, \tag{3.11}$$

the first moment of the distribution amplitude, subject to the constraints of eq. (2) and a fixed value of f_B. The extremal function has the form

$$\psi \;\propto\; \left(\bar{x^1} - x_0\right)\,\theta(\bar{x^1} - x_0),$$

where

$$\bar{x^1}(\delta\mathcal{M}^2) \;\equiv\; \frac{1}{2}\Big(1 \,+\, \frac{3m_b^4}{(\delta\mathcal{M}^2 + m_B^2)(\delta\mathcal{M}^2 + m_B^2 + 2m_b^2)}\Big)$$

is the average value of x^1 along a curve of constant $\delta\mathcal{M}^2$ [6], and x_0 parametrizes the class of constrained optimal functions. Thus we obtain the rigorous bound for any positive function $\psi(\delta\mathcal{M}^2)$

$$\left\langle x_b^1 \right\rangle \;<\; 0.84 \qquad \text{for} \qquad f_B \;=\; 190\sqrt{P_v(B)}\ \text{MeV} \quad . \tag{3.12}$$

This should be compared with the estimate $\left\langle x_b^1 \right\rangle = 0.90$ obtained in [7], which is (barely) consistent with the estimate of f_B in the same reference, but not with the currently preferred value. Similar constraints can be derived for any choice of $f_B/\sqrt{P_v(B)}$, as shown in Fig. 3.2. Note that the assumption $\mathrm{Re}[\psi] > 0$ is crucial. If we choose the value $f_B/\sqrt{P_v(B)} = 270$ MeV, which we believe to be a fairly conservative estimate, we obtain $\left\langle x^1 \right\rangle < 0.81$ and consequently $\langle 2x - 1 \rangle < 0.61$. This is a very stringent bound, applicable to a wide class of intuitively reasonable wavefunctions (though it can be circumvented by, for example, the introduction of a widely varying complex phase into the wavefunction).

It is a simple matter to derive similar bounds on other moments of the distribution amplitude; for example, with $f_B/\sqrt{P_v(B)} = 270$ MeV we obtain

$$\left\langle (2x-1)^2 \right\rangle \;<\; 0.41\ , \qquad \left\langle (2x-1)^3 \right\rangle \;<\; 0.35\ , \qquad \text{and} \qquad \left\langle (1-x)^{-1} \right\rangle \;<\; 14.2\ .$$

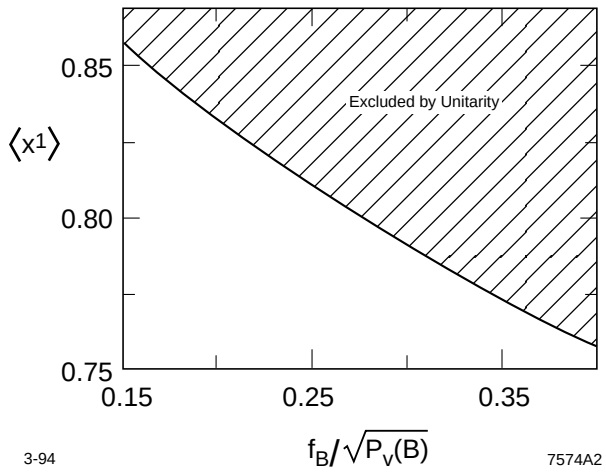

Fig. 3.2. The excluded region of $\langle x \rangle$ as a function of $f_B/\sqrt{P_v(B)}$. The assumptions underlying this derivation are described in the text.

One might expect that this method could also be used to improve our lower bound on $\langle \delta \mathcal{M}^2 \rangle$; however, it turns out that it serves only to duplicate the bound we have already derived. A little thought shows why; the wavefunction

$$\psi\big(\delta \mathcal{M}^2\big) \;\propto\; \big(\mathcal{M}^2_{\rm max} - \delta \mathcal{M}^2\big)\; \theta\big(\mathcal{M}^2_{\rm max} - \delta \mathcal{M}^2\big)$$

which realizes the bound is the same in both cases.

It must be emphasized that $\langle x^n \rangle$ represents a moment of the valence Fock state wavefunction only, rather than an expectation value, and that unitarity can provide no constraints on expectation values. However, the amplitudes for exclusive processes are determined by convolutions of wave functions, not of their squares; thus eq. (3.12) makes a strong statement about the shape of the wave function $\psi_{B \to b\bar{q}}$.

In sum, currently favored values for the meson decay constant f_B can only be reconciled with unitarity by allowing unexpectedly large values of $k_\perp$, and values of x far from unity, to make sizable contributions to the wave function.

References for Chapter 3

[1] P_v depends on the cutoff scale, in this case Q. However, in this work we find $Q \sim 1$ GeV everywhere, and neglect this dependence.

[2] S. J. Brodsky *et al.*, in *Banff 1981, Proceedings, Particles and Fields 2.*

[3] M. Neubert, SLAC–PUB–6263, and references therein; C. W. Bernard et al., Nucl. Phys. **B 30** (Proc. Suppl.), 465 (1993), and references therein. For an early look at expectations for f_B, see A. R. Zhitnitskiĭ, I. R. Zhitnitskiĭ and V. L. Chernyak, *Sov. J. Nucl. Phys.* **38**, 775 (1983) [*Yad. Fiz.* **38,** 1277 (1983)], and M. A. Shifman and A. Voloshin, *Sov. J. Nucl. Phys.* **45**, 242 (1987) [*Yad. Fiz.* **45,** 463 (1987)].

[4] Since this report was composed, estimates of $f_B \sim 190$ MeV have come to be favored by lattice computations. See, *e.g.*, C. W. Bernard *et al.*, UW/PT-93-06 (unpublished).

[5] NRQCD collaboration (G. P. Lepage, *et al.*), in *LATTICE 93.*

[6] This paper was originally circulated as SLAC-PUB-6383 (unpublished). Errors in that paper's treatment of the maximization of moments have been corrected in this version.

[7] M. A. Shifman and A. Voloshin, in ref. [3].

4. SUDAKOV EFFECTS AND PROTON-ANTIPROTON ANNIHILATION

In this chapter, we calculate the differential cross section for the process $\gamma\gamma \to p\bar{p}$, taking into account Sudakov suppression [1-2] in the manner given by Sterman, Botts and Li [3-4]. This process has previously been considered by Millers and Gunion [5] and by Farrar *et al.* [6]; our inclusion of the effects of Sudakov suppression allows us to refine their calculation and to more quantitatively examine its dependence on soft physics.

The chapter is organized as follows: Section 4.1 outlines the leading-order calculation. Section 4.2 discusses the use of proton distribution amplitudes. Section 4.3 is devoted to the perturbative computation of the hard-scattering amplitude. Section 4.4 discusses the origin of the Sudakov corrections, and summarizes the method of [3] for their calculation. Section 4.5 outlines our computational method; in Sec. 4.6, we display and comment on results for four candidate distribution amplitudes [7-10], and describe the sources of theoretical uncertainty. Section 4.7 summarizes the computation of the proton form factor, and presents results for the same distribution amplitudes. Finally, Sec. 4.8 contains our conclusions and evaluates future prospects for measuring the cross sections, and the possibility of gaining information about the distribution amplitude.

4.1. The Tree-Level Process

To leading twist, the amplitude for a hadronic process is given by [11]:

$$\mathcal{M}_{hh'}^{\lambda_1\lambda_2} = \sum_{m,(d)} \int [\mathrm{d}x]\ [\mathrm{d}y]\ [\mathrm{d}\vec{b}]\ [\mathrm{d}\vec{b}'] \times\ \phi_m(x,b,\mu)\ T_H^{m,(d)}(x,\tilde{h},b;y,\tilde{h}',b';Q,\mu)\ \phi_m(y,b',\mu)\ , \tag{4.1}$$

where

$[\mathrm{d}x] \equiv \mathrm{d}x_1\,\mathrm{d}x_2\,\mathrm{d}x_3\ \delta(1-\sum_i x_i)$, and $[\mathrm{d}\vec{b}] \equiv \mathrm{d}^2b_1\,\mathrm{d}^2b_2\,\mathrm{d}^2b_3\ \delta^2(\sum_i b_i)$;

m and d are the indices of the wavefunctions and the hard-scattering Feynman diagrams, respectively;

$\lambda_{1,2}$ are the photon helicities;

$\tilde{h}$ and $\tilde{h}'$ are the parton helicities within a hadron of helicity h or h' ;

$Q = \sqrt{|q^2|}$ is the hard process 4-momentum transfer; and

$\phi_m(x,b,\mu)$ is the distribution amplitude for partons with momentum fraction x and impact parameter b within the m^{th} wavefunction at 'separation scale' μ (the scale above which processes are deemed 'hard').

4.2. Distribution Amplitudes

At leading twist, only the 3-quark "valence" Fock state contributes to the scattering amplitude. The most general form of a distribution amplitude (neglecting transverse momentum) for this state is

$$\begin{aligned} \left|p_\uparrow\right\rangle = \frac{f_N}{8\sqrt{6}} \int [\mathrm{d}x]\ \phi_1(x) \left|u_\uparrow(x_1)\ u_\downarrow(x_2)\ d_\uparrow(x_3)\right\rangle \\ + \phi_2(x) \left|u_\uparrow(x_1)\ d_\downarrow(x_2)\ u_\uparrow(x_3)\right\rangle \\ + \phi_3(x) \left|d_\uparrow(x_1)\ u_\downarrow(x_2)\ u_\uparrow(x_3)\right\rangle , \end{aligned} \tag{4.2}$$

where f_N is a constant with units of GeV^2, determined by the value of the transverse wavefunction at the origin.

Note that x_2 is always attached to the negative-helicity quark. The ϕ_m are not independent; rather, we have [7]

$$\phi_3(x_1, x_2, x_3) = \phi_1(x_3, x_2, x_1) \quad \text{and} \quad \phi_2(x) = -\phi_1(x) - \phi_3(x) \ .$$

Although the amplitudes ϕ_m are known exactly [11] only in the limit $\mu \to \infty$, several estimates [7-10] based on QCD sum rules have been advanced as models for ϕ at $\mu^2 \simeq$ 1–2 GeV^2; they take the form

$$\phi_m(x_1, x_2, x_3) = 120\ x_1\, x_2\, x_3\ P_m(x_1, x_2, x_3) \ ,$$

where $P_m(x)$ is a quadratic polynomial. In Table 4.1, we show the decomposition of the model polynomials $P_1(x)$ into Appell polynomials, the eigenfunctions of the distribution amplitude evolution equation [11].

Evolution eigensolutions			coefficients in			
n	b_n	$\tilde{\phi}_n$	CZ[7]	COZ[8]	KS[9]	GS[10]
1	-1	1	1.0	1.0	1.0	1.0
2	2/3	$x_1 - x_3$	4.309	3.675	3.255	4.105
3	1	$3x_2 - 1$	-1.923	-1.484	-1.295	-2.060
4	5/3	$3(x_1 - x_3)^2 + x_2(5x_2 - 3)$	2.248	2.898	3.969	-4.720
5	7/3	$(x_1 - x_3)\,(4x_2 - 1)$	-1.156	-2.205	0.315	1.667
6	5/2	$14(x_2^2 + x_1 x_3) - 7x_2 - 1$	0.019	1.026	1.026	9.300

Table 4.1. Model distribution amplitude coefficients.

To minimize the effect of higher-order corrections, it is desirable to set the scale Q so as to avoid large logarithmic contributions. In addition to determining q^2 for each exchanged gluon, we must take into account the fact that the distribution amplitudes depend somewhat on the momentum transfer Q^2. For the eigenfunctions shown, their evolution equation becomes

$$\tilde{\phi}_n(x;Q) = \tilde{\phi}_n(x;\mu) \left(\frac{\ln \frac{Q^2}{\Lambda^2}}{\ln \frac{\mu^2}{\Lambda^2}} \right)^{-\gamma_n},$$

with $\gamma_n = (2C_B\, b_n + 3C_F/2)/\beta$ for the b_n given in Table 1; here $N_C = 3$ implies $C_B = 2/3$, $C_F = 4/3$, and $\beta = 11 - (2n_f/3)$ [11]. Botts and Sterman have shown [3] that we should choose the momentum transfer scale $Q = \omega \equiv \max_j\{|\tilde{b}_j|^{-1}\}$, where $\tilde{b}_j$ are the transverse separations of the quarks in position space. Thus we can easily extract the distribution amplitude analytically for a given b. Note that this form for the running of the distribution amplitude takes into account the running of f_N and the quark anomalous dimension [11].

4.3. Hard-Scattering Amplitude

Following [12], we classify the Feynman diagrams according to the topology of the gluon lines, as shown in Fig. 4.1.

Class (g) contains 42 diagrams, from the distinct attachments of the photon lines, but the color factor is zero; classes (a)–(f) each contain 56 diagrams, and the color factor is 4/9. Thus there are 336 diagrams to be evaluated, 192 of which are nonzero.

Fermion denominators in T_H are either linear in x and y or of the form $\bar{x}_i y_j$ or $x_i \bar{y}_j$ (throughout this work, we use $\bar{x}_i \equiv 1 - x_i$), but never proportional to $x_i y_j$; thus soft propagators are less of a problem, and we neglect fermion transverse momenta in $T_H^{(d)}$ [4]. Since T_H now depends only on sums of the form $k_{\perp,i} + k'_{\perp,i}$, we obtain a factor in T_H of $\delta^4(\vec{b} + \vec{b}')$, reflecting the heuristic notion that the $p\bar{p}$ pair is created at a point (the sign in the delta function is conventional; it arises from the fact that the p and $\bar{p}$ are back-to-back).

It proves convenient to use

$$T_H^{i,(d)} = 2\delta^4(\vec{b} + \vec{b}')\; C^{(d)}\, g^4\, e_m^{(d)}\, e^2\, \tilde{G}^{(d)}\, \tilde{T}^{(d)}\ , \tag{4.3}$$

where e and g are the QED and QCD charges, and $C^{(d)}$ and $e_m^{(d)}$ are the color factor and the product of the charges of the struck quarks, respectively; then $\tilde{G}^{(d)}$ is the product of the two gluon propagators, and $\tilde{T}^{(d)}$ is a (dimensionless) kinematic quantity containing the numerator factors and Dirac propagators. To calculate $\tilde{T}^{(d)}$, we found it convenient to parametrize the photon polarization vectors by [12]

$$\epsilon_1 = \alpha\epsilon_1(\uparrow) + \beta\epsilon_1(\downarrow)\ , \quad \text{and} \quad \epsilon_2 = \gamma\epsilon_2(\uparrow) + \delta\epsilon_2(\downarrow)\ ,$$

allowing us to calculate the four photon helicity amplitudes all in one piece.

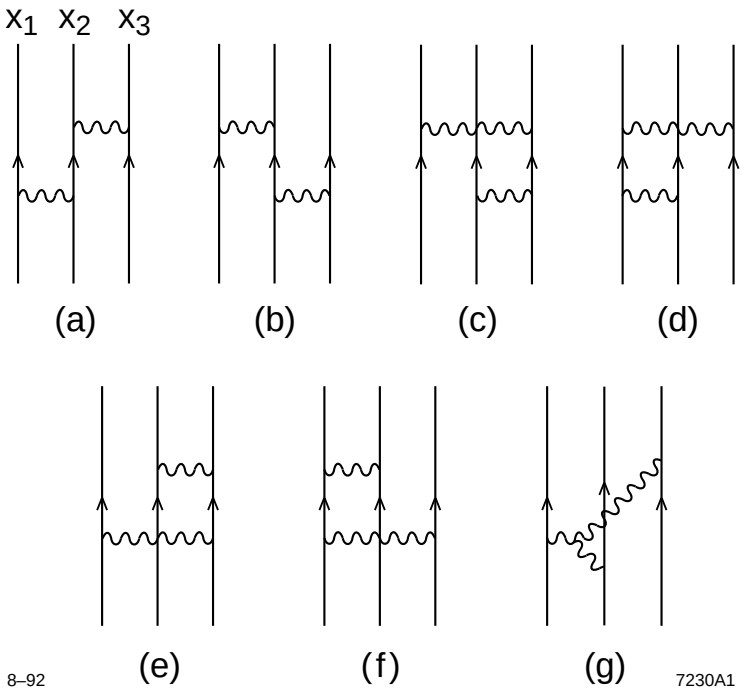

Fig. 4.1. Classes of hard-scattering Feynman diagrams. Arrows indicate fermion flow.

To leading twist, we may neglect quark masses so that the u and d quark differ only through their charge; then $\tilde{T}^{(d)}$ is flavor-independent, and the results for classes (b), (d), and (f) can be obtained from those of (a), (c), and (e), respectively, by the operation

$$\mathcal{E} : x_1 \leftrightarrow x_3 \ , \qquad y_1 \leftrightarrow y_3 \ , \qquad e_1 \leftrightarrow e_3 \ .$$

There is also a charge-conjugation symmetry

$$\mathcal{C} : x_i \leftrightarrow y_i \ , \qquad \alpha \leftrightarrow \beta \ , \qquad \gamma \leftrightarrow \delta \ , \qquad \theta \to \theta - \pi \ ,$$

which yields $T_H^{(\mathcal{C}d)} = \mathcal{C}(T_H^{(d)})$ for a diagram d; and $t \leftrightarrow u$ crossing symmetry

$$\mathcal{X} : \alpha \leftrightarrow \gamma \ , \qquad \beta \leftrightarrow \delta \ , \qquad \theta \to \theta - \pi$$

gives $T_H^{(\mathcal{X}d)} = \mathcal{X}(T_H^{(d)})$.

We calculated all diagrams in (a) and (c), and used the symmetries $\mathcal{X}$ and [in class (a)] $\mathcal{C} \circ \mathcal{E}$ to check the results. Our kinematic conventions are described in Appendix 4.A, and the values of $\tilde{T}^{(d)}$ are tabulated in Appendix 4.B.

We then derived the 'subamplitudes' $\tilde{T}$ for classes (b), (d), (e), and (f) by application of

$$\mathcal{E} \ : \ \text{(a)} \ \leftrightarrow \ \text{(b)} \ , \quad \text{(c)} \ \leftrightarrow \ \text{(d)} \ , \quad \text{(e)} \ \leftrightarrow \ \text{(f)} \ ,$$

and

$$\mathcal{C} \ : \ \text{(a)} \ \leftrightarrow \ \text{(b)} \ , \quad \text{(c)} \ \leftrightarrow \ \text{(e)} \ , \quad \text{(d)} \ \leftrightarrow \ \text{(f)} \ .$$

Since we neglect the quark mass, helicity is conserved along each fermion line, and there are only eight nonzero helicity amplitudes. Because of the symmetry of

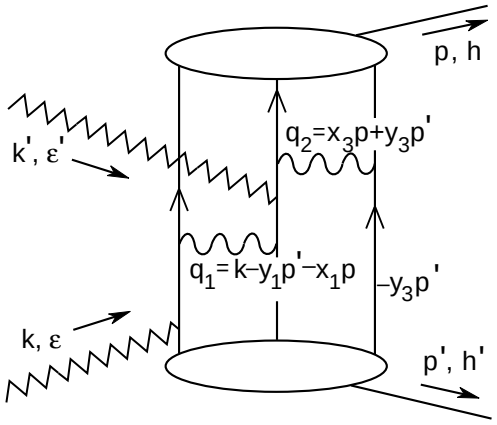

Fig. 4.2. Diagram A24. Here $|q_{\perp,1}| = |k_\perp| = |\vec{k}| \sin\theta_{\rm cm}$, while $q_{\perp,2} = 0$.

the theory under $\mathcal{P}$ and $\mathcal{C}$, only two of these amplitudes are independent. We will display results for $\gamma(\uparrow)\gamma(\uparrow) \to p_+\bar{p}_+$ and $\gamma(\uparrow)\gamma(\downarrow) \to p_+\bar{p}_+$.

The next problem which we face is the computation of $\tilde{G}$, the gluon propagator of eq. (3). To avoid difficulties in convergence and retain numerical tractability, we Fourier transform [4,13] only the unrenormalized propagator from $(q_l, q_\perp)$ space to $(q_l, b_\perp)$ space. In momentum space, the gluon denominator has the generic form

$$\frac{1}{q_l^2 - (q_\perp + l_{\perp,i} + l'_{\perp,i})^2} \ ,$$

where $q_\perp$ is the portion of the hard-scattering momentum transverse to the proton momentum (see Fig. 4.2), and $l_{\perp,i},\ l'_{\perp,i}$ are transverse momenta within the wavefunctions. For spacelike q_l, we take the Fourier transform to the hybrid $(q_l, b_\perp)$ space and average over possible orientations of b to obtain

$$D_{\text{space}} = -K_0\left(|b_i - b_j|\sqrt{-k^2}\ \right)\ J_0\left(|b_i - b_j||q_\perp|\right) \ ,$$

where K_0 is a modified Bessel function and i, j are the indices of the quark lines connected to the gluon [14-15].

To find the corresponding timelike propagator, we form the gluon momentum as a sum of on-shell outgoing parton momenta to obtain $(p_1+p_2)^2 = -(p_1-p_2)^2$; thus the timelike denominator has the same form as the spacelike denominator. Since $q_\perp \equiv 0$ for gluons of this type, we have the final form [16]

$$D_{\text{time}}(q_l, b) = K_0\left(|b|\sqrt{|q_l^2|}\ \right) \ . \tag{4.4}$$

For the running coupling constant, we use $\alpha_s(\max\{|q_l^2|, 1/|b_\perp|^2\})$ [4]; we shall see that Sudakov suppression confines the wavefunction to $|b| < \Lambda^{-1}$, so that no

further cutoff is needed. The physical justification for this choice is that very soft gluon exchange is suppressed in color singlets, so that for b small the coupling does not become strong. The region in which $|b| \to \Lambda$ is strongly Sudakov suppressed, so that the divergence of the coupling there does not greatly disturb our results.

4.4. Sudakov Effects

A color singlet with zero transverse size is effectively colorless, and initial- or final-state radiation of gluons does not occur. However, the transverse size of a physical hadron cannot be neglected; for example, if in a pion the quark and antiquark are separated by a distance b, then gluons with transverse momentum down to $1/b$ will distinguish the pair. The sum of one-gluon corrections to the baryon valence wavefunction is proportional to

$$\frac{C_F}{\pi} \int^Q \frac{\mathrm{d}^2 q_\perp}{q_\perp^2} \left[3 - \sum_{i<j} \exp\left\{ -i(b_i - b_j) \cdot q_\perp \right\} \right] \frac{\alpha_s(q_\perp^2)}{2\pi} \int_{q_\perp}^Q \frac{\mathrm{d}q_+}{q_+} \ .$$

The probability of no radiation is obtained by exponentiating this term [1-2], leading to the Sudakov suppression of exclusive processes for large b. In hadron-hadron scattering, Botts and Sterman have shown [3] that the effects of this suppression can, to leading-logarithmic order, be absorbed into the wavefunctions by the inclusion of a factor

$$\exp\left\{ -\sum_i \left[s(x_i Q, \tilde{b}_i) - \int_{1/\tilde{b}_i}^{\mu} \frac{\mathrm{d}\bar{\mu}}{\bar{\mu}} \, \gamma_q(\bar{\mu}) \right] \right\}. \tag{4.5}$$

Here $\tilde{b}_1 \equiv b_2 - b_3$, etc.; μ is the separation scale, γ_q the quark anomalous dimension, and

$$\begin{aligned} s(\xi Q, b) \;&= \frac{A^{(1)}}{2\beta_1} \;\; \hat{q} \ln\left(\frac{\hat{q}}{\hat{b}}\right) + \frac{A^{(2)}}{4\beta_1^2} \;\left(\frac{\hat{q}}{\hat{b}} - 1\right) - \frac{A^{(1)}}{2\beta_1} \;\; (\hat{q} - \hat{b}) \\ &- \frac{A^{(1)}\beta_2}{16\beta_1^3} \;\; \hat{q}\left(\frac{\ln(2\hat{b})+1}{\hat{b}} - \frac{\ln(2\hat{q})+1}{\hat{q}}\right) \\ &- \left[\frac{A^{(2)}}{4\beta_1^2} - \frac{A^{(1)}}{4\beta_1}\,(2\gamma - 1 - \ln 2)\right] \ln\left(\frac{\hat{q}}{\hat{b}}\right) \\ &- \frac{A^{(1)}\beta_2}{32\beta_1^3} \;\; \left[\ln^2(2\hat{q}) - \ln^2(2\hat{b})\right] \;, \end{aligned}$$

where

$$\hat{q} \equiv \ln\left(\tfrac{\xi Q}{\Lambda\sqrt{2}}\right) \;, \qquad \hat{b} \equiv \ln\left(\tfrac{b^{-1}}{\Lambda}\right) \;,$$

$$\beta_1 = \tfrac{33-2n_f}{12} \;, \qquad \beta_2 = \tfrac{153-19n_f}{24} \;,$$

$$A^{(1)} = \tfrac{4}{3} \;, \qquad A^{(2)} = \tfrac{67}{9} - \tfrac{\pi^2}{3} - \tfrac{10}{27}\, n_f + \tfrac{8}{3}\, \beta_1(\gamma - \ln 2) \;,$$

and Euler's constant $\gamma \simeq 0.577$. (Reference [3] defines $\hat{b} = +\log(b\Lambda)$; our notation is otherwise identical.)

It is the result (4.5) which we use to model the effects of the Sudakov suppression. As in [3-4,13], we impose the constraint that $s(\xi Q, b) > 0$, so that the 'suppression' does not lead directly to enhancement. Also, for very small b the function s becomes large; in this case, we set $s = 0$ since these contributions to s are from hard gluons (with momentum $\gtrsim b^{-1}$) and form a skewed subset of the higher-order hard-scattering contributions to T_H.

The advantage of this method is that it requires no unphysical parameters, such as a gluon mass, to retain finiteness. However, the method rests on an improved factorization obtained by retaining information about the transverse structure of the proton; thus, to implement it, we must be able to model that structure (at least in the valence state).

We can write

$$\phi_m(x, b, \mu) = \phi_m(x)\ \psi_x(b)\ ,$$

so that $\phi_m(x)$ is the familiar longitudinal distribution amplitude and $\psi_x(b)$ is an x-dependent transverse wavefunction. The definition of $\phi_m(x)$ requires the normalization [17]

$$\psi_x(\vec{b} = 0) = 1\ . \tag{4.6}$$

The form of the noninteracting light-cone Hamiltonian [11]

$$\mathcal{H}^0_{\rm LC} \equiv P^- P^+ - \vec{P}^2_\perp = \sum_i \frac{l^2_{\perp,i}}{x_i}$$

leads us to consider a transverse wavefunction proportional to [22]

$$\exp\left\{ -\sum_i\ \frac{l^2_{\perp,i}}{a^2 x_i} \right\}\ .$$

We must determine the numerical value of a in a manner consistent with its use here. We use the virial theorem. A transverse rescaling $b_\perp \to \lambda b_\perp$ affects the

'potential' (gluonic) energy of the proton by an amount parametrized by $n_{_U} \equiv (\lambda/\langle U\rangle)\,(\mathrm{d}\langle U\rangle/\mathrm{d}\lambda)$. Thus by the virial theorem, we must have

$$a^2 = \langle H^0_{\rm LC}\rangle = \frac{n_{_U}}{2+n_{_U}}\; m_p^2 \; .$$

We Fourier transform in $k_\perp$ space to obtain

$$\begin{aligned}\psi(b) = \;& \exp\left\{ -\frac{n_{_U} m_p^2}{4(2+n_{_U})} \right. \\ & \left. \times \left(x_1x_2(b_{\perp,1}-b_{\perp,2})^2 + x_2x_3(b_{\perp,2}-b_{\perp,3})^2 + x_3x_1(b_{\perp,3}-b_{\perp,1})^2 \right) \right\} \\ = \;& \exp\left\{ -\frac{n_{_U} m_p^2}{4(2+n_{_U})} \quad (x_1\,x_2\,\tilde{b}_3^2 + x_2\,x_3\,\tilde{b}_1^2 + x_3\,x_1\,\tilde{b}_2^2) \right\} \; .\end{aligned} \tag{4.7}$$

Note that $\sum_i \tilde{b}_i = 0$ and $[\mathrm{d}\tilde{b}] = 9\,[\mathrm{d}b]$.

Previous calculations [4,13] have set $n_{_U} = 0$, neglecting the b-dependence of the proton wavefunction. We take $n_{_U} = 3$ [18] for the results presented here, and use $n_{_U} \to 0$ to examine the sensitivity of our results. At $\sqrt{s} = 5$ GeV, this substitution increases the overall normalization by 14%, and introduces variations of less than 10% for the GS model [19] and 3% for the others.

At first glance, inclusion of this transverse wavefunction appears to aggravate the divergence at small x, since the available volume of $b_\perp$-space increases as any $x_i \to 0$. However, the Sudakov suppression contains the wavefunctions within the region where $|\tilde{b}_j| < \Lambda^{-1}$.

4.5. Calculations

Combining the results of (4.2–4.7) with (4.1), we obtain

$$\begin{aligned}\mathcal{M}_{hh'}^{\lambda_1\lambda_2} = \sum_m \int [\mathrm{d}x]\,\phi_m(x;\mu) \int [\mathrm{d}y]\,\phi_m(y;\mu) \int \frac{[\mathrm{d}\tilde{b}]}{9}\,\psi_x(\tilde{b})\,\psi_y(\tilde{b}) \\ \times \exp\left\{ -\sum_j \Big[s(x_j Q, \tilde{b}_j) - \int_{\tilde{b}_j^{-1}}^{\mu} \frac{\mathrm{d}\bar{\mu}}{\bar{\mu}}\,\gamma_q(\bar{\mu}) \Big] \right\} \\ \times \left[\sum_{(d)} 128\pi^3\,\alpha_{\mathrm{QED}}\,e_m^{(d)}\,C^{(d)}\,\alpha_s(q_1;\tilde{b})\,\alpha_s(q_2;\tilde{b})\,\tilde{G}^{(d)}\,\tilde{T}^{(d)}(\lambda_1,\lambda_2;h,h') \right] \\ \times \exp\left\{ -\sum_j \Big[s(y_j Q, \tilde{b}_j) - \int_{\tilde{b}_j^{-1}}^{\mu} \frac{\mathrm{d}\bar{\mu}}{\bar{\mu}}\,\gamma_q(\bar{\mu}) \Big] \right\}.\end{aligned} \tag{4.8}$$

To obtain definite predictions, we must make some simplifying assumptions. First, we replace the running coupling constant $\alpha_s(\mu^2)$ with the $n_f = 3$ form

$$\alpha_s(\mu^2) \;\equiv\; \frac{12\pi}{(33-2n_f)\ln\,(\mu^2/\Lambda^2)} \;\rightarrow\; \frac{4\pi}{9\ln\,(\mu^2/\Lambda^2)}\;;$$

we take $\Lambda \equiv \Lambda^{(3)}_{\overline{\mathrm{MS}}} = 200$ MeV. The range of momentum transfers which interest us runs from a few hundred MeV (b^{-1} where b is a typical quark impact parameter) to several GeV ($\sqrt{x_i y_i s}$, where x_i and y_i are typical parton momentum fractions and $\sqrt{s}$ ranges up to 7-8 GeV), which is almost exactly the region in which this approximation is viable. Certainly the resulting errors are minimal.

This form for the coupling constant allows us to rewrite (4.8) as

$$\mathcal{M}_{hh'}^{\lambda_1\lambda_2} = \frac{2^{12}5^2\pi^5}{3^7}\ \alpha_{QED}\ f_N^2\Big(\ln\frac{\mu^2}{\Lambda^2}\Big)^{4/3}$$

$$\times\ \sum_{m=1}^{3}\ \int\ [\mathrm{d}x]\,[\mathrm{d}y]\ x_1x_2x_3\ P_m(x)\ y_1y_2y_3\ P_m(y)$$

$$\times \int [\mathrm{d}\tilde{b}]\left[\sum_{(d)}\ \frac{e_m^{(d)}\ D(q_1,\tilde{b}_j)\,D(q_2,\tilde{b}_k)}{\ln\Big(\max\Big\{\frac{q_1^2}{\Lambda^2},\frac{1}{\tilde{b}_j^2\Lambda^2}\Big\}\Big)\ln\Big(\max\Big\{\frac{q_2^2}{\Lambda^2},\frac{1}{\tilde{b}_k^2\Lambda^2}\Big\}\Big)}\ \tilde{T}^{(d)}\,(\lambda_1,\lambda_2;h,h')\right]$$

$$\times\ \prod_{i=1}^{3}\left[\ \frac{\exp\Big\{-s(x_iQ,\tilde{b}_i)-s(y_iQ,\tilde{b}_i)-\frac{3m_p^2}{20}\ (\frac{x_1x_2x_3}{x_i}+\frac{y_1y_2y_3}{y_i})\ \tilde{b}_i^2\Big\}}{\big[-\ln(\tilde{b}_i^2\Lambda^2)\,\big]^{4/9}}\ \right],$$

where

$P_m(x)$ is a sum of Appell polynomials with weights determined by the input distribution amplitude and by $\omega \equiv \max_j\{|\tilde{b}_j|^{-1}\}$;

$e_m^{(d)}$ is the product of QED charges;

$D(q,\tilde{b})$ is the gluon propagator;

q_1, q_2 are the gluon longitudinal momenta;

$\tilde{b}_j$, $\tilde{b}_k$ are the transverse separations of the corresponding quark lines;

$\tilde{T}^{(d)}$ is the hard-scattering subamplitude of diagram d;

$s(xQ,b)$ is the Sudakov suppression of [3]; and

$3m_p^2/20$ is the inverse mean impact parameter for the wavefunction in our *ansatz*.

Many of the individual subamplitudes $\tilde{T}^{(d)}$ diverge as x_i^{-1}, and the gluon propagators diverge as $\ln(x_i)$. However, the distribution amplitude and transverse wavefunction contain factors of x_i, so that the integral remains convergent. To increase the numerical stability of integration, we use the change of variables

$$x_1 \;=\; \xi^2 \;, \qquad\qquad x_2 \;=\; \bar{x}_1 \;\frac{1+\sin\left[\pi(\eta-1/2)\right]}{2}$$

$$\Rightarrow \quad \int [\mathrm{d}x] = \int_0^1 \mathrm{d}\xi \int_0^1 \mathrm{d}\eta \;\; 2\pi\sqrt{x_1 x_2 x_3} \;,$$

and similarly for $[\mathrm{d}y]$.

We integrated the resulting form numerically, obtaining the results shown in Figs. 4.3–4.7; in all cases, the statistical errors of the numerical integration were less than 4%, small enough to make no discernible contribution to the overall theoretical uncertainties.

4.6. Results and Comments

In this chapter, we have considered three effects which lead to refinement of the results of refs. [5–6]: the Sudakov suppression itself; the consideration of the transverse wavefunction; and the running of the distribution amplitude.

The full amplitudes are shown in Fig. 4.3 for same-helicity photons and in Fig. 4.4 for opposite-helicity, with $s = 25$ GeV^2 in both cases. The same-helicity amplitude is odd in $\cos\theta_{\mathrm{cm}}$ due to crossing symmetry.

The effects of replacing the Sudakov correction with the cutoff $\alpha_s \leq 1$ are shown in Fig. 4.5. It is notable that for some values of θ_{cm}, the "suppression" actually leads to an enhancement in $\gamma_\uparrow\gamma_\downarrow \to p\bar{p}$.

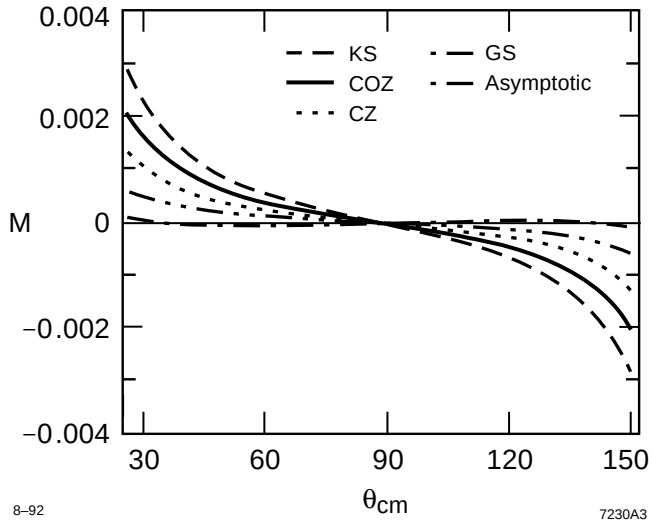

Fig. 4.3. Amplitudes for $\gamma_\uparrow\gamma_\uparrow \to p\bar{p}$ (with $s = 25$ GeV^2).

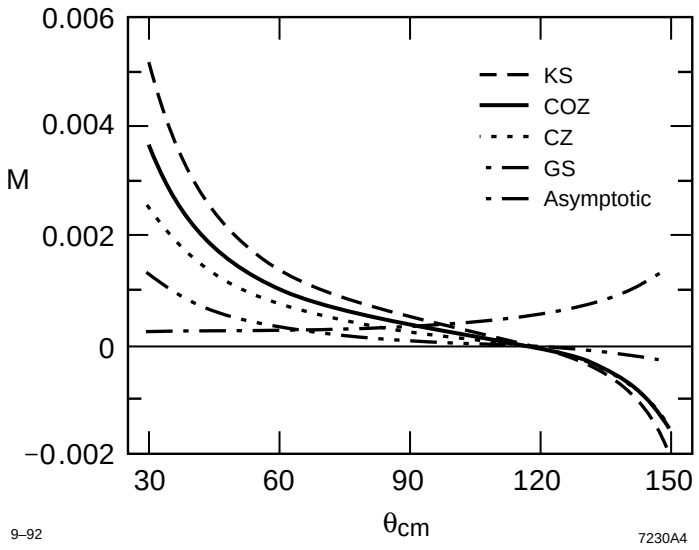

Fig. 4.4. Amplitudes for $\gamma_\downarrow\gamma_\uparrow \to p\bar{p}$.

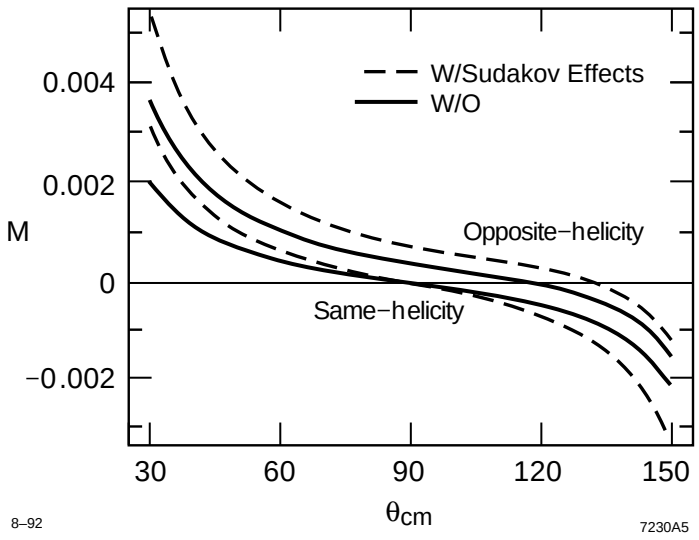

Fig. 4.5. Effects of Sudakov suppression on $\mathcal{M}(\gamma\gamma \to p\bar{p})$, with COZ wavefunction.

Scaling of amplitudes is exhibited in Fig. 4.6(a) for same-helicity photons (remember that the amplitude is odd in $\cos\theta$) and in Fig. 4.6(b) for opposite-helicity. Both adhere closely to the dimensional-counting expectation $\sigma \propto s^{-4}$ when $s \gtrsim (5\ \mathrm{GeV})^2$; this is a sign that our method is trustworthy at these energies.

Figure 4.7 presents our predictions for the timelike Compton cross section. The size is quite sensitive to the choice of distribution amplitude. Recall that the cross section is proportional to f_N^4; f_N has been determined only approximately [7] ($f_N = 5.1 \pm 0.3 \times 10^{-3}\ \mathrm{GeV}^2$). This uncertainty, combined with inevitable experimental normalization uncertainties, means that the total cross section alone is not a good test of the validity of a distribution. A more valid test, the shape of the cross section, is nearly the same for the three main distribution amplitudes we consider.

Note the piece of the cross section shown for the asymptotic wavefunction, which resembles none of the candidates in this energy regime.

4.7. The Proton Timelike Form Factor

The methods discussed above can also be used to derive the timelike proton form factor

$$F_1^p(q^2 > 0) \equiv \frac{\mathcal{M}(e^+e^- \to p\bar{p})}{\mathcal{M}(e^+e^- \to \mu^+\mu^-)} .$$

In fact, the calculation of the form factor (neglecting F_2) offers several simplifications:

- the number of hard-scattering Feynman diagrams is greatly reduced (to 42, 28 of which vanish).
- all internal gluon momenta are timelike and purely longitudinal.

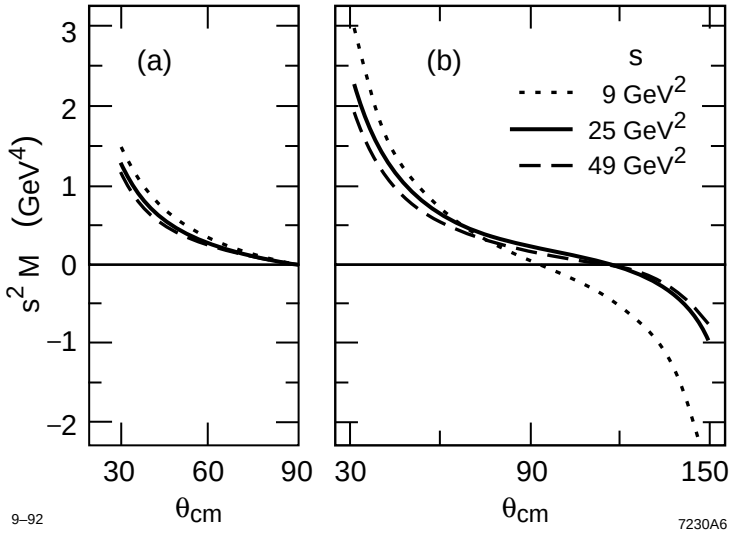

Fig. 4.6. Violation of scaling in (a) $\gamma_\uparrow\gamma_\uparrow \to p\bar{p}$; (b) $\gamma_\downarrow\gamma_\uparrow \to p\bar{p}$, with COZ wavefunction.

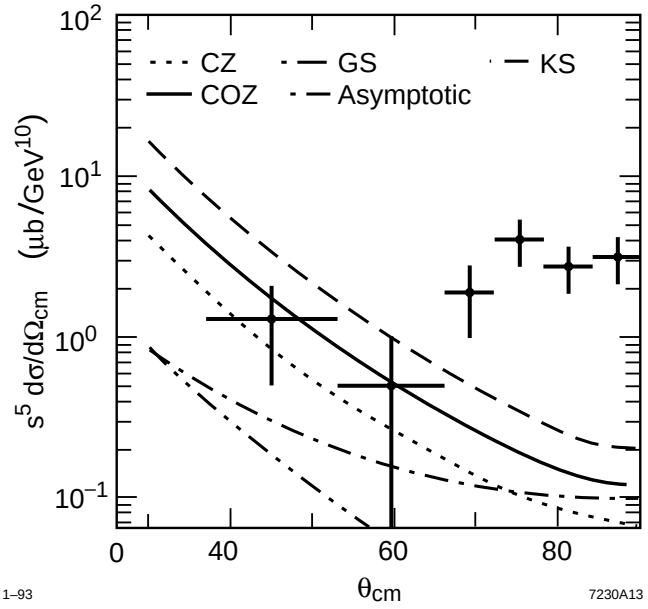

Fig. 4.7. Normalized unpolarized differential cross section for $\gamma\gamma \to p\bar{p}$ (calculated at $s = 25\text{GeV}^2$). Data are from the JADE Collaboration, *Phys. Lett.* **174B**, 350(1986).

- there is no nontrivial angular or spin dependence.

The highest-energy currently available measurements of this form factor are those of FNAL E760 [20]. Figure 4.8 shows our predictions for the form factor and the data of [20] as a function of q^2. Again, the dimensional-counting rules are very accurate. Further experiments at FNAL E760 hopefully will extend the measurement of F_1^p to higher s.

Figure 4.9 shows the dependence of the normalized form factor on a cutoff $\tilde{b} < b_{\max}$. Note the upward kink at $b_{\max} \simeq 0.9$; in this region, the one-loop running coupling α_s begins to grow large for small q_l, but the Sudakov suppression is not yet forceful. The interplay between factors contained in $\mathcal{M}$ at given b is illustrated in Fig. 4.10, in which we have chosen for definiteness $q_1^2 = q_2^2 = 35\Lambda^2$, a typical gluonic momentum for $\sqrt{s} \simeq 5$ GeV. At small b, the logarithmic divergence of $K_0(bQ)$ is cancelled by the lack of phase space; as $b \to \Lambda^{-1}$, the divergence of the coupling constant is overwhelmed by the Sudakov suppression. The dominant region in our example is around $b_{\max} \sim 0.6\Lambda^{-1}$, while the threatening 'kink' region is just above $b_{\max} = 0.9\Lambda^{-1}$. In the high-energy limit, this kink will entirely disappear as the Sudakov suppression begins to force $b_{\max} \lesssim Q^{-1}$.

The size of the 'kink contribution' is a measure of the unreliability of our results; it is about 30% at $\sqrt{s} = 3$ GeV, but decreases to 10-15% for $\sqrt{s} = 5$ GeV. This is comparable to the difference in the predictions for the COZ and CZ or KS wavefunctions; thus measurement of the form factor alone is not a powerful test of the proton distribution amplitude.

The neutron form factor F_1^n and the amplitude for $\gamma\gamma \to n\bar{n}$ can be calculated in identical manner. It is unlikely that these measurements can be extended to such high energies, but proposed experiments at Frascati [21] may measure the cross

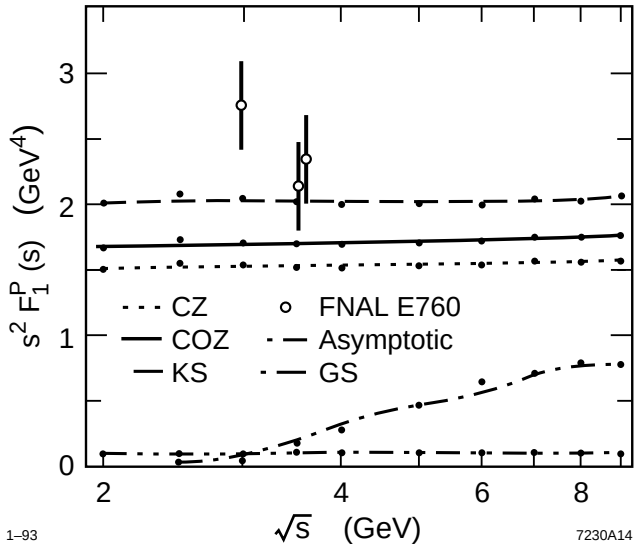

Fig. 4.8. Normalized proton timelike form factor $q^4 F_1^p(q^2)$. Data are from Ref. [20].

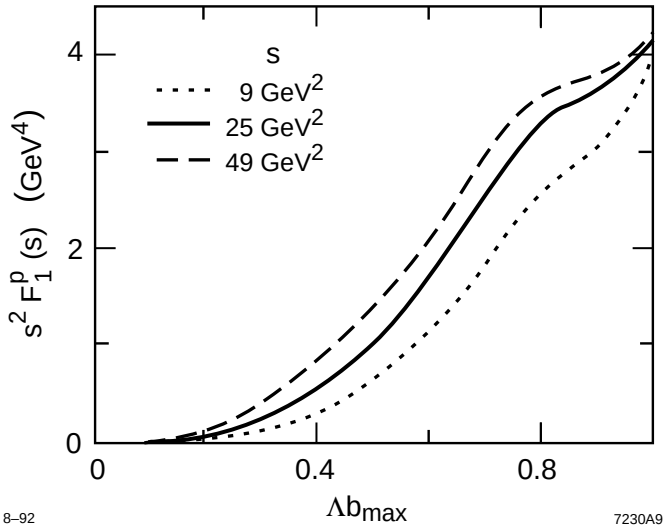

Fig. 4.9. Accumulation of $s^2 F_1^p$ as $b_{\max} \equiv \max_i\{\tilde{b}_i\}$ increases, with COZ wavefunction.

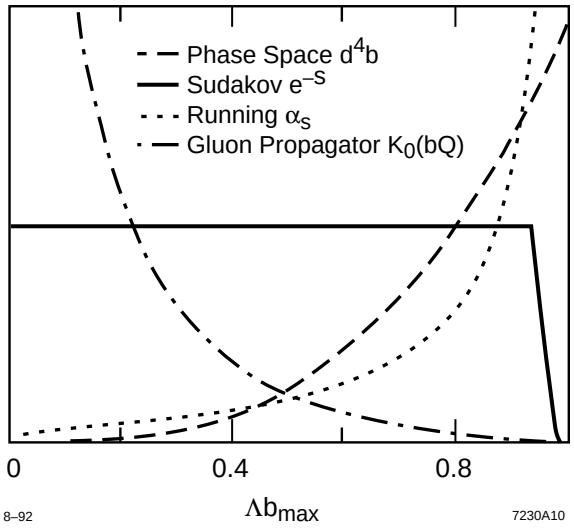

Fig. 4.10. Factors contributing to $\mathrm{d}\mathcal{M}/\mathrm{d}b_{\max}$.

Model	CZ [7]	COZ [8]	KS [9]	GS [10]	asymptotic
F_1^n/F_1^p	0.237	0.240	0.218	0.042	0.253
$\bar{R}_{e^+e^-/\gamma\gamma}$	0.180	0.113	0.081	0.052	0.005

Table 4.2. Model distribution results for $\bar{R}_{e^+e^-/\gamma\gamma}$ and F_1^n/F_1^p.

section $e^+e^- \to n\bar{n}$ at $\sqrt{s} \gtrsim 3$ GeV. Thus we present here our predictions for the ratios F_1^n/F_1^p (see Table 2) and $\sigma(\gamma\gamma \to n\bar{n})/\sigma(\gamma\gamma \to p\bar{p})$ (Fig. 4.11).

Perhaps the most interesting quantity, due to its freedom from theoretical and experimental normalization uncertainties, is the ratio

$$R_{e^+e^-/\gamma\gamma} \equiv \frac{\mathrm{d}\sigma/\mathrm{d}\Omega\,(p\bar{p} \to e^+e^-)}{\mathrm{d}\sigma/\mathrm{d}\Omega\,(p\bar{p} \to \gamma\gamma)} \ .$$

Figure 4.12 shows our predictions for this quantity. This ratio is much smaller for all of the candidate distributions than for the asymptotic, reflecting the strong suppression of the form factor using the asymptotic wavefunction. The values given include a correction of about 8% resulting from the running of α_{QED}.

The major source of model dependence in $R_{e^+e^-/\gamma\gamma}$ is the $n_{_U}$-dependence. The results presented here were obtained with $n_{_U} = 3$; using the flat wavefunction $n_{_U} = 0$ decreases the predictions by 14% at $\sqrt{s} = 5$ GeV (10% at $\sqrt{s} = 7$ GeV). Certainly the flat wavefunction represents an unphysical limiting case; we maintain that this difference can be treated as a generous upper bound on the uncertainty due to variation in $n_{_U}$.

The overall ratio

$$\bar{R}_{e^+e^-/\gamma\gamma} \ \equiv \ \frac{\sigma(p\bar{p} \to e^+e^-; \theta_{\mathrm{cm}} > 30^\circ)}{\sigma(p\bar{p} \to \gamma\gamma; \theta_{\mathrm{cm}} > 30^\circ)}$$

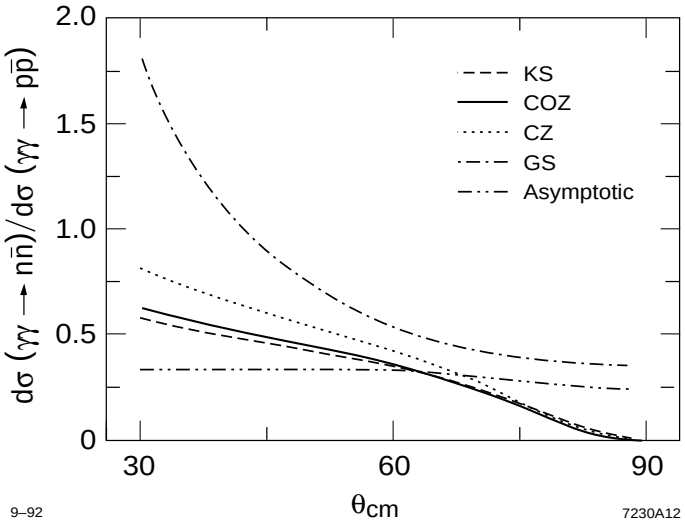

Fig. 4.11. Ratio $\mathrm{d}\sigma(\gamma\gamma \to n\bar{n})/\mathrm{d}\sigma(\gamma\gamma \to p\bar{p})$ for the candidate distribution amplitudes under consideration.

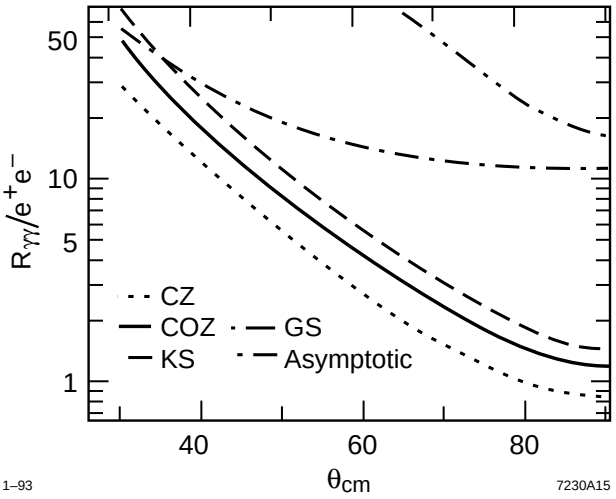

Fig. 4.12. Ratio $R_{e^+e^-/\gamma\gamma}$ for candidate distributions at $s = 25$ GeV^2. Part of the curve for the asymptotic wavefunction in also shown.

is displayed in Table 2 for each candidate distribution. This ratio is highly sensitive to the choice of distribution; it is also much easier to measure than either the shape of the $\mathrm{d}\sigma/\mathrm{d}\Omega(p\bar{p} \to \gamma\gamma)$ or the running of $Q^4 F_1^p$. Hence, it is probably one of the best tests of the proton distribution amplitude.

4.8. Conclusion

The value of the formalism of [3] is that it allows a consistent perturbative treatment of hadronic processes without resorting to arbitrary cutoffs. Thus the results we have just derived are (to next-to-leading log) trustworthy predictions of QCD; the size of potential errors is estimated by the magnitude of the kink contribution in the form factor, and of scaling violations in $p\bar{p} \to \gamma\gamma$. It is our belief that the model dependence of our main result, the prediction of $R_{\gamma\gamma/e^+e^-}$, is less than 15%, which is certainly adequate to allow tests of model distribution amplitudes.

High precision measurement of $R_{e^+e^-/\gamma\gamma}$ may be attainable at FNAL E760, an antiproton accumulator experiment, or at the proposed SuperLEAR facility. This would open the door to precision tests of the proton wavefunction, and set us on the road toward understanding QCD at the amplitude level.

Appendix 4.A. Kinematics and Conventions

We computed all amplitudes in the center-of-momentum frame, with the outgoing proton momentum along the positive z-axis, and the y-axis perpendicular to the scattering plane. That is,

$$\begin{aligned} p &= E(1,0,0,1) && \text{proton ;} \\ p' &= E(1,0,0,-1) && \text{antiproton ;} \\ k &= E(1,\sin\theta,0,\cos\theta) && \text{photon } \gamma_1 \text{ ;} \\ k' &= E(1,-\sin\theta,0,-\cos\theta) && \text{photon } \gamma_2 \,. \end{aligned}$$

For the photon polarization vectors, we chose

$$\epsilon_1(\uparrow) = \tfrac{1}{\sqrt{2}}(\cos\theta, i, -\sin\theta) \;, \qquad \epsilon_1(\downarrow) = \tfrac{1}{\sqrt{2}}(-\cos\theta, i, \sin\theta) \;;$$

$$\epsilon_2(\uparrow) = \tfrac{1}{\sqrt{2}}(\cos\theta, -i, -\sin\theta) \;, \qquad \epsilon_2(\downarrow) = \tfrac{1}{\sqrt{2}}(-\cos\theta, -i, \sin\theta) \;.$$

We worked in the helicity formalism [22], in which the Dirac matrices are

$$\gamma^0_\pm = -\mathbf{1} \;, \qquad \gamma^i_\pm = \mp\sigma^i \;.$$

This yields

$$\not{p}_+ = \not{p}'_- = -2E \begin{pmatrix} 1 & 0 \\ 0 & 0 \end{pmatrix}, \qquad \not{p}_- = \not{p}'_+ = -2E \begin{pmatrix} 0 & 0 \\ 0 & 1 \end{pmatrix},$$

$$\not{k}_+ = \not{k}'_- = -2E \begin{pmatrix} c^2 & sc \\ sc & s^2 \end{pmatrix}, \qquad \not{k}_- = \not{k}'_+ = -2E \begin{pmatrix} s^2 & -sc \\ -sc & c^2 \end{pmatrix},$$

where $s \equiv \sin(\theta/2)$, $c \equiv \cos(\theta/2)$; the polarization vectors become

$$\epsilon_{1+} = -\epsilon_{1-} = \sqrt{2} \begin{pmatrix} sc\alpha - sc\beta & -c^2\alpha - s^2\beta \\ s^2\alpha + c^2\beta & -sc\alpha + sc\beta \end{pmatrix},$$

$$\epsilon_{2+} = -\epsilon_{2-} = \sqrt{2} \begin{pmatrix} sc\gamma - sc\delta & s^2\gamma + c^2\delta \\ -c^2\gamma - s^2\delta & -sc\gamma + sc\delta \end{pmatrix}.$$

For an external quark line, we need a factor $x^{-1/2} u_\pm(xp) = u_\pm(p)$. These spinors are

$$u_+(p) = \sqrt{2E} \ \begin{pmatrix} 1 & 0 \end{pmatrix} \ , \qquad u_-(p) = \sqrt{2E} \ \begin{pmatrix} 0 & 1 \end{pmatrix} \ ,$$

for the outgoing quarks, and

$$v_+(p') = \sqrt{2E} \ \begin{pmatrix} 0 \\ 1 \end{pmatrix} \ , \qquad v_-(p') = \sqrt{2E} \ \begin{pmatrix} -1 \\ 0 \end{pmatrix} \ ,$$

for the antiquarks [12]; the subscript denotes the helicity.

We find it convenient to adopt the notation

$$(x_i, y_j) \equiv \left(x_i p + y_j p' - k \right)^2 = -x_i \bar{y}_j \, s^2 - \bar{x}_i y_j \, c^2 \ .$$

APPENDIX B: HARD-SCATTERING AMPLITUDES

The nonzero contributions $\tilde{T}$ to T_H are tabulated here. In each case, we list $\tilde{T}^{(d)}$ for only one of the class of diagrams generated by the symmetries $\mathcal{C}$, $\mathcal{E}$, and $\mathcal{X}$. In obtaining the amplitudes not listed, one must bear in mind that $\mathcal{X}$ interchanges photon helicities and $\mathcal{C}$ reverses them. Parentheses indicate repeated diagrams.

d $\mathcal{X}$(d)	$\mathcal{E}$(d) $\mathcal{X}\circ\mathcal{E}$(d)	$\mathcal{C}$(d) $\mathcal{X}\circ\mathcal{C}$(d)	$\mathcal{C}\circ\mathcal{E}$(d) $\mathcal{X}\circ\mathcal{C}\circ\mathcal{E}$(d)	$\tilde{T}^{\uparrow\uparrow}_{+-}$	$\tilde{T}^{\uparrow\downarrow}_{+-}$	$\tilde{T}^{\downarrow\uparrow}_{+-}$	$\tilde{T}^{\downarrow\downarrow}_{+-}$
A12 A21	B67 B76	B21 B12	A76 A67	$\frac{c}{s}\,\frac{1}{\bar{x}_1 y_1}$	0	$\frac{c}{s}\,\frac{1}{x_1 y_1}$	0
A13 A31	B63 B36	B25 B52	A75 A57	$sc\,\frac{\bar{x}_2}{x_2(x_1,\bar{y}_3)}$	$sc\,\frac{1}{(x_1,\bar{y}_3)}$	$sc\,\frac{\bar{x}_1\bar{x}_2}{x_1x_2(x_1,\bar{y}_3)}$	$sc\,\frac{\bar{x}_1}{x_1(x_1,\bar{y}_3)}$
A14 A41	B64 B46	B24 B42	A74 A47	$-s\,\frac{x_1}{\bar{x}_1(x_1,\bar{y}_3)}$	$\frac{c^3}{s}\,\frac{1}{(x_1,\bar{y}_3)}$	$-sc\,\frac{1}{(x_1,\bar{y}_3)}$	$\frac{c^3}{s}\,\frac{\bar{x}_1}{x_1(x_1,\bar{y}_3)}$
A16 A61	B61 B16	B27 B72	A72 A27	$-sc\,\frac{1}{(x_1,\bar{y}_3)}$	$-\frac{c}{s}\,\frac{x_2+x_3c^2}{x_3(x_1,\bar{y}_3)}$	$-sc\,\frac{\bar{x}_1}{x_1(x_1,\bar{y}_3)}$	$-\frac{c}{s}\,\frac{\bar{x}_1(x_2+x_3c^2)}{x_1x_3(x_1,\bar{y}_3)}$
A17 A71	B62 B26	(B26) (B62)	(A71) (A17)	$\frac{c^3}{s}\frac{\bar{y}_3}{y_3(x_1,\bar{y}_3)}$	$\frac{c^3}{s}\frac{1}{(x_1,\bar{y}_3)}$	$\frac{c^3}{s}\,\frac{\bar{x}_1\bar{y}_3}{x_1y_3(x_1,\bar{y}_3)}$	$\frac{c^3}{s}\,\frac{\bar{x}_1}{x_1(x_1,\bar{y}_3)}$
A22 A2$\bar{2}$	B77 B7$\bar{7}$	B1$\bar{1}$ B11	A6$\bar{6}$ A66	$-\frac{c}{s}\,\frac{1-y_1c^2}{\bar{x}_1y_1\bar{y}_1}$	$-\frac{c^3}{s}\,\frac{1}{\bar{x}_1\bar{y}_1}$	$sc\,\frac{1}{\bar{x}_1\bar{y}_1}$	$-sc\,\frac{1}{\bar{x}_1\bar{y}_1}$
A23 A32	B73 B37	B15 B51	A65 A56	$-\frac{s}{c}\,\frac{\bar{x}_2(y_2+y_1c^2)}{x_2y_1(x_1,\bar{y}_3)}$	$-\frac{s}{c}\,\frac{y_2+y_1c^2}{y_1(x_1,\bar{y}_3)}$	$-\frac{s^3}{c}\,\frac{\bar{x}_2}{x_2(x_1,\bar{y}_3)}$	$-\frac{s^3}{c}\,\frac{1}{(x_1,\bar{y}_3)}$
A24 A42	B74 B47	B14 B41	A64 A46	$\frac{s}{c}\,\frac{x_1\bar{y}_1s^2+\bar{y}_3c^2}{\bar{x}_1y_1(x_1,\bar{y}_3)}$	$-sc\,\frac{\bar{x}_1y_2-x_1y_3}{\bar{x}_1y_1(x_1,\bar{y}_3)}$	$\frac{s^3}{c}\,\frac{x_1}{\bar{x}_1(x_1,\bar{y}_3)}$	$-sc\,\frac{1}{(x_1,\bar{y}_3)}$

Appendix B. Hard-scattering amplitudes (continued)

d $\mathcal{X}$(d)	$\mathcal{E}$(d) $\mathcal{X}\circ\mathcal{E}$(d)	$\mathcal{C}$(d) $\mathcal{X}\circ\mathcal{C}$(d)	$\mathcal{C}\circ\mathcal{E}$(d) $\mathcal{X}\circ\mathcal{C}\circ\mathcal{E}$(d)	$\tilde{T}_{+-}^{\uparrow\uparrow}$	$\tilde{T}_{+-}^{\uparrow\downarrow}$	$\tilde{T}_{+-}^{\downarrow\uparrow}$	$\tilde{T}_{+-}^{\downarrow\downarrow}$
A25 A52	B75 B57	B13 B31	A63 A36	$-\frac{c}{s}\frac{1}{\bar{x}_1 y_1}$	$-\frac{c}{s}\frac{\bar{y}_2}{\bar{x}_1 y_1 y_2}$	0	0
A26 A62	B71 B17	(B17) (B71)	(A62) (A26)	$\frac{s}{c}\frac{y_2+y_1c^2}{y_1(x_1,\bar{y}_3)}$	$-\frac{s}{c}\frac{x_1y_3-x_2y_2+x_3y_1c^2}{x_3y_1(x_1,\bar{y}_3)}$	$\frac{s^3}{c}\frac{1}{(x_1,\bar{y}_3)}$	$\frac{s}{c}\frac{x_2+x_3c^2}{x_3(x_1,\bar{y}_3)}$
A34 A43	B34 B43	B54 B45	A54 A45	$-sc\bar{x}_2x_2(\bar{x}_1,y_3)$	$\frac{c^3}{s}\frac{\bar{x}_2y_3}{x_2\bar{y}_3(\bar{x}_1,y_3)}$	$-sc\frac{1}{(\bar{x}_1,y_3)}$	$\frac{c^3}{s}\frac{y_3}{\bar{y}_3(\bar{x}_1,y_3)}$
A35 A53	B35 B53	(B53) (B35)	(A53) (A35)	$-\frac{c^3}{s}\frac{\bar{x}_2}{x_2(\bar{x}_1,y_3)}$	$-\frac{c^3}{s}\frac{\bar{x}_2\bar{y}_2}{x_2y_2(\bar{x}_1,y_3)}$	$-\frac{c^3}{s}\frac{1}{(\bar{x}_1,y_3)}$	$-\frac{c^3}{s}\frac{\bar{y}_2}{y_2(\bar{x}_1,y_3)}$
A44 A4$\bar{4}$	B44 B4$\bar{4}$	(B4$\bar{4}$) (B44)	(A4$\bar{4}$) (A44)	$sc\frac{x_1c^2+\bar{y}_3s^2}{\bar{x}_1\bar{y}_3(\bar{x}_1,y_3)}$	$sc^3\frac{\bar{x}_1-y_3}{\bar{x}_1\bar{y}_3(\bar{x}_1,y_3)}$	$-s^3c\frac{\bar{x}_1-y_3}{\bar{x}_1\bar{y}_3(\bar{x}_1,y_3)}$	$sc\frac{\bar{x}_1s^2+y_3c^2}{\bar{x}_1\bar{y}_3(\bar{x}_1,y_3)}$
C11 C1$\bar{1}$	D66 D6$\bar{6}$	E2$\bar{2}$ E22	F7$\bar{7}$ F77	$-sc\frac{1}{\bar{x}_1\bar{y}_1}$	$-\frac{c^3}{s}\frac{1}{\bar{x}_1\bar{y}_1}$	$sc\frac{1}{\bar{x}_1\bar{y}_1}$	$-\frac{c}{s}\frac{1-x_1c^2}{x_1\bar{x}_1\bar{y}_1}$
C12 C21	D67 D76	E21 E12	F76 F67	0	0	$\frac{c}{s}\frac{1}{x_1y_1}$	$\frac{c}{s}\frac{1}{x_1\bar{y}_1}$
C13 C31	D64 D46	E24 E42	F75 F57	0	0	$-\frac{s}{c}\frac{\bar{x}_2(s^2-x_2)}{x_1x_2(\bar{x}_2,y_1)}$	$-\frac{s}{c}\frac{s^2-x_2}{x_1(\bar{x}_2,y_1)}$

Appendix B. Hard-scattering amplitudes (continued)

d $\mathcal{X}$(d)	$\mathcal{E}$(d) $\mathcal{X}\circ\mathcal{E}$(d)	$\mathcal{C}$(d) $\mathcal{X}\circ\mathcal{C}$(d)	$\mathcal{C}\circ\mathcal{E}$(d) $\mathcal{X}\circ\mathcal{C}\circ\mathcal{E}$(d)	$\tilde{T}^{\uparrow\uparrow}_{+-}$	$\tilde{T}^{\uparrow\downarrow}_{+-}$	$\tilde{T}^{\downarrow\uparrow}_{+-}$	$\tilde{T}^{\downarrow\downarrow}_{+-}$
C14 C41	D65 D56	E23 E32	F74 F47	0	0	$\frac{c}{s}\frac{s^2-x_2}{x_1(\bar{x}_2,y_1)}$	$-\frac{c}{s}\frac{x_2\bar{y}_2+y_2s^2}{x_1y_2(\bar{x}_2,y_1)}$
C15 C51	D61 D16	E27 E72	F73 F37	0	$-\frac{c}{s}\frac{1}{x_3\bar{y}_1}$	$-\frac{s}{c}\frac{1}{x_1\bar{y}_1}$	$-\frac{1}{sc}\frac{\bar{x}_3s^2+\bar{x}_1c^2}{x_1x_3\bar{y}_1}$
C16 C61	D62 D26	E26 E62	F72 F27	0	0	$sc\frac{\bar{x}_2}{x_1\bar{y}_1(\bar{x}_2,y_1)}$	$sc\frac{x_2}{x_1\bar{y}_1(\bar{x}_2,y_1)}$
C17 C71	D63 D36	E25 E52	F71 F17	0	0	$-\frac{c}{s}\frac{(s^2-x_2)\bar{y}_3}{x_1y_3(\bar{x}_2,y_1)}$	$-\frac{c}{s}\frac{s^2-x_2}{x_1(\bar{x}_2,y_1)}$
C25 C52	D71 D17	E17 E71	F63 F36	0	$\frac{s}{c}\frac{1}{x_3y_1}$	0	$\frac{s}{c}\frac{1}{x_3\bar{y}_1}$
C35 C53	D41 D14	E47 E74	F53 F35	0	$-\frac{c}{s}\frac{\bar{x}_2(c^2-x_2)}{x_2x_3(x_2,\bar{y}_1)}$	0	$-\frac{c}{s}\frac{c^2-x_2}{x_3(x_2,\bar{y}_1)}$
C45 C54	D51 D15	E37 E73	F43 F34	0	$\frac{s}{c}\frac{c^2-x_2}{x_3(x_2,\bar{y}_1)}$	0	$-\frac{s}{c}\frac{x_2\bar{y}_2+y_2c^2}{x_3y_2(x_2,\bar{y}_1)}$
C55 C5$\bar{5}$	D11 D1$\bar{1}$	E7$\bar{7}$ E77	F3$\bar{3}$ F33	$sc\frac{1}{\bar{x}_3\bar{y}_1}$	$\frac{c^3}{s}\frac{1}{\bar{x}_3\bar{y}_1}$	$-sc\frac{1}{\bar{x}_3\bar{y}_1}$	$\frac{c}{s}1-x_3c^2x_3\bar{x}_3\bar{y}_1$
C56 C65	D12 D21	E76 E67	F32 F23	0	0	$-sc\frac{\bar{x}_2}{x_3\bar{y}_1(\bar{x}_2,y_1)}$	$-sc\frac{x_2}{x_3\bar{y}_1(\bar{x}_2,y_1)}$
C57 C75	D13 D31	E75 E57	F31 F13	0	0	$\frac{c}{s}\frac{\bar{y}_3(s^2-x_2)}{x_3y_3(\bar{x}_2,y_1)}$	$\frac{c}{s}\frac{s^2-x_2}{x_3(\bar{x}_2,y_1)}$

References for Chapter 4

[1] V. V. Sudakov, *Sov. Phys.–JETP* **3**, 65 (1956).

[2] A. H. Mueller, *Phys. Rept.* **73**, 237 (1981).

[3] J. Botts and G. Sterman, *Nucl. Phys.* **B325**, 62 (1989).

[4] H. Li and G. Sterman, *Nucl. Phys.* **B381**, 129 (1992).

[5] D. Millers and J. F. Gunion, *Phys. Rev.* **D34**, 2657 (1986).

[6] G. R. Farrar *et al.*, *Nucl. Phys.* **B311**, 585 (1989).

[7] V. L. Chernyak and A. R. Zhitnitsky, *Nucl. Phys.* **B246**, 52 (1984).

[8] V. L. Chernyak, A. A. Ogloblin and I. R. Zhitnitskiĭ,, *Yad. Fiz.* **48**, 841 (1988); *Sov. J. Nucl. Phys.* **48**, 536 (1988).

[9] I. D. King and C. T. Sachrajda, *Nucl. Phys.* **B297**, 785 (1987).

[10] M. Gari and N. G. Stefanis, *Phys. Lett.* **B175**, 462 (1986); *Phys. Rev.* **D35**, 1074 (1987).

[11] G. P. Lepage and S. J. Brodsky, *Phys. Rev.* **D22**, 2157 (1980); S. J. Brodsky and G. P. Lepage, *Phys. Rev.* **D24**, 1808 (1981). For a recent review see S. J. Brodsky, SLAC–PUB–5849 (1992).

[12] A. N. Kronfeld and B. Nižić, *Phys. Rev.* **D44**, 3445 (1991).

[13] H. Li, *Phys. Rev.* **D48**, 4243 (1993).

[14] This is slightly inaccurate when $q^2 = q_l^2 - q_\perp^2 < 0 < q_l^2$. It depends on the approximation $l_\perp \ll q_\perp$, which fails in the region $|q_\perp + l_\perp| \sim \sqrt{q_l^2}$ when $q_l^2 \simeq q_\perp^2$. However, we use it anyway since the spacelike gluon denominators, like the fermion denominators, do not contain terms like $x_i y_j$; thus the errors induced will be less than those from the neglect of transverse momentum in the fermion propagators.

[15] When both gluons carry the transverse hard momentum $q_\perp$, we must use $J_0(\sqrt{|q_\perp||(b_i - b_j) + (b_j - b_k)|})$, reflecting the fact that we take only one angular average, rather than $J_0(\sqrt{|q_\perp||b_i - b)j|})J_0(\sqrt{|q_\perp||b_j - b_k|})$.

[16] For timelike gluons, the simple analytic continuation $K_0(bQ) \to K_0(ibQ) = (i\pi/2)\ H_0^{(1)}(bQ)$ of the spacelike propagator, where the imaginary part comes from integrating $k_\perp$ through the singularity at $l_\perp^2 = q_l^2$, must be unphysical. The reason is that in $\gamma\gamma \to p\bar{p}$, the only timelike momentum a gluon can carry is the sum of some subset of the outgoing, on-shell quark momenta; thus the region $q_l^2 - l_\perp^2 = q^2 < 0 < q_l^2$ is excluded.

[17] G. P. Lepage et al., in *Banff 1981, Proc. Particles and Fields 2*.

[18] The immediate effect of the scaling might be an factor λ^1 (as in the long-distance quarkonium potential), but is more likely λ^2 since the nucleon can be thought of as saturated with a gluon field. In addition, we must account for the increased strength of the running coupling as the transverse momentum scale decreases. This effect, if approximated by a power-law factor, seems to contribute roughly an additional λ^1.

[19] The GS model is distinguished by pronounced asymmetry; this has been criticized by V. L. Chernyak, A. A. Ogloblin and I. R. Zhitnitskiĭ, *Z. Phys.* **C42**, 583 (1989).

[20] FNAL E760 Collaboration, FNAL–PUB–92/244–E, submitted to Phys. Rev. Lett.

[21] R. Baldini, private communication.

[22] G. R. Farrar and F. Neri, *Phys. Lett.* **130B**, 109 (1983).

5. SEMIEXCLUSIVE MESON PRODUCTION

The study of hadronic properties through exclusive processes [1] is by now an established industry [2]. Grozin and Baier [3] proposed an alternative type of process, which the author independently rediscovered and dubbed *semiexclusive* production, whose analysis holds promise of illuminating the structure of mesons with greater precision than is achievable with exclusive reactions.

Exclusive processes, in which the final state is completely specified, are inevitably suppressed by powers of Q^2 at high energies, where Q is the momentum scale apposite to the hard process under consideration [1]. The degree of this suppression in the amplitude can be shown to be $(\mu/Q)^{n_s}$, where $\mu \sim \Lambda_{\rm QCD}$ is a typical hadronic momentum scale and $n_s = n_{\rm partons} - n_{\rm hadrons}$ is the number of 'spectators' to the hard scattering, which must emerge collinear to the hadrons they constitute [4]. For example, the proton form factor falls like Q^{-4}, so that the associated cross sections are proportional to Q^{-10}.

In semiexclusive reactions, we specify the properties of one directly produced meson and demand a high degree of isolation (*e.g.*, isolation in a hemisphere in the center-of-momentum frame, or by a large rapidity gap) in order to eliminate inclusive backgrounds. Since we do not specify the content of the recoil system, we pay the minimum possible penalty in the cross section: there is only a single spectator quark. Thus semiexclusive meson production, which will be the focus of this chapter [5], occurs with cross sections proportional to Q^{-4} (compared to total event cross sections of order Q^{-2}). For example, consider the current data sample of the CLEO detector at CESR, about 2 fb^{-1}. This represents about 10^7 events of all types. The semiexclusive production cross sections are about 2–3 fb for each meson, so several such events are expected even in the current data sample. On the

other hand, the cross section for exclusive $\pi^+\pi^-$ production is on the order of 1 fb, and that for $p\bar{p}$ production is about 10^{-2} fb.

The less drastic suppression of semiexclusive cross sections with increasing energy allows us to study these processes at higher energies than the study of exclusive processes can reach, putting us in a region where the perturbation expansion is more reliable, and higher-twist terms more thoroughly suppressed.

Semiexclusive processes have a further advantage in the study of hadronic structure; the fraction z of the beam energy carried by the isolated meson can be measured, and the differential cross section $\mathrm{d}\sigma/\mathrm{d}z$ reconstructed. The shape of this cross section depends on the distribution amplitude of the isolated meson; thus extraction of valence distribution amplitudes with high precision should become feasible. This is in contrast to the situation in purely exclusive scattering in which the angular distribution is trivial (as is the case for form factors) or is insensitive to the distribution amplitude [6-7].

These advantages are partially, but not entirely, neutralized by the added complications due to the hadronization of the recoil system, which introduces nonperturbative physics into the computation of experimental results. Much of this work focuses on the extraction of viable results which take into account the behavior of the hadronizing system.

Our computational scheme is that of Lepage and Brodsky [1]. The amplitude for any process in which a 'hard' scale Q can be identified is written as a convolution of a hard-scattering subprocess amplitude, calculable in perturbative QCD (pQCD), with one or more process-independent nonperturbative light-cone hadron wavefunctions:

$$\mathcal{M} = \sum_i \int \mathrm{d}x \; \mathrm{d}^2 k_\perp \; T_{Hi}(x, k_\perp; Q) \psi_i(x, k_\perp; Q),$$

where T_H is a pQCD amplitude for the hard scattering of free partons, ψ_i is the projection of the wavefunction onto the i^{th} Fock state, and Q is the 'separation scale' above which processes are deemed hard; processes with momentum transfer smaller than Q are absorbed into the wavefunction.

To leading twist, we may ignore the dependence of T_H on $k_\perp \sim \mu \ll Q$. Then, defining [8]

$$\phi(x; Q) \equiv \int^Q \mathrm{d}^2 k_\perp \; \psi(x, k_\perp; Q), \tag{5.1}$$

we obtain the simpler form (valid up to terms of $O(\mu^2/Q^2)$ where $\mu \lesssim 1$ GeV is a typical hadronic momentum scale)

$$\mathcal{M} = \int \mathrm{d}x \; T_H(x; Q) \phi(x; Q). \tag{5.2}$$

Another crucial simplification results from the neglect of all terms of higher twist: the amplitude thus calculated depends only on the projection of the wavefunction onto the Fock state of smallest particle number and with no orbital angular momentum, the 'valence' Fock state [1]. Thus the tremendous complexity of the hadronic structure is reduced to the single valence distribution amplitude ϕ. Gupta [9] has shown that the factorization theorems from exclusive processes are also valid in the semiexclusive case, so that the distribution amplitudes extracted from the study of semiexclusive processes are indeed universal.

Figure 1 shows the Feynman diagrams contributing at tree level to the simplest semiexclusive process, $e^+e^- \to K^- X$ (of course, any light meson may be produced

by the same mechanism). In this work, we will systematically explore the properties of the resulting system, obtaining a set of reliable predictions of experimentally measurable quantities.

This chapter is organized as follows: Section 5.1 computes the tree-level amplitudes at leading twist for the processes of interest and comments on their structure. Section 5.2 is devoted to next-to-leading twist corrections to these results, arising from the inclusion of quark and meson mass terms, intrinsic transverse momenta, and higher Fock states. Section 5.3 explores the effects of Sudakov suppression and the running of the QCD coupling α_s. Section 5.4 describes the effects of other higher-order pQCD processes on our results. Section 5.5 explores the collinear divergence of the naive tree-level amplitude which arises when one quark is created nearly parallel to the produced meson; a more accurate, convergent form is used for this region, and the effect on measurements away from the collinear region is explored. Section 5.6 uses standard Monte Carlo methods to study the relation between the isolation of the directly produced meson in the partonic system and the experimentally measured isolation from hadrons produced in fragmentation. Finally, Section 5.7 presents our results, extracts experimentally accessible quantities, and discusses the prospects for constraining hadronic distribution amplitudes.

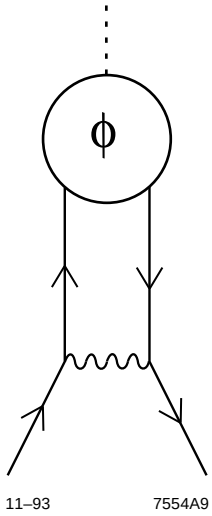

Fig. 5.1. Feynman diagrams contributing to the semiexclusive process $e^+e^- \to HX$. Here we show only the hadronic event topology; a sum over all possible attachments of the incoming γ^* is assumed. All external particles are outgoing; arrows indicate fermion flow.

5.1. Tree-Level Amplitudes

In this section, we calculate the tree-level amplitudes for the semiexclusive process $e^+e^- \to HX$, where H is some meson. The amplitudes take their simplest form in the center-of-momentum frame if we define

the hadron momentum fraction

$$z \equiv \frac{E_H + |\vec{p}_H|}{\sqrt{s}};$$

the antiquark and quark (respectively) back-momenta (light-cone momenta in the frame antiparallel to $\vec{p}_H$)

$$y_i\sqrt{s} \equiv E_i - \frac{\vec{l}_i \cdot \vec{p}_H}{|\vec{p}_H|},$$

with $y_1 + y_2 = 1 - m_H^2/zQ^2$;

the beam scattering angles θ and ϕ, where θ is the e^--to-H polar angle, and ϕ is the angle between the H-q-$\bar{q}$ plane and the plane containing the beam and H [10]; and

$s \equiv \sin(\theta/2)$ and $c \equiv \cos(\theta/2)$.

In these terms, the unpolarized differential cross section is

$$\mathrm{d}\sigma = \frac{1}{1024\pi^4}\; z\bar{z}\mathrm{d}z\; \mathrm{d}y_1\; \mathrm{d}\Omega\; \frac{1}{2}\sum_{\text{spins}} |\mathcal{M}|^2, \tag{5.3}$$

where we have introduced the notation $\bar{z} \equiv 1 - z$; recall that $\mathcal{M}$, for a process with three final-state particles, has dimensions of mass^{-1}.

For leading-twist calculations, we use the helicity formalism of Ref. [11]; the spinors and polarization vectors are tabulated in Appendix 5.A. We do not need to compute the interference effects between different quark helicity amplitudes, even if the resulting hadron helicities are identical, because our neglect of resonance effects in the recoil system is tantamount to treating the recoil quarks as observable particles. Thus pseudoscalar states $|{+-}\rangle - |{-+}\rangle$ and longitudinally polarized vector states $|{+-}\rangle + |{-+}\rangle$ will yield identical hard-scattering amplitudes.

This assumption means that our results will be valid only in the region in which duality holds; we expect that it will be very accurate when the invariant mass $\bar{z}Q^2$ of the hadronizing recoil system is larger than about $(2\ \mathrm{GeV})^2$ [12]. This will provide an upper limit on the values of z at which our computed cross sections are reliable; however, at $Q \sim 10$ GeV the restriction is almost unnoticeable due to the factor of $\bar{z}$ in eq. (5.3), which ensures that the differential cross section $\mathrm{d}\sigma/\mathrm{d}z$ vanishes as $z \to 1$.

5.1.1. Distribution Amplitudes

To leading twist, the hadron wavefunction enters only through the valence-state distribution amplitude of eq. (5.1). In eqs. (5.1) and (5.2), we will let x denote the light-cone momentum fraction carried by the heavier parton, be it quark or antiquark. Thus we expect $\langle x \rangle \geq 0.5$.

While the asymptotic behavior of the distribution as $Q^2 \to \infty$ is simple and well understood, the approach to asymptopia is very slow [1]. One interesting approach

to extraction of distribution amplitudes at moderate Q^2 is the sum-rule approach [13-16]. This method relates moments of the distribution, of the form

$$\int_0^1 (x-\bar{x})^n \phi(x) \mathrm{d}x,$$

to the observed spectrum of hadron masses. It has so far yielded predictions in good agreement with experiment [17]; one of our aims is to provide a more precise test of its accuracy.

Since the distribution amplitude must vanish like $x\bar{x}$ at each endpoint, it is customary to expand it as a series of Gegenbauer polynomials [18], which are orthogonal under the measure with weight $x\bar{x}$:

$$\phi(x) = \frac{f_h}{\sqrt{2}} x\bar{x} \sum_{i=0}^{\infty} a_i P_i(x), \quad \text{where} \quad \int_0^1 x\bar{x} P_i(x) P_j(x) \mathrm{d}x = \delta_{ij}, \tag{5.4}$$

and f_h is the hadron decay constant, which can be measured experimentally in semileptonic decay.

A major advantage of this expansion is that the Gegenbauer polynomials are the eigenfunctions of the one-loop evolution equation for the meson valence distribution amplitude [1]. Thus the running of the coefficients a_i is simple and easily calculable. We will take advantage of this fact in our analysis of semiexclusive production in Z decays (Sec. 5.1.7). Our normalization ensures that a_0, which does not run with increasing Q^2 for scalar or longitudinally polarized mesons [1], is equal to 1.

The first few Gegenbauer polynomials are

$$
\begin{aligned}
P_0 &= \sqrt{6} \\
P_1 &= \sqrt{30}(x-\bar{x}) \\
P_2 &= 2\sqrt{21}(1-5x\bar{x}) \\
P_3 &= 6\sqrt{5}(x-\bar{x})(1-7x\bar{x}) \\
P_4 &= \sqrt{330}(42x^2\bar{x}^2-14x\bar{x}+1) \\
P_5 &= \sqrt{546}(x-\bar{x})(66x^2\bar{x}^2-18x\bar{x}+1) \\
P_6 &= 2\sqrt{210}(429x^3\bar{x}^3-198x^2\bar{x}^2+27x\bar{x}-1)\ldots
\end{aligned}
$$

To proceed from the moments derived from QCD sum rules to definite models of the distribution amplitude, we fit the required moments with a sum over the first few Gegenbauer polynomials. In general, it is far simpler to test the resulting model than to extract the moments from experiment; however, the resulting confrontation with theory is somewhat oblique. We will discuss the problem of addressing the sum-rule predictions more directly in Sec. 5.7.5.

We will find it useful to define the integrals

$$
\begin{aligned}
A(z) &\equiv \int_0^1 \frac{\phi(x)}{\bar{x}(1-zx)}\mathrm{d}x, \quad \bar{A}(z) \equiv \int_0^1 \frac{\phi(x)}{x(1-z\bar{x})}\mathrm{d}x; \\
B &\equiv A(0) = \int \frac{\phi(x)}{\bar{x}}\mathrm{d}x, \quad \bar{B} \equiv \bar{A}(0); \\
C(z) &\equiv \int_0^1 \frac{\phi(x)}{x\bar{x}(1-zx)}\mathrm{d}x, \quad \bar{C}(z) \equiv \int_0^1 \frac{\phi(x)}{x\bar{x}(1-z\bar{x})}\mathrm{d}x, \\
\text{and} \quad D &\equiv C(0) = \bar{C}(0) = \int_0^1 \frac{\phi(x)}{x\bar{x}},
\end{aligned}
\tag{5.5}
$$

which control the behavior of the cross section. These quantities are related by

$$C(z) = zA(z) + D, \quad \bar{C}(z) = z\bar{A}(z) + D, \qquad \text{and} \quad D = B + \bar{B}.$$

Note that A and C are logarithmically divergent as $z \to 1$; however, we find that their contributions to cross sections are always suppressed by one or more powers of $1-z$, so that we obtain consistently finite results. The Dirac form factors of mesons are determined solely by B and $\bar{B}$: *e.g.*, $F^1_{K^-} \propto |q_s B^2_K - q_u \bar{B}^2_K|$.

The foremost goal, when measuring the semiexclusive cross section, is the precise extraction of the functions $A(z)$ and $\bar{A}(z)$, from which the distribution amplitude $\phi(x)$ may be reconstructed. In terms of the Gegenbauer coefficients of eq. (5.4), these integrals can be written

$$\begin{aligned}
A(z) &= -\frac{f_H}{\sqrt{2}} \sum_{i=0}^{\infty} \text{FINITE}\Big[\frac{a_i P_i(z^{-1}) \ln(1-z)}{z^2}\Big]; \\
\bar{A}(z) &= -\frac{f_H}{\sqrt{2}} \sum_{i=0}^{\infty} \text{FINITE}\Big[\frac{(-1)^i a_i P_i(z^{-1}) \ln(1-z)}{z^2}\Big]; \\
B &= \frac{f_H}{\sqrt{2}} \sum_{i=0}^{\infty} a_i \sqrt{\frac{2i+3}{(i+1)(i+2)}}; \\
\bar{B} &= \frac{f_H}{\sqrt{2}} \sum_{i=0}^{\infty} (-1)^i a_i \sqrt{\frac{2i+3}{(i+1)(i+2)}}; \\
C(z) &= -\frac{f_H}{\sqrt{2}} \sum_{i=0}^{\infty} \text{FINITE}\Big[\frac{a_i P_i(z^{-1}) \ln(1-z)}{z}\Big]; \\
\bar{C}(z) &= -\frac{f_H}{\sqrt{2}} \sum_{i=0}^{\infty} \text{FINITE}\Big[\frac{(-1)^i a_i P_i(z^{-1}) \ln(1-z)}{z}\Big]; \text{and} \\
D &= \frac{f_H}{\sqrt{2}} \sum_{i=0}^{\infty} \big(1 + (-1)^i\big) a_i \sqrt{\frac{2i+3}{(i+1)(i+2)}}.
\end{aligned}$$

Here we define FINITE$[f(x)]$ to be the finite part of the Laurent expansion of f in x (or, equivalently, the residue after $x \to 0$ divergences have been removed by minimal subtraction); for instance,

$$\begin{aligned}\text{FINITE}\Big[\frac{-\ln(1-x)}{x^3}\Big] &= \text{FINITE}\Big[x^{-2} + \frac{x^{-1}}{2} + \frac{1}{3} + \frac{x}{4} + \cdots\Big] = \frac{1}{3} + \frac{x}{4} + \cdots \\ &= \frac{-\ln(1-x) - x - x^2/2}{x^3}.\end{aligned}$$

5.1.2. Modeling the Distribution Amplitude

To obtain concrete predictions for production cross sections, we must have a specific model of the distribution amplitude. The simplest 'model' is simply the known asymptotic form [1]:

$$\phi(x) = f_H \sqrt{3}\; x\bar{x}.$$

However, there is good reason to believe that the distribution amplitudes at moderate Q^2 are very different: predictions of exclusive cross sections based on this distribution, for example, systematically predict values far below the experimental results [13].

The distribution amplitudes predicted from QCD sum rules are in substantially better agreement with present experimental results [14–17]. Table 5.1 presents the coefficients of the Gegenbauer polynomials in the models we use. We also present the coefficients for two toy models, which we will use for purposes of comparison to test the power of the analysis. The first of these models is the simple toy model

$$\phi_K(x) = 2\sqrt{3} f_K x^2 \bar{x},$$

which we will use for strange mesons; the second is a 'stealth' model, with the coefficients a_1 and a_2 chosen such that the integrals B_K and $\bar{B}_K$ match those from

Distribution	Coefficients				Integrals	
	a_0	a_1	a_2	a_3	B	$\bar{B}$
Asymptotic	1.0	0	0	0	$0.87 f_h$	
ZZC K	1.0	0.24	0.64	0.13	$1.43 f_K$	$0.99 f_K$
ZZC π	1.0	0	1.07	0	$1.44 f_\pi$	
ZZC ρ_L	1.0	0	0.27	0	$1.01 f_\rho$	
ZZC ρ_T	1.0	0	-0.27	0	$0.72 f_\rho$	
ZZC K_L^*	1.0	0	0.11	0	$0.93 f_{K^*}$	
ZZC ϕ	1.0	0	-0.05	0	$0.84 f_\phi$	
Toy K	1.0	0.45	0	0	$1.16 f_K$	$0.58 f_K$
'stealth' K	1.0	0.34	0.64	0	$1.43 f_K$	$0.99 f_K$

Table 5.1 Coefficients of the Gegenbauer polynomials in each model distribution amplitude.

the ZZC sum-rule model. The stealth model necessarily bears a strong resemblance to the sum-rule model, as shown in Fig. 5.2. The resemblance of the transforms $A(z)$ and $\bar{A}(z)$ is even more extreme; in fact, $A(z)$ and $\bar{A}(z)$ differ by no more than 6% over the range $z < 0.95$, and these differences are strongly anticorrelated. Thus the stealth wavefunction serves to illustrate the range of variation in the distribution which can be concealed in semiexclusive production. Of course, the ZZC and stealth distributions yield precisely the same Dirac form factor as well.

Figure 5.4 shows the model wavefunctions obtained by a fit to the sum-rule moment predictions for the π and ρ mesons [14,15]. The symmetry of these wavefunctions under $x \to \bar{x}$ implies $A(z) = \bar{A}(z)$. A striking prediction of the sum rules is that ϕ_π is strongly peaked near the endpoints, giving it the bimodal structure

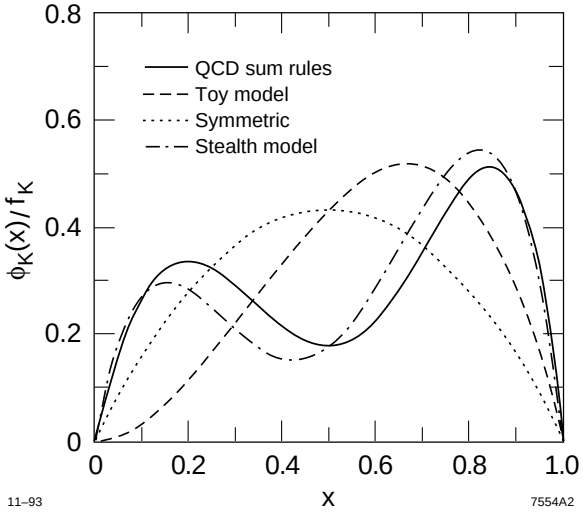

Fig. 5.2. Models of the distribution amplitude ϕ_K. The curve marked 'QCD sum rules' is the model of Ref. [15]; the symmetric curve shows the asymptotic large-Q limit. The toy and 'stealth' models are described in the text.

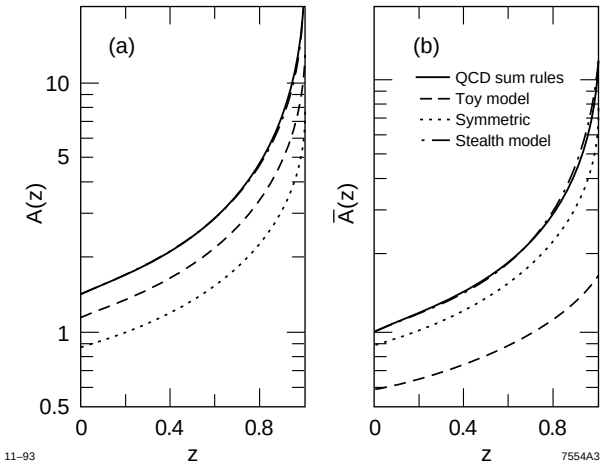

Fig. 5.3. The transforms $A_K(z)$ and $\bar{A}_K(z)$ corresponding to the distribution amplitudes shown in Fig. 5.2. Note the extremely close resemblance between the 'stealth' model and the sum-rule model prediction.

shown; in contrast, ϕ_{ρ_T} is strongly peaked at $x = 1/2$ and drops off sharply near the endpoints. Thus it is predicted that the transform $A_\pi(z)$ will be much greater than $A_\rho(z)$, and the cross section correspondingly larger.

5.1.3. Evolution of the Distribution Amplitude

The sum-rule models are obtained at a momentum transfer $Q_0^2 \simeq 1.5\ \mathrm{GeV}^2$; since the processes in which we are interested probe the distribution amplitude at somewhat larger Q^2, we must take the evolution of the distribution into account. Since the Gegenbauer polynomials are eigenfunctions of the evolution equation, this is easily accomplished by the substitution [1]

$$a_n(Q^2) = a_n(Q_0^2)\Big[\frac{\ln(Q^2/\Lambda^2)}{\ln(Q_0^2/\Lambda^2)}\Big]^{-\gamma_n}, \quad \text{where } \gamma_n \equiv \frac{C_F}{\beta}\Big(1+4\sum_{k=2}^{n+1}\frac{1}{k}-\frac{2\delta_{\lambda\bar{\lambda}'}}{(n+1)(n+2)}\Big),$$

$C_F = 4/3$ is the color factor, $\beta = 11 - 2/3n_f$ is the one-loop QCD beta function, λ and λ' are the quark and antiquark helicities within the pion, and $\bar{\lambda}' \equiv -\lambda'$. For pseudoscalar or longitudinally polarized mesons, $\delta_{\lambda\bar{\lambda}'} = 1$, and the first few anomalous dimensions γ_n are

$$\gamma_0 = 0, \qquad \gamma_1 = \frac{8C_F}{3\beta}, \qquad \gamma_2 = \frac{25C_F}{6\beta}, \qquad \text{and} \quad \gamma_3 = \frac{157C_F}{30\beta};$$

for transversely polarized vector mesons, $\delta_{\lambda\bar{\lambda}'} = 0$, and

$$\gamma_0 = \frac{C_F}{\beta}, \qquad \gamma_1 = \frac{3C_F}{\beta}, \qquad \gamma_2 = \frac{13C_F}{3\beta}, \qquad \text{and} \quad \gamma_3 = \frac{16C_F}{3\beta}.$$

It is noteworthy that the quark mass terms do not enter into the evolution potential [1,22]. Thus heavy-quark mesons evolve in the same way as light mesons.

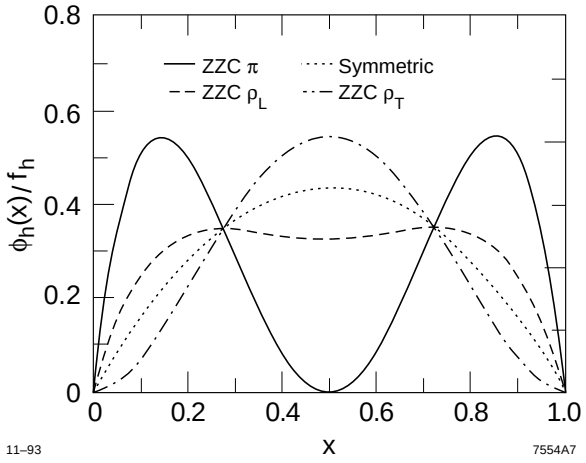

Fig. 5.4. Sum-rule distribution amplitudes for the π and ρ mesons [14,16].

We expect that at low momentum transfer the heavy quark will carry a large momentum fraction, so that $1 - \langle x \rangle \ll 1$; thus it is worth while to consider the evolution of $\langle x \rangle$ with Q^2. We find that in terms of the parameter

$$\xi \equiv \ln \ln \frac{Q^2}{\Lambda^2},$$

the heavy-quark momentum fraction obeys the evolution equation

$$\frac{\mathrm{d}}{\mathrm{d}\xi} \langle x \rangle = -\Big(1 + \frac{\delta_{\lambda\bar{\lambda}'}}{3}\Big) \frac{C_F}{\beta} + O(1 - \langle x \rangle),$$

independent of the shape of the distribution amplitude. Thus we derive the approximate relation for heavy-light pseudoscalar mesons

$$\big\langle x; Q^2 \big\rangle \simeq \big\langle x; Q_0^2 \big\rangle - \frac{4C_F}{3\beta} \Big(\ln \ln \frac{Q^2}{\Lambda^2} - \ln \ln \frac{Q_0^2}{\Lambda^2} \Big).$$

For $Q_0^2 = 1.5\ \mathrm{GeV}^2$ and $\big\langle x; Q_0^2 \big\rangle = 0.95$, this implies $\big\langle x; Q^2 = (10\ \mathrm{GeV})^2 \big\rangle \sim 0.79$ and $\big\langle x; Q^2 = m_Z^2 \big\rangle \sim 0.70$. Clearly the $O(1 - \langle x \rangle)$ corrections begin to be important before this stage; nonetheless, we see that the evolution of the distribution amplitude will quickly smooth any sharp peaks. Since a substantial cross section for semiexclusive production at very high energies, *e.g.* in Z decays, depends on large values of the parameters B and $A(z)$ and therefore on a strongly peaked distribution amplitude, consideration of the evolution of the distribution amplitude greatly decreases both the expected cross sections and the efficacy with which we will be able to discriminate among models; see Fig. 5.5. We will return to this point in Sections 5.7.3 and 5.7.4.

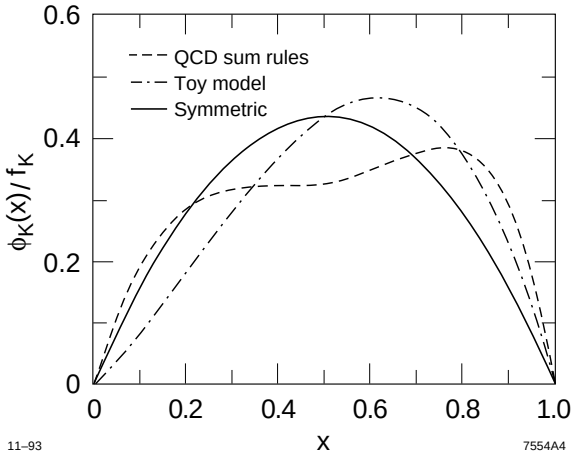

Fig. 5.5. The distribution amplitudes of Fig. 5.2, evolved to $Q = m_Z$.

5.1.4. Mesons with Flavor

In the production of mesons with a nonzero flavor quantum number (including isospin), only the four Feynman diagrams of Fig. 5.1 contribute. We will specialize to the case $H = K^-$ or $H = K^{*-}$, for the sake of definiteness; of course, our results are equally valid for all light flavored mesons. In addition, we will omit an overall factor of $e^2 g_s^2/Q^2 = 16\pi^2\alpha\alpha_s/s$, which is understood to be included in all the amplitudes we will present.

For pseudoscalar mesons or longitudinally polarized vector mesons (*i.e.*, for anti-aligned quark spins) the hard-scattering amplitude is

$$\begin{aligned} T_H^{(+)} = C_F \Bigg\{ & \frac{y_2\bar{x}q_u - y_1 x q_s}{zx\bar{x}\sqrt{y_1 y_2}} \left[\left(s e^{-i\phi} - \sqrt{\frac{\bar{z}y_2}{y_1}}\, c \right) \left(c - \sqrt{\frac{\bar{z}y_1}{y_2}}\, s e^{-i\phi} \right) \right] \\ & + \frac{1}{x}\sqrt{\frac{y_2}{y_1}}\, s e^{-i\phi} q_u \left(c - \sqrt{\frac{\bar{z}y_2}{y_1}}\, \frac{s e^{-i\phi}}{1 - z\bar{x}} \right) \\ & - \frac{1}{\bar{x}}\sqrt{\frac{y_1}{y_2}}\, c q_s \left(s e^{-i\phi} - \sqrt{\frac{\bar{z}y_1}{y_2}}\, \frac{c}{1 - zx} \right) \Bigg\}, \end{aligned} \tag{5.6}$$

with the color factor $C_F = 4/3$. The superscript $(+)$ refers to the case in which the incoming electron and outgoing s quark share the same helicity; it is a simple matter to show that the opposite-helicity amplitude can be obtained by the substitution $c \leftrightarrow s$ (see Appendix 5.A).

The corresponding amplitude for transversely polarized vector meson production is

$$T_H^{(+)} = c^2\sqrt{\bar{z}} \left[\frac{q_s}{\bar{x}(1 - zx)y_2} - \frac{q_u}{x(1 - z\bar{x})y_1} \right]. \tag{5.7}$$

In the exclusive limit ($z \to 1$), the $\sin^2\theta$ angular dependence required by hadron helicity conservation is regained [21,22]. Note that the naive expectation that the

cross section vanishes for $q_u \to q_s$ is violated even when $\bar{A}(z) = A(z)$ and $y_1 = y_2$; the photon probes the partonic rather than the overall hadronic structure. From (2), one can see that the angular dependence of the interference term leaves a cross section proportional to $z\bar{z}^2(A^2 + \bar{A}^2)$; thus, in the exclusive limit, the cancellation again becomes complete.

The factor $\sqrt{\bar{z}}$ in eq. (5.7) is also noteworthy; it leads to the vanishing of the amplitude in the exclusive limit, as required by hadron helicity conservation [21]. It must be noted that the light-cone wavefunctions of vector mesons depend on the polarization; thus the total unpolarized cross section for vector meson production will sum contributions from two distinct distribution amplitudes. However, the simple $1+\cos^2\theta$ angular distribution of the cross section for production in transverse polarization states should aid in disentangling the two processes. Also, the decays of vector mesons are to some extent self-analyzing; the polarization of, *e.g.*, a ρ meson can be estimated from the angular distribution of its decay products. Thus at given z, the observed distribution at leading twist of semiexclusive events, integrated over $\mathrm{d}\phi$, should be an incoherent sum of three simple distributions (longitudinal with shape $\sin^2\theta$, and longitudinal or transverse with shape $1 + \cos^2\theta$). Unfortunately, the cross section is dominated by the term proportional to $(1 + \cos^2\theta)$, which mixes both transverse and longitudinal contributions with further contamination from backgrounds (which will have the $1 + \cos^2\theta$ distribution common to inclusive processes). However, we will discuss the potential to extract the other components of the cross section.

5.1.5. Mesons without Flavor

Some mesons, such as the η or π^0, have no nonzero flavor quantum numbers (excepting isospin). Thus they might be formed by diagrams like that of Fig. 5.6, recoiling against a gg system. Note that only pseudoscalar mesons can receive such a contribution at leading twist, as the quark and antiquark spins are anti-aligned.

For definiteness, we will consider $h = \eta$. In computing the amplitude for production of ηgg, we must sum over quark helicities and flavors (since in this case the helicities are no longer observable). We choose to absorb this factor in the hard-scattering amplitude; that is, we present the amplitude

$$\frac{1}{\sqrt{2}}\Big[T_H(e^+e^- \to q_+\bar{q}_- gg) - T_H(e^+e^- \to q_-\bar{q}_+ gg)\Big],$$

but call it T_H since we will obtain the full amplitude by convolving it with the distribution amplitude, as always. The result is

$$T_H(e^-_+e^+_- \to \eta g_\uparrow g_\uparrow) = C_F q_i s^2 \sqrt{\frac{2\bar{z}}{y_{\min}y_{\max}}}\left(\frac{1}{x(1-z\bar{x})} - \frac{1}{\bar{x}(1-zx)}\right); \tag{5.8}$$

$$T_H(e^-_+e^+_- \to \eta g_\uparrow g_\downarrow) = \frac{C_F q_i}{zx\bar{x}}\sqrt{\frac{\bar{z}}{2y_\uparrow y_\downarrow}}\left(c^2 y_\downarrow - s^2 e^{2i\phi} y_\uparrow\right)\left(\frac{1}{1-zx} - \frac{1}{1-z\bar{x}}\right); \tag{5.9}$$

$$T_H(e^-_+e^+_- \to \eta g_\downarrow g_\downarrow) = C_F q_i c^2 \sqrt{\frac{2\bar{z}}{y_{\min}y_{\max}}}\left(-\frac{1}{x(1-z\bar{x})} + \frac{1}{\bar{x}(1-zx)}\right). \tag{5.10}$$

In this case, the color factor is $C_F = \sqrt{2/3}$, not 4/3. In eq. (5.9), we have used the notation $y_{\uparrow,\downarrow}$ instead of $y_{1,2}$ to refer to the two gluon momenta, since the labels 1 and 2 are arbitrary; in eqs. (5.8) and (5.10), we define $y_{\min} = \min\{y_i\}$ and $y_{\max} = \max\{y_i\}$.

The amplitudes for negative-helicity electrons (positive-helicity positrons) are obtained, as always, by the substitution $s \leftrightarrow c$ (Appendix 5.A). However, in either

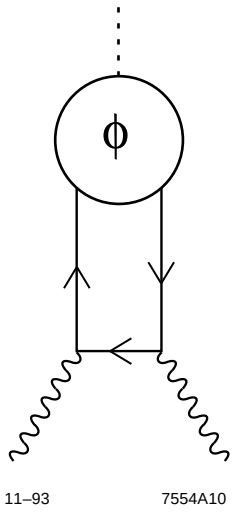

Fig. 5.6. Additional Feynman diagrams which must be considered in the case of flavorless pseudoscalar mesons. As in Fig. 5.1, a sum over attachments of the incoming γ^* is implicit.

case, the amplitudes of eqs. (5.8)–(5.10) are antisymmetric under $x \leftrightarrow \bar{x}$. The wavefunction must be symmetric; thus the full amplitude, obtained by convolving ϕ with T_H, vanishes. We need not treat such mesons any differently than we would flavored states.

5.1.6. Mesons with gg Fock States

Scalar mesons, with spin-parity 0^+, have no $q\bar{q}$ valence Fock state but can mix with a gg state. The lightest and best measured such meson is the $f_0(975)$, which we now consider.

Production in the gg Fock state recoiling against a $q_i\bar{q}_i$ system, shown in Fig. 5.7, proceeds with the hard-scattering amplitude

$$T_H = -C_F \frac{q_i}{2zx\bar{x}y_1y_2}\left[\sqrt{\bar{z}}y_2(1-zx^2)c^2+2\sqrt{y_1y_2}(zx\bar{x}+\bar{z})sce^{i\phi}+\sqrt{\bar{z}}y_1(1-z\bar{x}^2)s^2e^{2i\phi}\right]; \tag{5.11}$$

again, the color factor $C_F = \sqrt{2/3}$.

In eq. (5.11) the quark spins are considered observables, and the quark and antiquark are distinguishable, in contrast to eq. (5.9) in which we sum over spin states in the amplitude, leading to destructive interference in the large-z limit and to antisymmetry under $x \leftrightarrow \bar{x}$. This should emphasize the importance of studying semiexclusive processes only in the domain in which the assumption of duality is accurate; in the exclusive limit $z \to 1$, the processes corresponding to eqs. (5.9) and (5.11) become identical, and both amplitudes vanish.

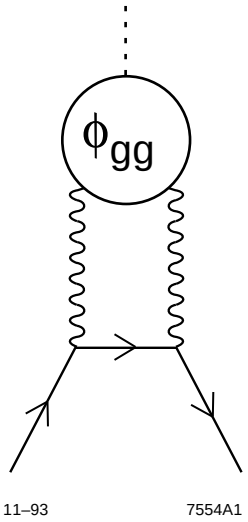

Fig. 5.7. Feynman diagrams contributing to production of a meson in a gg Fock state. Again, a sum over attachments of the γ^* is implicit.

The result of eq. (5.11) shows that the amplitude for scalar meson production in a gg Fock state depends on the distribution amplitude through the quantity

$$f_{h\to gg} \equiv 2\sqrt{3}\int_0^1 \phi_{h\to gg}(x)\mathrm{d}x,$$

where the constant factor is analogous to that of eq. (5.4), and through the integrals B_{gg}, $\bar{B}_{gg}$, and D_{gg}, as defined in eq. (5.5), where the subscript gg reminds us that the distribution amplitude in question is $\phi_{h\to gg}$. However, the distribution amplitude must be symmetric under $x \leftrightarrow \bar{x}$, so we have $B_{gg} = \bar{B}_{gg} = D_{gg}/2$.

The lack of valence $q\bar{q}$ Fock states of 0^+ mesons is a boon to our analysis; any observation of $f_0(975)$ production at leading twist is an unambiguous signal of formation in the gg Fock state. The $f_0(975)$ decays primarily to $\pi\pi$, which should provide a clear experimental signal if it can be distinguished from $\rho(770) \to \pi\pi$.

We can also compute the amplitude for creation of transversely polarized 2^+ mesons in the gg Fock state by requiring that the gluon spins be aligned. The amplitude for this process is

$$T_H{}^{(++)} = -C_F q_i \frac{\sqrt{\bar{z}}}{z^2 x\bar{x}} \frac{1}{y_1 y_2}(c\sqrt{y_2} + se^{i\phi}\sqrt{\bar{z}y_1})(c\sqrt{\bar{z}y_1} - se^{i\phi}\sqrt{y_2}) \tag{5.12}$$

when the gluons have the same helicity as the electron and the outgoing antiquark; the other amplitudes are obtained by $y_1 \leftrightarrow y_2$ and $s \leftrightarrow c$. The lightest such meson is the $f_2(1270)$; again, its signature is decay to $\pi\pi$. The most important backgrounds in this case come from the $f_0(1400)$ and $\rho(1450)$, both of which can also decay to two pions. Also, the suppression of higher-twist terms is less severe at larger mass, so that contamination from $q\bar{q}$ states with $L = S = 1$ must be considered. We will touch upon this point again in Sec. 5.2.3.

Semiexclusive production cross sections for 2^{++} mesons, like those for 1^{--} mesons, sum contributions from the transverse and longitudinal polarization states. Thus the quantities $f_{h\to g_\uparrow g_\downarrow}$, $D_{gg/L}$, and $D_{gg/T}$, where the subscripts L and T denote transverse and longitudinal polarization states, will contribute to the measured cross section for $f_2(1270)$ production.

5.1.7. Z^0 Decays

The channel $e^+e^- \to Z^0 \to HX$ can also contribute to semiexclusive production. Although the suppression by μ^2/Q^2 is far more severe at the Z peak than at the energies we have so far considered, we can still obtain detectable cross sections.

Bjorken *et al.* [23-24] have pointed out that the requirement of a rapidity gap is a natural and effective way to identify processes involving production of color singlets. That is, we may require that the candidate directly-produced meson be isolated in rapidity (or pseudorapidity) with respect to its own axis by some gap ΔY. Indeed, the condition of isolation in a hemisphere can be thought of as a special case of the rapidity gap, where $\Delta Y = \ln(2zE/m_H)$ is a function of z.

For light mesons, *e.g.* $H = K$, isolation in a hemisphere is equivalent to $\Delta Y = 6 + \ln z$. This is unnecessarily drastic; values of $\Delta Y \simeq 4$ should be more than adequate to screen out backgrounds from the hadronization process [25].

Following Ref. [24], we write the weak charge of a fermion as

$$\mathbf{Q}_f \equiv \begin{pmatrix} Q_{f_L} \\ Q_{f_R} \end{pmatrix},$$

containing both the right- and left-handed couplings to the Z. Then the amplitudes for semiexclusive production in Z decays can be obtained from those derived in the

last two sections by the simple substitution $q_f \to \mathbf{Q}_f$, with the understanding that the dot product $\mathbf{Q}_{f_1} \cdot \mathbf{Q}_{f_2}$ is to replace the sum over spins $\sum q_{f_1} q_{f_2}$ in the unpolarized cross section.

We will later see that while the cross sections are much smaller at this energy, the experimental separation of interesting higher-twist physics is somewhat easier. Thus we can hope to observe semiexclusive Z^0 decays.

5.1.8. Crossing

It should be noted that semiexclusive production $e^+e^- \to HX$ is the crossed process corresponding to deep inelastic scattering (DIS) $e^-H \to e^-X$. Thus we expect the cross sections calculated here to bear some relation to the structure functions of DIS.

Indeed, carrying out the crossing operation and evaluating the variables q^2 and x governing DIS, we find $q^2 = -Q^2$, $x = z^{-1}$. Thus semiexclusive production can be said to measure the continuation of the structure function to the region $x > 1$. Indeed, the quantity $[A(z)]^2$ of eq. (5.5) for $z > 1$ shows some properties of a structure function, with a leading-twist pole contribution at $x = z^{-1}$; the resemblance would be more pronounced had we not implemented the simplification of eq. (5.1).

As we shall see in Sec. 5.5, this pole corresponds to the collinear singularity at $y_i = 0$ in semiexclusive production. Part of our task will be to separate the interesting but higher-twist central region where y_i is not small from contamination due to the collinear pole.

5.2. Higher-Twist Corrections

So far, we have been concerned with the leading-twist behavior of semiexclusive amplitudes. In obtaining our results so far, we have made several simplifying assumptions:

- We have neglected all quark masses, which give rise to corrections of order m^2/Q^2 to the helicity amplitudes we have calculated and introduce helicity-flip amplitudes at order m/Q [21].
- We have neglected the mass of the meson H as well as that of the hadronizing quarks in defining our kinematic variables; a more careful definition will change our results by terms on the order of m_H^2/Q^2.
- We have assumed that the quark constituents are perfectly collinear with the hadron comprising them; if we relax this assumption to allow quark transverse momenta $k_\perp$, we will obtain a correction of order $k_\perp^2/Q^2$ [26]. In addition, we have entirely neglected the effects of Sudakov suppression [27] on the amplitude.
- Finally, we have considered only the valence Fock state of the meson, and ignored the possibility of mixing with qqg states. The corrections resulting from a correct treatment of such states, while still suppressed by μ^2/Q^2, have the potential to be numerically large because of the contribution they receive from the endpoints of the distribution amplitude, when one of the constituent partons is very soft.

Let us deal with these corrections, one at a time.

5.2.1. Quark and Meson Mass Effects

Terms of order m/Q in the amplitude involve helicity flips; thus they will contribute only at order m^2/Q^2 to the cross section, as will interference terms between leading-twist amplitudes and $O(m^2/Q^2)$ corrections. We can only hope to distinguish contributions of subleading twist if they show some signature distinguishing them from the leading-twist cross section, which the interference terms will not have. Thus we do not consider such terms, but instead choose to restrict our discussion to the computation of the leading helicity-flip amplitudes.

We account for quark mass terms to first order in m/Q in internal lines by computing all single Higgs insertions on the internal quark line. The effect of mass insertions on external lines is to alter the quark spinor by the substitution (see Appendix 5.A)

$$u_\pm(p) \to u_\pm(p) + \frac{m}{E+|\vec{p}|} u_{(\pm\to\mp)}(p) + O(m^2); \tag{5.13}$$

$u_{(\pm\to\mp)}$ considered as a two-component spinor is numerically identical to $u_\pm$, but corresponds to opposite helicity (*i.e.*, $u_{(\pm\to\mp)} = \gamma^0 u_\pm$, while $v_{(\pm\to\mp)} = -\gamma^0 v_\pm$).

Since we are interested in obtaining quantities with experimental signatures distinct from those of leading-twist semiexclusive production, we must consider the production of transversely polarized vector mesons with an angular distribution other than the $(1+\cos^2\theta)$ distribution obtained from eq. (5.7).

As an example, we consider the amplitude for $e^+e^- \to D^*_\uparrow \bar{c}_+ u_-$. Naively calculating with the substitution of eq. (5.13) yields a divergent expression from the region $x \to 0$, in which the quantity m/xzQ becomes large. In this limit, of course, the first-order expansion in m is invalid. We choose to contain the divergence

by keeping terms of order m^2 in the gluon denominator $(xp + l_1)^2$, which yields uniformly finite expressions.

We are interested in the part of the above amplitude which is proportional to $sce^{i\phi}$. This is (omitting the usual factor of $e^2 g_s^2/Q^2$)

$$-\frac{m_c}{Q}\frac{\sqrt{\bar{z}}}{zx}\left[\frac{2}{z\bar{x}}\frac{y_1}{y_2}q_c + \frac{z + 2\bar{z}y_2}{xy_1 + \bar{z}y_2 m_c^2/z^2 x}q_u\right]. \tag{5.14}$$

The expression in brackets is not numerically large, especially when one considers that the wavefunction is likely concentrated at fairly large x. In fact, it is generally smaller than the amplitude of eq. (5.7), even before the m/Q suppression is taken into account. Thus the higher-twist contribution to the cross section from quark mass terms will be not more than $m_{\mathbf{q}}^2/Q^2$: 3% for D mesons at the Υ_{4s}, and less than 0.5% for B mesons at the Z^0 peak. Since such terms must be disentangled from both the $(1 + \cos^2\theta)$ distribution of most semiexclusive events and the $\sin^2\theta$ component of the distribution of longitudinally polarized mesons, it seems that their experimental measurement is out of the question.

Corrections to the denominators in the expression of the amplitude contribute only at $O(m^2/Q^2)$, and may generally be neglected. However, we must consider their effect on the endpoint behavior in z and y.

The former is fairly simple. The upper bound $z_{\max}$ on z is determined by our assumption of duality; if the mass of the hadronizing system, $\sqrt{\bar{z}}Q$, is too small, that assumption fails, and our predictions are vulnerable to large corrections from poorly understood resonance physics. For light-quark systems, we require $\sqrt{\bar{z}}Q > 2$ GeV [28]. For systems containing a single heavy quark, we should then require $\sqrt{\bar{z}}Q > m_{\mathbf{q}} + 2$ GeV, decreasing the upper limit $z_{\max}$.

The kinematic limit on the back momentum y_1 of the heavy (anti)quark is then $y_1 > m_{\mathbf{q}}^2/\bar{z}Q^2$. The *prima facie* effect of this limit is simply to excise a region of the cross section. However, more careful consideration shows that the interplay between $m_{\mathbf{q}}$ and y_1 also affects the experimental acceptance; we will return to this point in Sec. 5.6.4.

5.2.2. Non-valence Fock States

This is the greatest technical challenge we must face. The difficulty arises from the fact that the regulation of infrared divergences in inclusive processes relies on the cancellation between graphs like those of Figs. 5.8(a) and (b); however, when we demand that the collinear final-state particles form a meson, we risk spoiling this cancellation.

In the consideration of exclusive production in the valence state, the incomplete cancellation of infrared divergences leads to the 'Sudakov suppression' of exclusive production[7,27,29]. The Sudakov form factor for exclusive production of a bare colored particle vanishes in the absence of an infrared cutoff. However, in production of color-singlet states the transverse size of the hadron itself provides a natural infrared cutoff, rendering the Sudakov form factor finite.

Our aim, then, is to compute the contribution from $q\bar{q}g$ Fock states, which correspond to infrared-divergent hard-scattering amplitudes, in a manner consistent with the existing treatment of Sudakov effects. To this end, we consider the prescription of Ref. [1] for the calculation of exclusive amplitudes. In the graphs of Figs. 5.8(b) and (d), let $k_\perp$ denote the gluon's transverse momentum with respect to the hadron direction of motion. If $k_\perp^2$ is smaller than the factorization scale Q^2, we are required to absorb these (possibly nonperturbative) terms into the bound-state

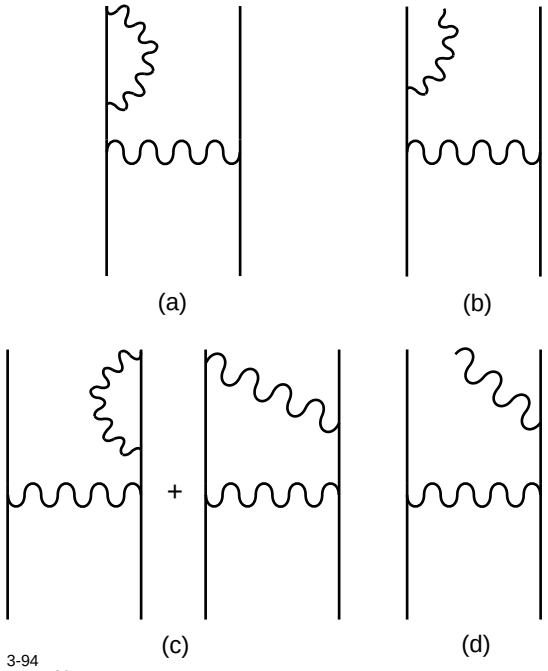

Fig. 5.8. Diagrams which cancel to provide infrared-finite predictions for inclusive amplitudes. (a) shows a higher-order correction to the process of Fig. 5.1; (b) shows a diagram whose collinear divergence cancels against that of (a). In exclusive production, we must consider the diagrams of (a) and (c) to obtain the Sudakov-corrected amplitude for color-singlet production. The factorization prescription, meanwhile, tells us that (b) and (d) are to be excluded from the hard-scattering calculation (but see Fig. 5.9(b)).

dynamics, rather than compute them in pQCD. Conversely, if $k_\perp^2 > Q^2$, the gluon is no longer sufficiently collinear to be included in the distribution amplitude defined in eq. (5.1). Thus we should consistently drop contributions from all such diagrams. One might worry that the remaining sum of diagrams will lack gauge invariance; however, we have verified by explicit computation that the diagrams thus discarded become gauge-invariant in the collinear limit.

Figure 5.9 shows the Feynman diagrams we must evaluate to compute the amplitude for production in the one-gluon Fock state. These diagrams possess no collinear divergences, and their calculation is straightforward. We obtain the hard-scattering amplitude

$$\begin{aligned} T_H^{(+)} = \frac{c^2}{z\sqrt{y_1 y_2}}\Big[\frac{q_s y_1}{\bar{x}_1 x_2(1-zx_1)y_2} - \frac{q_u y_2}{x_1\bar{x}_2(1-zx_2)y_1}\Big]\times \\ \times\Big[C_1(\bar{z}+zx_3)+C_3(\bar{z}+2zx_3)\Big] \\ + C_2 sce^{i\phi}\sqrt{\bar{z}}\Big[\frac{q_s}{x_2(1-z\bar{x}_2)y_2} - \frac{q_u}{x_1(1-z\bar{x}_1)y_1}\Big] \end{aligned} \tag{5.15}$$

for production of pseudoscalar or of longitudinally polarized vector mesons. The color factors $C_1 = -1/3\sqrt{3}$, $C_2 = 8/3\sqrt{3}$, and $C_3 = i\sqrt{3}$ correspond to the diagrams of Figs. 5.9(a), (b), and (c), respectively.

Like the helicity-violating amplitudes of the previous section, the amplitudes for production in a non-valence state can best be measured in regions where leading-twist production is forbidden. Thus we again consider the production of transversely polarized vector mesons. The full hard-scattering amplitude is quite awkward; however, since we are interested in production with a $\sin^2\theta$ angular distribution, we present only the part proportional to $\sin\theta$:

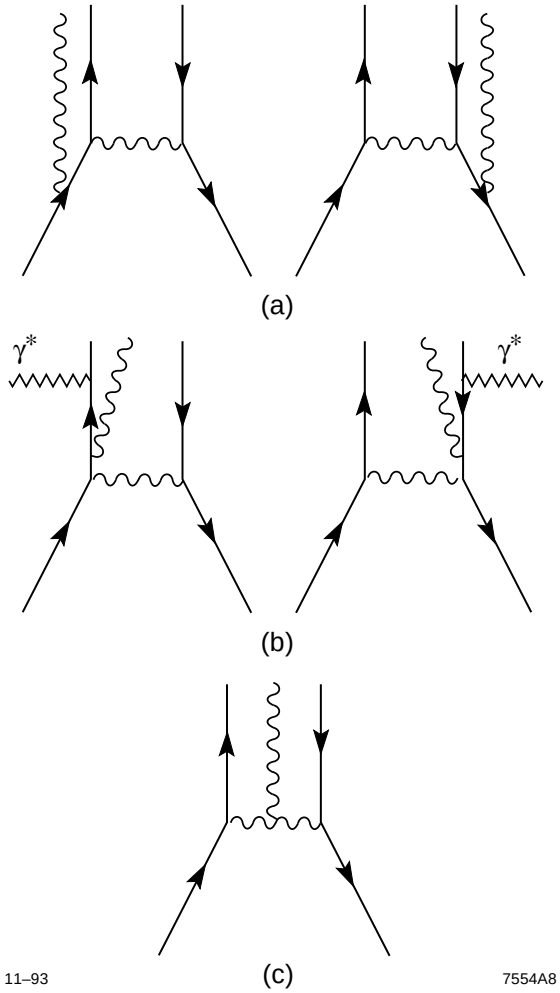

Fig. 5.9. The Feynman diagram topologies which must be included in the amplitude for production of a meson in a $q\bar{q}g$ Fock state. In (a) and (c), a sum over all possible attachments of the γ^* is implicit. In (b), however, only the specific attachment shown should be used; the rest are considered in Figs. 5.8(b) and (d).

$$\tilde{T}_H^{(+)} = \frac{e^2 g_s^3}{Q^3}\sqrt{\bar{z}}\Bigg\{ -\frac{C_1 q_u}{x_1(1-z\bar{x}_1)}\frac{y_2}{y_1} + \frac{C_3 q_s}{z\bar{x}_1 x_2}\Big[\frac{1}{y_1} - \frac{z+y_1}{zy_2} + \frac{1}{1-zx_1}\Big] + \frac{2C_2}{z^2}\Bigg(\frac{q_s}{x_2 y_2}\Big[\frac{1}{x_3\bar{x}_3} - \frac{y_1}{\bar{x}_1}\Big] - \frac{q_u}{x_3}\Big[\frac{1-zx_3}{x_1\bar{x}_3} + \frac{y_2}{\bar{x}_2 y_1}\Big]\Bigg)\Bigg\}. \tag{5.16}$$

Again, no numerically large coefficients appear. While the gluon is expected to carry less average momentum than the quarks, the distribution amplitude is suppressed by x_3^2 as $x_3 \to 0$, because a very soft gluon cannot couple to a singlet $q\bar{q}$ state. Thus $\langle x_3^{-1} \rangle$ is not extremely large. Also, in this case the suppression factor is μ/Q, where $\mu \lesssim 0.5$ GeV does not depend on quark masses; thus higher-twist contribution to the cross section will probably be invisibly small. To proceed further, we need information about the distribution amplitude $\phi_{h\to q\bar{q}g}$; this is the subject of the next section.

5.2.3. Non-valence Distribution Amplitudes

In order to estimate the size of the contribution to the semiexclusive cross section from the higher-twist terms of the preceding section, we must have some model of the meson distribution amplitudes for the non-valence states in question.

One approach to this problem is undertaken by Zhitnitskiĭ *et al.* [30], who extend the sum-rule approach of Refs. [13–15] to wavefunctions of nonleading twist. They propose model distribution amplitudes for the $q\bar{q}g$ states of the π and ρ: we are interested in the distribution $\phi_{3\rho}^V$ of transversely polarized ρ mesons [31]. The sum-rule model distribution is

$$2520 f_{3\rho} x_1 x_2 x_3^2 (x_1 - x_2)(7 - 15x_3),$$

where $f_{3\rho} \simeq 3.5 \cdot 10^{-3}$ GeV^2; thus, when convolving the hard-scattering amplitude and distribution amplitude, we must replace

$$\frac{1}{\bar{x}_2 x_3} \to -14 f_{3\rho}, \qquad \frac{1}{\bar{x}_1 x_2} \to 28 f_{3\rho}, \qquad \text{and} \quad \frac{1}{x_2 x_3 \bar{x}_3} \to 35 f_{3\rho} \simeq 0.12 \text{ GeV}^2. \tag{5.17}$$

Thus the extreme smallness of $f_{3\rho}/Q$ more than counterbalances the numerical enhancement from the factors of x_i in the denominator.

Comparison of eqs. (5.14) and (5.16)–(5.17) suggests that, in light mesons, quark mass effects are more important than effects from non-valence Fock states for $m_{\mathbf{q}} \gtrsim 700$ MeV. Of course, this is an extremely rough estimate. However, for our purposes it is sufficient to demonstrate that production in non-valence Fock states does not provide a measurable signal.

5.2.4. Orbital Angular Momentum

We can compute the corrections of order μ/Q resulting from our neglect of Fock states with nonzero orbital angular momentum by including a small transverse momentum $\pm\epsilon_\perp$ in the spinors $u_\pm(p)$ of Appendix 5.A. Specifically, we wish to consider the contribution from hard scatterings like $e^+e^- \to s_- \bar{d}_- X \to K_L^* X$.

The wavefunction must carry a unit of orbital angular momentum, in order to offset the difference in the spin states of the meson and of its quark constituents. Thus the moment of $\epsilon_x + i\epsilon_y$, and with it all such terms in the amplitude, vanished, while $\epsilon_x + i\epsilon_y$ may be replaced with some typical transverse momentum μ.

For example, the term of order μ/Q and proportional to $\sin\theta$ in the amplitude for semiexclusive production of longitudinally polarized K^* mesons is

$$sce^{-i\phi}\sqrt{\bar{z}}\Big[\frac{xq_s}{\bar{x}(1-zx)y_2} - \frac{\bar{x}q_d}{x(1-z\bar{x})y_1}\Big]. \tag{5.18}$$

Neglecting the factor μ/Q, this is numerically smaller than the corresponding term in eq. (5.14); thus the error which its neglect introduces into our calculations is negligible, while the chance of measuring its contribution separately is remote.

5.3. Sudakov Effects and the Running Coupling

So far, we have neglected the running of the strong coupling constant α_s. While this is technically a correction at next-to-leading logarithmic order, it assumes great importance in exclusive reactions because of the divergence of the one-loop running coupling

$$\alpha_s(Q^2) \equiv \frac{4\pi}{\beta \ln(Q^2/\Lambda^2_{\rm QCD})}$$

as $Q^2 \to \Lambda^2$.

It is our belief that too much has been made of this divergence, which stems from an extrapolation using the lowest-order (one-loop) QCD β function into precisely that region in which the lowest-order approximation is invalid. Nonetheless, in the absence of a better form, one would be obliged to use this coupling. The recent work of Mattingly and Stevenson [32] suggests that there is, indeed, a better form; we shall return to this point in Sec. 5.4.1.

The soft divergence of α_s affects the computation of exclusive amplitudes even at large momentum transfer, because the gluon virtuality can still be small near the endpoints $x \to 0$, $x \to 1$. In a proper higher-order treatment, we would use a scale-setting procedure, such as BLM [33], to fix the argument of the running coupling α_s through the entire process. However, this is not satisfactory for our purposes for two reasons.

The first and most concrete is that the scale can only be set to given order in α_s when the perturbative coefficients have been obtained to one higher order. Thus no scale-setting is possible when only a tree-level amplitude has been computed, as is the case here.

The second objection is more fundamental: since the momentum transfer through the internal gluon depends on the hadron's distribution amplitude, a single scale cannot consistently be set for all possible distributions. Instead, the model wavefunction enters into the scale, resulting in a formula of redoubled complexity. This is a true physical effect, not an artifact of the procedure; for example, a wavefunction which is very strongly suppressed at the endpoints will certainly yield a larger mean value of q^2 than will one which is concentrated there.

Thus we must allow the argument of α_s to depend on the momentum fraction x in the hard-scattering process. At first glance, this seems to threaten the finiteness of our results. However, the work of Sudakov and of Mueller [27] demonstrates that exclusive amplitudes remain finite.

Heuristically, the picture is as follows: the coupling can only grow large when the gluon propagates for a large distance (of order $\Lambda_{\rm QCD}^{-1}$) in transverse position space. In this case, the constituents of the final-state hadron are widely separated and have a large color dipole moment. Thus the probability that they will emit final-state radiation, in which case the process is *ipso facto* not exclusive, approaches 1.

Mueller [27] derived the quantitative effects of this Sudakov suppression to leading logarithmic order, and Botts and Sterman [29] extended them to next-to-leading order (in $\ln Q$). We do not wish to use the entire machinery thus derived, but instead will take the low road, absorbing the leading effects of Sudakov suppression into an effective coupling constant $\alpha_{\rm eff}$.

To incorporate Sudakov suppression into the calculation of exclusive amplitudes, we must undo the simplification of eq. (5.2). However, we use the wavefunction and propagator not in momentum space, but in the hybrid space of longitudinal momentum and transverse position:

$$\frac{\alpha_s(q^2)}{q^2} \to \frac{1}{\pi}\int \mathrm{d}^2 b\; K_0(b|q|)\alpha_s(q^2), \tag{5.19}$$

where K_0 is a modified Bessel function. The form of eq. (5.1) is regained if we assume that the wavefunction is independent of b (*i.e.*, that it is proportional to $\delta^2(k_\perp)$). Here and in the following, we assume that q is a purely longitudinal momentum (otherwise see Ref. [7]).

When q^2 is small the proper argument of α_s is not q^2, but rather $\max\{q^2, b^{-2}\}$: the coupling cannot grow large if the gluon propagates over only a short distance [34].

The form of the Sudakov suppression given by Botts and Sterman [29] vanishes as $|b| \to \Lambda^{-1}$ sufficiently rapidly to contain the divergence of α_s in the same limit. For $q^2 > \Lambda^2$, the effect of Sudakov suppression is expressed by the substitution

$$\int K_0(b|q|)\alpha_s(q^2) b\; \mathrm{d}b \to \int_0^{\Lambda^{-1}} e^{-S(b,q)} K_0(b|q|)\alpha_s\big(\max\{q^2, b^{-2}\}\big) b\; \mathrm{d}b, \tag{5.20}$$

where $S(b,q)$ diverges as $b \to \Lambda^{-1}$. The contribution from the region $b > \Lambda^{-1}$ in eq. (5.19) is in any case suppressed by e^{-q^2/Λ^2}, so the main effect for substantial q^2 is the correction to α_s for very small b (which contributes at $O(1/\ln q^2)$ to the amplitude).

For small q^2, the problem is much thornier; the quantitative behavior of the Sudakov suppression comes into play. We take advantage of the fact that the factor

$\alpha_s(b^{-2})$ which enters into the tree-level amplitude as computed by eq. (5.19) is precisely the same as the coupling α_s which controls final-state radiation and leads to the Sudakov suppression, and use in place of eq. (5.20) the *ansatz*

$$\int^{\Lambda^{-1}} \min_{b' \le b} \Big\{ K_0(b'|q|) \alpha_s\big(\max\{q^2, b'^{-2}\}\big) \Big\} b \, \mathrm{d}b \equiv \frac{\alpha_{\mathrm{eff}}(q^2)}{q^2}. \tag{5.21}$$

That is, we postulate that the physical amplitude for exclusive processes does not increase with b and use that assumption to derive a finite form for the effective gluon propagator. In fact, since $K_0(x)$ diverges only logarithmically as $x \to 0$, this formula yields

$$\alpha_{\mathrm{eff}}(q^2) \sim \frac{q^2}{2\Lambda^2} \frac{4\pi}{\beta \ln(\Lambda^2/q^2)} \qquad \text{as } q^2 \to 0;$$

the finite size of hadrons means that the amplitude for exclusive production increases more slowly than $1/q^2$ for small q^2.

This procedure requires some justification. Our reasoning is that the exclusive production amplitude should not increase with increasing transverse size, as demonstrated in the observation of color transparency [35]. At large q^2, where the Sudakov suppression is well understood, our method reproduces the results of Refs. [27,29] to leading order in $\ln q^2$. Thus we are willing to accept its predictions in the comparatively poorly understood region of small q^2, where the results of Ref. [29] are themselves subject to substantial parametric uncertainties [36].

Finally, this method offers striking ease of computation. Equation (5.21) can be integrated numerically to obtain the values of α_{eff} at all q^2. The result is shown in Fig. 5.10. The only parameter involved in the determination of α_{eff} is Λ_{QCD} itself.

Unfortunately, this parameter is not yet well determined; current experimental results give

$$\Lambda^{(3)}_{\overline{\rm MS}} = 318^{+58}_{-51}\ {\rm MeV}.$$

The resulting uncertainty in our cross sections is 15%, which is numerically equal to the uncertainty in $\alpha_s(Q = 3\ {\rm GeV})$: that is, the Λ-dependence of the cross section does not reflect a sensitivity to soft physics, but an imprecision in the size of the QCD coupling at moderate momentum transfer.

It must be emphasized that the effective coupling $\alpha_{\rm eff}$ has no applicability outside the domain of exclusive or semiexclusive reactions, since its finiteness results from the finite transverse size of hadrons. It could be argued that we have underestimated $\alpha_{\rm eff}$ by ignoring the possibility that the final-state radiation might be absorbed into the hadron, thus preserving the exclusivity of the reaction; however, such an effect involves the intrinsically soft process of long-distance hadronization, and the events resulting from it will share the characteristics of soft events, rather than of the hard direct processes in which we are interested. Thus we regard such a contribution not as an additional component of the signal, but as a part of the background which should be amenable to calculation with standard Monte Carlo techniques. Also note that the vanishing of the effective coupling, which seems strongly counter-intuitive, is in fact simply a restatement of the fact that the effective propagator diverges less slowly than $1/q^2$ for small q: clearly, the same result is obtained in methods using intrinsic transverse momentum smearing or an artificial gluon mass.

The latter technique is commonly used in the computation of spacelike scattering amplitudes, since an effective gluon mass regulates the divergence of the propagator [37]. This is intended to model the physical effects of the intrinsic transverse

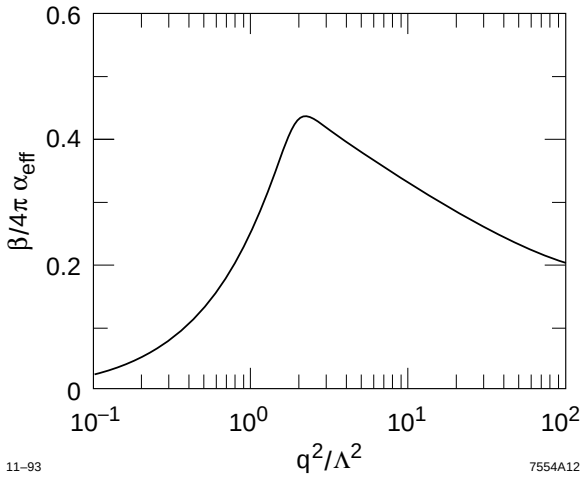

Fig. 5.10. The effective coupling constant $\alpha_{\rm eff}$ as a function of the gluon virtuality q^2.

momenta within the hadron, which serve to eliminate collinear divergences. We could extend the same approach to the timelike process under consideration, though an imaginary gluon mass would be required. A more accurate treatment could be achieved by inserting a term representing the transverse distribution of the wavefunction [7],

$$\psi_x(k_\perp) \equiv \frac{\psi(x, k_\perp)}{\phi(x)},$$

into the integration of eq. (5.19), again obtaining an effective coupling which will vanish as $q^2 \ln q^2$ at small longitudinal momentum transfer.

In practice, however, hadronic amplitudes are insensitive to the transverse wavefunction. This is especially true when the Sudakov suppression, which forces the hadron to be formed at small impact parameter, is also considered [7]. Thus we do not expect intrinsic transverse momenta to have a great effect on our results.

In order to test the sensitivity of our results to our assumptions about the effective coupling, we also computed the cross sections with the effective coupling

$$\alpha_s = \frac{4\pi}{\beta \ln (Q^2 + m_g^2)/\Lambda^2}, \tag{5.22}$$

where $m_g = 1.2\ \Lambda$ was chosen to match the value

$$\lim_{q^2 \to 0} \alpha_s(q^2) = 0.82$$

obtained by Mattingly and Stevenson [32,38]. The predicted cross sections at $\sqrt{s} \simeq 10$ GeV were altered by less than 10%, illustrating the relative insensitivity of semiexclusive production to the niceties of soft physics.

5.4. Higher-Order Corrections

Before we can have faith in the results we have derived thus far, we must know whether they will be overwhelmed by $O(\alpha_s)$ corrections. We begin by classifying all such corrections.

The first-order corrections to the production mechanism of Fig. 5.1 are obtained by attaching an additional gluon line to the hadronic topology. Some of the ways in which it may be attached are familiar and have already been dealt with in other contexts.

For example, the higher-order corrections of Fig. 5.11(b) are precisely analogous to those which modify the total cross section $\sigma_{\rm tot}(e^+e^- \to \text{hadrons})$, since they are completely internal to the color-singlet recoil system. Thus we can, with no calculation whatsoever, be assured that their entire effect is to increase the total measured cross section by a factor $(1 + \alpha_s(\bar{z}Q^2)/\pi)$[39].

Similarly, the diagrams of Fig. 5.11(c) are the same as those which contribute to the study of purely exclusive processes. When the internal gluon momentum q is small compared to the momentum scale Q of the hard process, it may be considered internal to the meson and treated as a correction to the wavefunction.

This brief catalog leaves only two cases uncovered. First, differentiation between diagrams like that of Figs. 5.11(b) and (c) is not perfectly well-defined, and there will be cases where $q \sim Q$. However, the resulting corrections are suppressed by $\log(Q^2/\mu^2)$ relative to those in which one of the gluon momenta is soft, and we may safely ignore them in this work.

Second, there are unfactorized soft contributions like that shown in Fig. 5.12. As described in Ref. [29], these give rise to the Sudakov suppression of exclusive

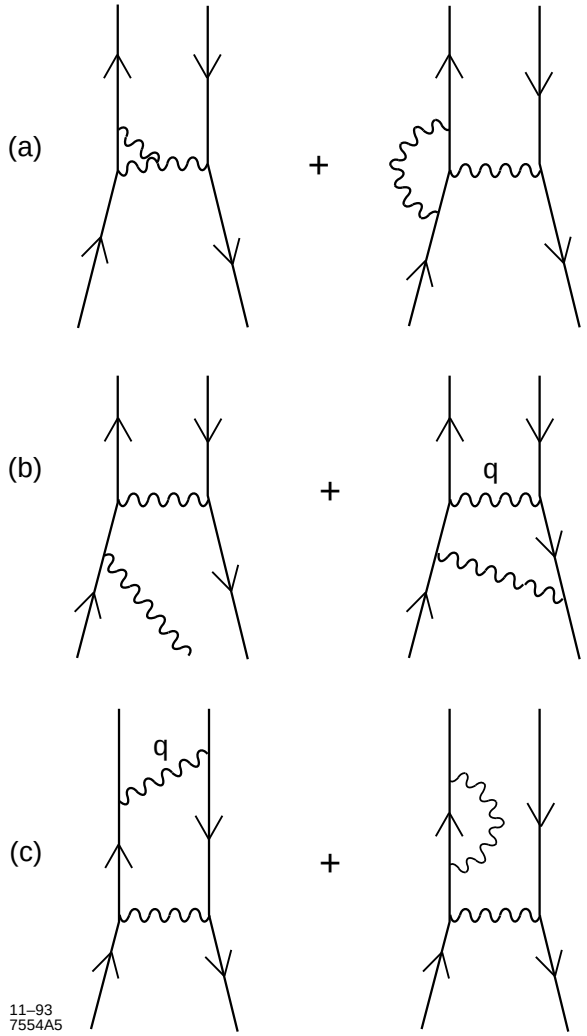

Fig. 5.11. Some diagrams which will yield $O(\alpha_s)$ corrections to the amplitude. (a) is simply a vertex correction. (b) is familiar, when $q^2 \sim Q^2$, from the analysis of inclusive production. (c), with $q^2 \ll Q^2$, is 'factorizable' – internal to the meson – and will have the same effect here as in exclusive processes.

amplitudes; the same suppression applies in the semiexclusive case, and we considered its effects in Sec. 5.3.

5.4.1. The Infrared-stable Coupling

In a recent paper [32], Mattingly and Stevenson show that the third-order corrections to $R_{e^+e^-}$ [40] lead, through the use of perturbation theory optimized with the PMS scale-setting method [41], to a form of the coupling which approaches a constant limit as $q^2 \to 0$. A fit to experimental data on $R_{e^+e^-}$ yields a limiting value $\alpha_s(q^2 \to 0) \simeq 0.82$.

Thus we may choose to adopt a more conservative approach than that described in Sec. 5.3, and merely use the coupling of Ref. [32] throughout our numerical calculation [38]. In actuality, neither approach is perfectly satisfactory. The suppression of the effective coupling due to the finite size of hadrons is a physical effect, which the naive insertion of α_s into exclusive amplitudes ignores; but the form of Ref. [29] for the Sudakov suppression is partly predicated on the low-q^2 divergence of the coupling, and is now subject at least to quantitative revisions which are outside the scope of this thesis.

In practice, the use of $\alpha_{\rm eff}$ has the virtue that it naturally incorporates Sudakov effects which serve to contain the collinear (small-y_i) divergence that appears in the tree-level amplitudes of eqs. (5.6) and (5.7), and to improve the numerical behavior near the endpoints. The physics of this apparent divergence and the means by which the correct endpoint behavior may be computed are the subjects of the next section.

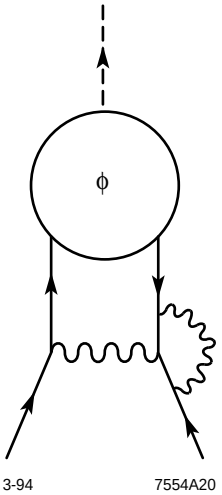

Fig. 5.12. Non-factorizable soft contributions to the hard-scattering amplitude T_H, which lead to Sudakov suppression.

5.5. The Small-y Collinear Divergence

The tree-level amplitudes of eqs. (5.6)–(5.11) diverge for $y_i \to 0$, as the internal gluon approaches its mass shell. This apparent divergence is in fact controlled by several corrections which become important in this limit. We will discuss some of them, in order of importance.

5.5.1. Wavefunction vs. Distribution Amplitude

The factorization of eq. (5.1), which assumes that T_H depends only weakly on the internal momenta $k_\perp$, is clearly invalid when the momentum transfer $y_i Q^2$ of the exchanged gluon becomes comparable to a typical hadronic momentum scale μ^2.

At this point, we must undo the factorization used in eq. (5.2), and instead consider diagrams like those shown in Fig. 5.13. In this region, the diagram of Fig. 5.13(b) is suppressed by a factor of y_i relative to that of Fig. 5.13(a) and may safely be neglected. The amplitude may then be evaluated in terms of the quark fragmentation amplitude $\psi_{q\to hQ}$. To leading order in y_i, we obtain

$$\mathcal{M}^{(+)} = e^2 q_i C_F \, c^2 \psi_{q\to hQ}(z, j_\perp), \qquad \text{where} \quad j_\perp^2 = z^2 \bar{z} y_i Q^2,$$

the color factor $C_F = \sqrt{3}$, and q_i is the QED charge of the quark q.

Thus

$$\begin{aligned} \int_0^{y_{\rm crit}} \mathrm{d}y_1 \; |\mathcal{M}^{(+)}|^2 &= 3e^4 q_i^2 \, c^4 \int_0^{zQ\sqrt{\bar{z}y_{\rm crit}}} \frac{\mathrm{d}^2 j_\perp}{\pi z^2 \bar{z} Q^2} |\psi(z, j_\perp)|^2 \\ &= \frac{768\pi^4 \alpha^2 q_i^2}{z^2 \bar{z} Q^2} \, c^4 \tilde{g}_{h/q}(z; zQ\sqrt{\bar{z}y_{\rm crit}}), \end{aligned} \tag{5.23}$$

where

$$\int^{Q_0} \frac{\mathrm{d}^2 k_\perp}{16\pi^3} |\psi(x, k_\perp)|^2 \equiv \tilde{g}_{h/q}(x; Q_0) \le G_{h/q}(x; Q_0);$$

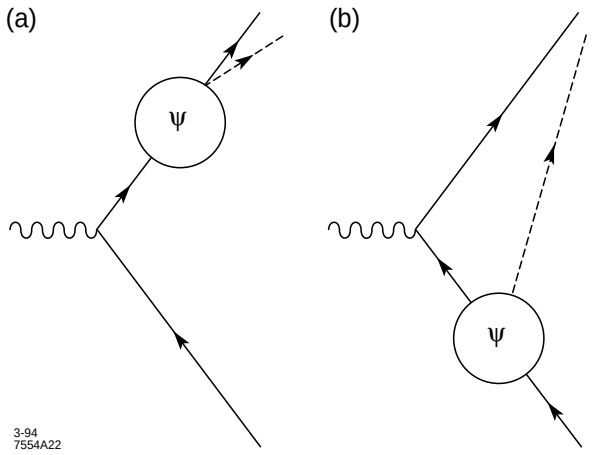

Fig. 5.13. The diagrams contributing to the semiexclusive production amplitude at small y_1. (a) shows the leading-twist part, (b) a higher-twist part.

here $G_{h/q}(x)$ is the fragmentation function for finding a meson h inside the quark q at momentum transfer Q_0. The full fragmentation amplitude G differs from $\tilde{g}$ in that G includes a sum over all Fock states, while $\tilde{g}$ receives a contribution only from the exclusive 'decay' $q \to hQ$. At large z, however, this difference should vanish; it is expected that the valence Fock state dominates the structure and fragmentation functions at large x.

Combining eqs. (5.23) and (5.3), we find that the total spin-averaged contribution to the cross section from the region $y < y_{\rm crit}$ is

$$\mathrm{d}\sigma = \frac{3\pi\alpha^2 q_i^2}{8zQ^2}\tilde{g}_{h/q}(z; zQ\sqrt{\bar{z}y_{\rm crit}})(1+\cos^2\theta)\mathrm{d}\cos\theta\,\mathrm{d}z. \tag{5.24}$$

We have integrated out the trivial ϕ-dependence.

Several things about the contribution to the cross section given by eq. (5.24) are noteworthy. First, and most disturbing, it is leading-twist; the suppression of the cross section is only Q^{-2}. Thus we must take great care to separate the higher-twist direct production in which we are interested from this 'direct fragmentation' contamination.

That this is possible at all is due to the nature of the hadronization process. At high energies, where the extra Q^{-2} suppression of the semiexclusive signal is severe, the jets inherit the parton momenta; thus the small-y region can be identified and discarded with great accuracy. In order to pass cuts designed to ensure that the meson is produced with a high degree of isolation, the events described by eq. (5.24) must be transformed in the hadronization process into events in which no jet is near the meson; the probability that this will occur is suppressed by Q^{-2} for large Q. The leopard can change his spots, but it requires an intrinsically higher-twist

process. Thus the signal for semiexclusive production at moderate y_i is in principle measurable even at arbitrarily large Q^2.

In fact, the signal from the collinear region which passes the event shape cuts resembles a higher-order correction to the tree-level semiexclusive signal. To see this, recall that a hard gluon must be exchanged between the quark and antiquark in the recoil system, so that jets will not form near the meson. Adding this gluon to the tree-level diagram of Fig. 5.1, we get the diagram of Fig. 5.11(c); the soft gluon which appears in near-collinear tree-level production corresponds to a soft gluon internal to the meson in the more complete picture.

Two complications, however, prevent us from lightly discarding the collinear region from consideration. First, many interactions can take place between the near-collinear quark and meson, rather than the single gluon exchange which appears in the perturbative computation. Second, the momentum transfer between the outgoing quark and antiquark also need not be carried by a single gluon, since we do not demand exclusivity and are unable to completely specify the final-state momenta. As a result, such contributions lack a perturbatively calculable hard scattering and must be treated by Monte Carlo techniques.

To estimate the contribution to the measured semiexclusive cross section, we need to model the fragmentation function $\tilde{g}$. Since we are interested in the region of large z, we will assume

$$\tilde{g}(z) = G(z); \tag{5.25}$$

this is a somewhat pessimistic but not inaccurate assumption. The structure functions $G(x)$ near $x = 1$ are expected to have the form

$$G(x; Q^2) = C(1-x)^2 + \frac{D}{Q^2},$$

where C is a dimensionless constant parametrizing the leading-twist behavior, and D represents higher-twist terms [22]. The approximate forms

$$G_{\pi^+/u}(x) = G_{\pi^-/d}(x) = 1.54(1-x)^2 \qquad \text{and} \quad G_{\pi^-/u}(x) = G_{\pi^+/d}(x) = 0.54(1-x)^2$$

fit the experimental observations [42] within statistical errors. We are not interested in the higher-twist corrections, which share the Q^{-4} behavior of the semiexclusive signal and will make a negligible contribution to the signal after experimental cuts.

Thus, summing over quark and antiquark flavors and assuming $SU(3)$ symmetry, we obtain the estimate

$$\mathrm{d}\sigma = C_h \frac{\alpha^2}{Q^2} \frac{\bar{z}^2}{z} \mathrm{d}z \; (1 + \cos^2\theta) \mathrm{d}\cos\theta, \tag{5.26}$$

where $C_h = 1.50$ for π and $K^\pm$, and $C_h = 1.11$ for K^0 and $\bar{K}^0$. This is not a small effect, but rather comprises a substantial fraction of all events!

Since the backgrounds of this sort are so substantial and involve no short-distance physics in the jet formation process, we expect that they will be well simulated by Monte Carlo models. Thus we defer further analysis of this region to Sec. 5.6, where we will examine hadronization effects. We will see that a judicious combination of experimental cuts can reduce the contamination from the endpoints to acceptable levels.

5.5.2. Multiple Scatterings and $y_{\rm crit}$

To accurately predict the rate of semiexclusive production, we must obtain a good estimate of the value $y_{\rm crit}$ at which the factorization of eq. (5.2) is no longer reliable.

Let us consider the physical picture of direct pQCD production, shown in Fig. 5.14. Semiexclusive production depends on the hadron's undergoing no final-state interactions, and this can only proceed if the quark interacts with the antiquark before scattering from the hadron.

Thus we parametrize the rates A_h and $A_{\bar{q}}$ for the quark to interact with the hadron and antiquark, respectively. Neglecting for the moment the running of the coupling strength, we obtain

$$\frac{A_h}{A_{\bar{q}}} = \frac{\bar{z}^2\mu^2}{z^2 y_2^2 Q^2} \qquad \Rightarrow \quad y_{\rm crit} \simeq \frac{\bar{z}}{z}\Big(\frac{\mu}{Q}\Big); \tag{5.27}$$

the factor of μ^3/Q^2 comes from comparison of the $1/r^2$ behavior of the interactions between nonsinglet particles to their $1/r^4$ 'tidal' interactions with singlet particles [43]. As Q increases, the degree of collinearity of the meson constituents increases, and $y_{\rm crit}$ must decrease. Including the running of the QCD coupling would decrease this estimate somewhat, but since the energy of the qh system grows as a power of Q, the behavior given in eq. (5.27) will still hold.

The wavefunction of Fig. 5.13 takes into account all such multiple scatterings; $G_{h/q}(z)$ should be interpreted as the amplitude for the hard probe from the recoil antiquark to find the quark in a qh state. Thus the prediction of eq. (5.24) is unaffected by multiple hard scatterings, as long as the assumption of eq. (5.25) holds.

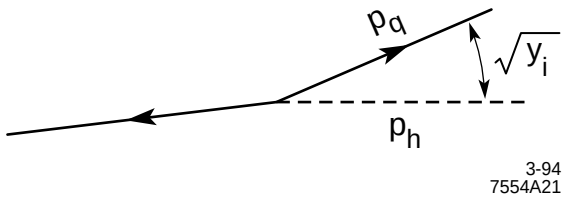

Fig. 5.14. The physical picture of direct meson production at leading order. Final-state interactions are more likely between particles which emerge in close proximity.

For $y > y_{\rm crit}$, the squared invariant mass of the qh system is at least $zy_{\rm crit}Q^2 \simeq \bar{z}\mu Q \gg \mu^2$, so that once multiple scattering occurs the probability of finding the original qh system again in a qh state may be neglected. Thus we account for the possibility of multiple scattering for $y > y_{\rm crit}$ by including a suppression factor

$$\frac{A_{\bar{q}}}{A_h + A_{\bar{q}}} = \left(1 + \frac{y_{\rm crit}^2}{y^2}\right)^{-1}$$

in the computation of the cross section.

5.5.3. Other Soft Corrections

Other intrinsically soft processes will affect the behavior of the amplitude near the collinear pole. For example, terms proportional to the intrinsic transverse momenta will be less thoroughly suppressed, so that formation in Fock states with $L_z \neq 0$ will proceed with probability $\mu/y_{\rm crit}Q$; however, this is still a small number, scaling as $Q^{-1/2}$. Since we will see that our experimental cuts effectively exclude the small-y region, we do not consider this possibility further.

The finite size of hadrons, as enforced by Sudakov suppression [7,27,29,44], where the tendency of large color dipoles to emit final-state radiation suppresses the effective wavefunction at large impact parameter b, has been dealt with in Sec. 5.3. The conclusions reached there are certainly invalid at the collinear pole itself, however, since the process by which the hadron is formed is itself soft. Indeed, the result of eq. (5.24) implicitly accounts for all soft corrections by absorbing them into the measured fragmentation function. However, Sudakov effects should be important for $y_i > y_{\rm crit}$; we will return to this point in the next section.

5.5.4. Sensitivity to $y_{\rm crit}$

Our focus will be on finding experimental cuts which isolate the 'good' region $y > y_{\rm crit}$ from the dangerous region in which multiple scattering becomes important. We must, however, be able to estimate the contribution from the small-y endpoints, so that we may be sure that our predictions are trustworthy.

We have now dealt with the region $y < y_{\rm crit}$ unambiguously, and have found that standard Monte Carlo techniques should represent it accurately. One difficulty remains: the sensitivity of our results to $y_{\rm crit}$. Clearly, in a correct treatment which accounts properly for the contributions from all values of y, the precise value of $y_{\rm crit}$ should be irrelevant. However, this is far from the case here—since the differential cross section from eq. (5.6) diverges like y_i^{-2}, we may see a power-law dependence on $y_{\rm crit}^{-1} \sim Q/\mu$ in our results.

What physical mechanisms are important in this region? Since the transfer is of order $y_i Q^2 \sim \mu Q$, the process is still perturbative, but approaching the soft region. This is precisely the domain in which Sudakov effects become important [44].

With the effective coupling program implemented in Sec. 5.3, we find that the inclusion (albeit in a somewhat naive manner) of Sudakov effects naturally regulates the small-x and small-y divergences of amplitudes like that of eq. (5.6). While we cannot trust the inherently perturbative mechanisms employed in this derivation in the region $y < y_{\rm crit}$, they should be reasonably accurate in the region $y > y_{\rm crit}$ where the momentum transfer $y_i Q^2$ is large enough to allow a perturbation expansion. Thus in this region the effective-coupling method is insensitive to parametric variations[45]. One feature of this effective coupling is its $q^2 \ln q^2$ behavior at small q^2. Since the gluon virtuality vanishes in the limit $y_i \to 0$ with which we are concerned, use of the effective coupling replaces the

$1/y$ divergences of eqs. (5.6)–(5.12) with integrable $\ln y$ divergences. However, the numerical behavior at the endpoints is still unfriendly, and depends on the value of $\Lambda_{\rm QCD}$. We will depend on stringent experimental cuts to eliminate the dependence on endpoint behavior, and thus on our treatment of soft physics, of the observed cross sections after integration over y.

5.6. Hadronization Effects

In Refs. [3] and [5], it was assumed that the width of the (angular or rapidity) gap by which the directly produced meson was isolated would be unchanged by the hadronization process; *i.e.*, that the products of hadronization will fill the region of phase space spanned by the free partons, but not spill out of it. We shall see that this naive assumption is highly misleading.

Since we are concerned with the intrinsically soft process of hadronization, we may use a phenomenological model of such processes, the Lund Monte Carlo generator [46].

Most of our attention will be devoted to two cases: $Q \simeq 10$ GeV, where B factories may operate in the near future, and $Q = m_Z$. In the former case we will enforce the condition of isolation by requiring either an angular gap (in the center-of-momentum frame) or a rapidity gap [24] between the candidate directly produced meson and the other products of hadronization; in the latter, we will use isolation in rapidity space exclusively.

5.6.1. Isolation Cuts

The first order of business is to demand a high degree of isolation of the candidate directly produced meson in order to reject backgrounds from inclusive processes. In each case, we used the LUND Monte Carlo generator to model the development of the recoil system. As explained previously, since the hard physics does not influence the hadronization process, we expect such a simulation to be very accurate. We studied the hadronization of $u\bar{u}$ systems with the initial state momenta given by the kinematics of Sec. 5.1.

Most of the systems we are interested in are asymmetric systems such as $u\bar{s}$; however, since the dynamics of hadronization are flavor independent, we confidently expect that the errors thus introduced are negligible for light (uds) systems. We will return to the issue of heavy quarks later.

Given the kinematic variables z and y_1, we can define cumulative acceptance functions:

- $P_{\rm ang}(\theta; z, y_1)$ is the fraction of events at given z and y_1 in which the directly produced meson is isolated by a cone of opening half-angle θ in the event center-of-momentum frame;
- $P_{p_z}(p_{\rm cut}; z, y_1)$ is the fraction of events in which no particle except the directly produced meson has $p_z > p_{\rm cut}$ [47]; and
- $P_{\rm rap}(Y_{\rm max}; z, y_1)$ is the fraction of events in which no particle has rapidity greater than $Y_{\rm max}$ along the $\hat{z}$-axis [24,48].

The regions of momentum space excluded by these cuts are shown in Fig. 5.15. Intuitively, one can see the advantage of the rapidity gap: it is not greatly affected by either soft physics in the same hemisphere or hard physics at large angles.

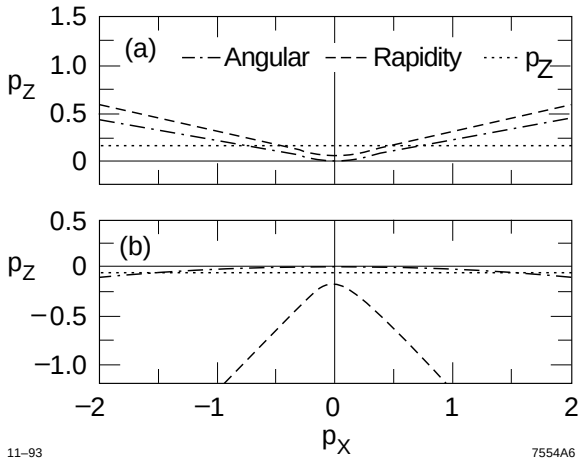

Fig. 5.15. The regions of momentum space excluded by the isolation cuts we consider. The numerical values shown are those used for $Q = 10.58$ GeV and (a) $z = 0.7$, (b) $z = 0.95$. In each case, the isolation cut is given by the requirement that the phase space above the line be empty except for the candidate directly produced meson itself. It must be emphasized that the stringency of the cuts is not a matter of taste, but is chosen to maximize the figure of merit U of eq. (5.28).

We obtained numerical values for $P(x; z, y_1)$ with the Monte Carlo generator, typically in runs of 20,000 events. We then optimized the cut with the figure of merit

$$U \equiv \frac{\int_0^1 P(x; z, y_1) \mathrm{d}y_1}{\sqrt{P(x; z, y_1 = 0)}}. \tag{5.28}$$

This method of optimization is chosen to reflect the fact that the dominant source of background noise is the direct fragmentation contribution of eq. (5.24). Truly inclusive events are comparatively easy to exclude, especially given the severity of the cuts which maximize U.

Maximizing this figure of merit for each choice of z, we find that the resulting $\theta(z)$ are well described by

$$\cot\theta = \frac{0.370 - 0.438z}{1 - z}. \tag{5.29}$$

Note that the angular isolation is still extreme even at moderate z; for example, we demand that a meson with $z = 0.5$ be isolated by 73°. The stringent cuts are necessary mainly to reduce the background from direct fragmentation, eq. (5.24).

We also optimized the cuts p_{cut} and y_{max} at each value of z; the results of this optimization agreed well with the fits

$$p_{\mathrm{cut}} = (0.70 - 0.79z) \text{ GeV} \tag{5.30}$$

and

$$Y_{\mathrm{max}} = \frac{0.463 - 0.541z}{1 - z}. \tag{5.31}$$

It is interesting to note that the point at which the angular cutoff is equivalent to the requirement of isolation in a hemisphere ($z = 0.845$) is nearly identical to the

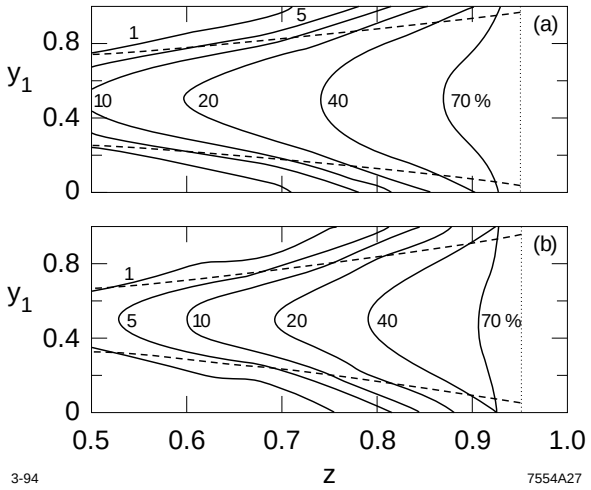

Fig. 5.16. Contours of constant acceptance in the zy_1-plane for $Q = 10.577$ GeV, with the cuts (a) $\cos\theta < 0.172$ and (b) $\cos\theta < 0$, corresponding to 80° and 90° isolation respectively. Dotted lines show the acceptance cuts resulting from the neglect of hadronization effects, which are valid in the large-Q^2 limit but at this energy drastically overestimate the acceptance at moderate z.

corresponding point for the rapidity cut ($z = 0.856$). We will make us of this fact shortly.

The acceptance curves with $Y_{\max}$ defined by eq. (5.31) and those with θ given by eq. (5.29) are shown in Fig. 5.17(a). For moderate z, the rapidity cut is clearly superior to the angular isolation requirement; for large z, however, the rapidity cut is too restrictive, suppressing the signal as well as the small-y noise.

A little thought shows the reason for this. When $z < 0.85$, the situation is as depicted in Fig. 5.15(a); the rapidity cut is insensitive to very soft physics. For $z > 0.85$, however, the cuts are as shown in Fig. 5.15(b); now the rapidity cut forces every particle to have some substantial momentum in the $-\hat{z}$ direction. Thus the rapidity cut is more likely to reject semiexclusive events due to soft physics in the hadronization process, and the angular cut is superior.

With this reasoning, we choose to implement a hybrid cut. For $z < 0.85$, we impose a rapidity cut with

$$Y_{\max} = 0.551 \, \frac{0.85 - z}{1 - z}; \tag{5.32}$$

for $z > 0.85$ we use an angular cut with

$$\frac{x}{\sqrt{1 - x^2}} = -0.429 \, \frac{z - 0.85}{1 - z}. \tag{5.33}$$

This yields the cleanest event sample over the full range of z. The resulting acceptance is shown in Fig. 5.16(b).

This represents a step towards cleaning up the semiexclusive signal. However, our numerical results show that the cuts given so far cannot by themselves adequately restrict the contamination from the small-y region. For this, a further cut is necessary.

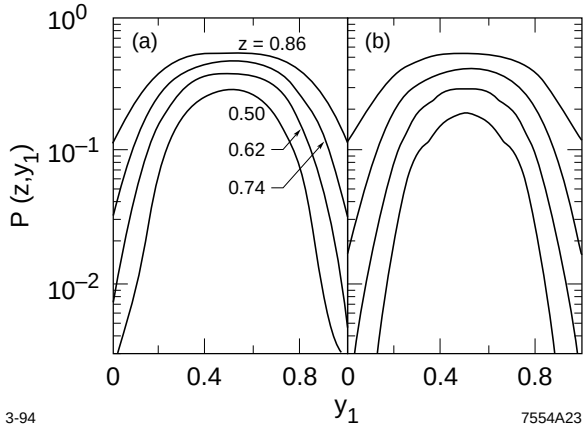

Fig. 5.17. The acceptance $P(z, y_1)$ with (a) the rapidity cut defined in eq. (5.31) and (b) the angular cut of eq. (5.29).

5.6.2. Event Shape Cuts

As described in Sec. 5.5.2, events from the small-y region carry their own signature—the jets tend to be aligned with the hadron momentum, which we define to lie along the $\hat{z}$-axis. This allows the isolation cut to preferentially exclude those events to some extent. However, we can improve the discrimination by going directly to the heart of the matter and examining the shape of the hadronizing system.

We first impose a minimum cut on the thrust

$$T \equiv \max_{\hat{n}} \left\{ \frac{\sum_i |p_i \cdot \hat{n}|}{\sum_i |p_i|} \right\} > T_{\min}.$$

Events with low T are somewhat amorphous, and thus carry little information about their original orientation.

We could attempt to impose a condition on the angle between the thrust axis and $\hat{z}$. However, it turns out to be more efficacious to restrict the 'z-component' of thrust [49]:

$$T_z \equiv \frac{\sum_i |p_i \cdot \hat{z}|}{\sum_i |p_i|} < T_{\max,z}.$$

We again optimized the cuts $T_{\min}$ and $T_{\max,z}$ through numerical evaluation of the figure of merit U. In the end, we found it best to choose the isolation cut

$$Y_{\max} = 0.88 - z, \tag{5.34}$$

and to use the event shape cuts

$$T_{\min} = 0.90 - \frac{0.036}{1-z} \quad \text{and} \quad T_{\max,z} = 0.34. \tag{5.35}$$

To eliminate low-multiplicity inclusive backgrounds, we also required that the recoil system contain at least six particles. The resulting acceptance $P(z, y_1)$ is shown in

Figs. 5.18 and 5.19. The rejection of small y is now nearly perfect; as a result, we will be able to isolate a clean semiexclusive signal from the region of moderate y.

5.6.3. Acceptances at the Z Peak

In precisely the same manner as above, we can define, optimize, and compute acceptances $P(z, y_1)$ at $Q = m_Z$. In this case, we replace eqs.(5.34) and (5.35) with the requirements

$$Y_{\max} = 1.6 - 1.4z, \quad T_{\min} = 0.90 - \frac{0.004}{1-z}, \quad \text{and} \quad T_{\max,z} = 0.57 - 0.23z. \quad (5.36)$$

Figure 5.20 shows the results of these constraints. The acceptances are substantially larger in the central region, and much better suppressed at the endpoints in y_i, than the acceptances at $Q = m_\Upsilon$. This serves to offset the increased predominance of the leading-twist collinear contribution, as described in Sec. 5.5.1.

5.6.4. Quark Mass Effects

To examine the interesting cases of semiexclusive D production at the Υ resonance and B production at the Z^0 pole, we must allow for nonzero quark masses, and the concomitant energetic weak decays, in the computation of the acceptance $P(z, y_1)$. This does not involve any conceptual changes to the approach we have described; in particular, Monte Carlo simulation of the hadronizing system should still provide physically reliable results.

Figure 5.21 shows the results of this analysis. Note that the restriction on the mass of the hadronizing system leads to a much more severe constraint on z; otherwise, the results are qualitatively similar to those of Sec. 5.6.2.

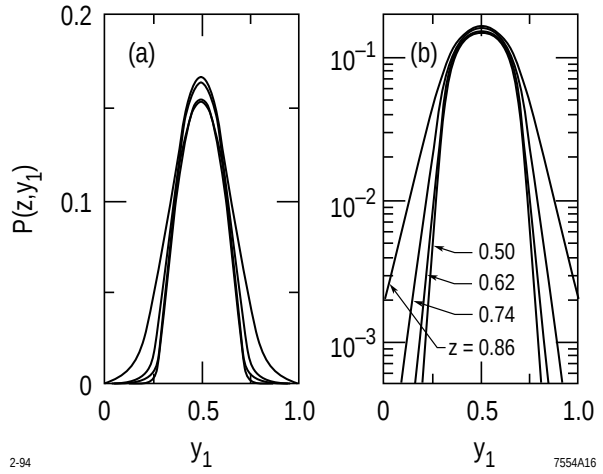

Fig. 5.18. The acceptance $P(z, y_1)$ with the combination of event shape and isolation cuts of eqs. (5.34) and (5.35): (a) is linear, (b) a semilog plot.

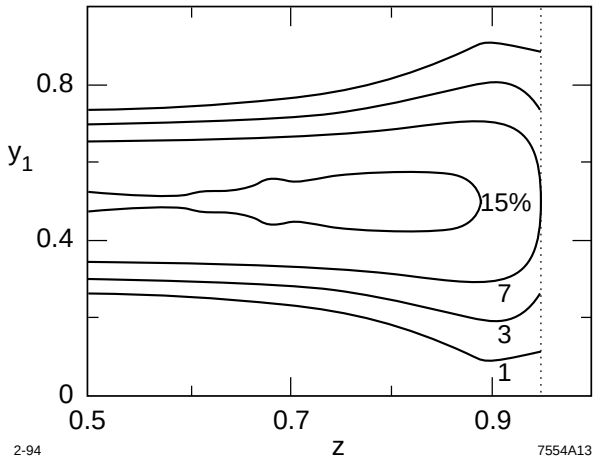

Fig. 5.19. Contours of equal acceptance in the zy_1-plane, with the cuts of eqs. (5.34)-(5.35).

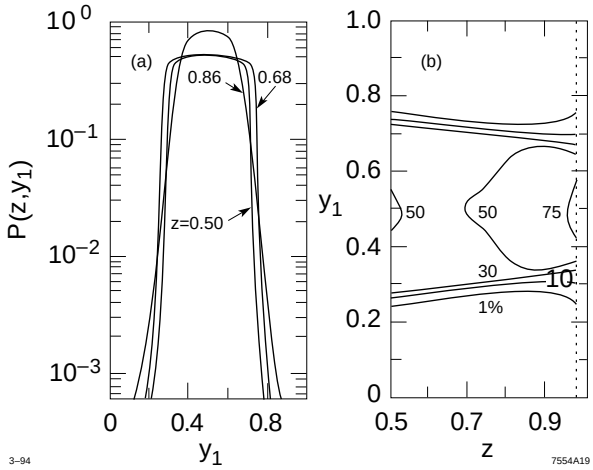

Fig. 5.20. The acceptance $P(z, y_1)$ at $Q = m_Z$, with the cuts of eq. (5.36): (a) is a semilog plot, (b) a contour plot.

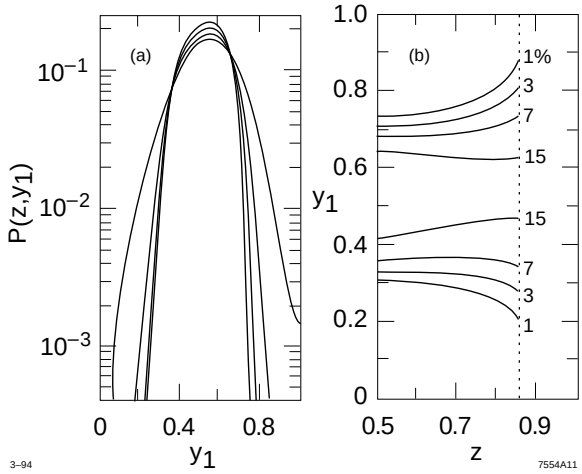

Fig. 5.21. The acceptance $P(z, y_1)$ for semiexclusive production of charmed mesons at the Υ_{4s} resonance. Here $y_1 = y_c$ is the back momentum of the $\bar{c}$ quark in the hadronizing system.

Similarly, we must account for the B mass and weak decay channels in analyzing the acceptance for B production at the Z peak. Figure 5.22 shows the results of this analysis; again, the effects of the quark mass are not very large.

At moderate z, the b quark is heavy compared to the scale of hadronization but light enough that its weak decay products are collimated in the direction of its motion. This is an ideal situation, as is reflected in the wide and high plateaus of $P(z, y_1)$ shown in Fig. 5.22. At large z, when the mass of the hadronizing system is not much larger than m_b, this situation deteriorates rapidly. However, at $z \sim 0.95$ the recoil system still has a mass of more than 20 GeV, so that the endpoint region can be excluded with great accuracy. Thus the rates which we will predict for semiexclusive B production are extremely insensitive to physics at any scale softer than $\min\{\bar{z}, z y_i \langle \bar{x} \rangle\} m_Z^2$.

5.7. Results

We can now combine the results of the previous sections to obtain predictions for observable cross sections at realistic energies.

We first perform the convolution of hard-scattering amplitudes and distribution amplitudes; using eqs. (5.6) and (5.7) and the definitions of eq. (5.5), we obtain after some rearrangement

$$\begin{aligned}\mathcal{M}^{(+)} = C_F \frac{16\pi^2 \alpha \alpha_s}{zQ^2} \Bigg[& 2sce^{-i\phi} \Big(q_u \bar{B} \sqrt{\frac{y_2}{y_1}} - q_s B \sqrt{\frac{y_1}{y_2}} \Big) \\ & + \sqrt{\bar{z}} s^2 e^{-2i\phi} \Big(q_s B - q_u \big[\bar{B} + z \bar{A}(z) \big] \frac{y_2}{y_1} \Big) \\ & - \sqrt{\bar{z}} c^2 \Big(q_u \bar{B} - q_s \big[B + z A(z) \big] \frac{y_1}{y_2} \Big) \Bigg]\end{aligned}$$

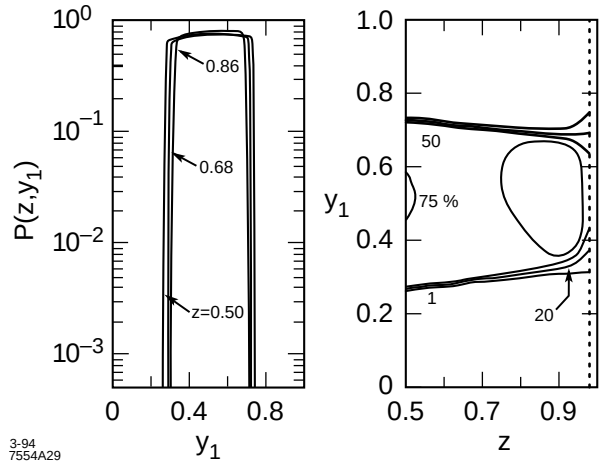

Fig. 5.22. The acceptance $P(z, y_1)$ for semiexclusive production of B mesons at the Z^0 peak. Here $y_1 = y_b$ is the back momentum of the $\bar{b}$ quark in the hadronizing system.

for K^- or longitudinally polarized K^*, and

$$\mathcal{M}^{(+)} = C_F \frac{16\pi^2 \alpha \alpha_s}{Q^2} c^2 \bar{z} \Big[\frac{q_s A(z)}{y_2} - \frac{q_u \bar{A}(z)}{y_1} \Big]$$

for transversely polarized K^* mesons. Again, the same result holds for any light flavored meson.

The argument of α_s depends on the diagram; in general, we can use the substitutions

$$q_s \alpha_s \rightarrow q_s \alpha_s(\bar{x} z y_2 Q^2) \text{ and}$$
$$q_u \alpha_s \rightarrow q_u \alpha_s(x z y_1 Q^2).$$

We will not exhibit the explicit dependence of α_s on the momentum transfer in the equations which follow. However, the final results we present are obtained by a numerical integration procedure which takes into account the running of α_s for each model wavefunction and for each value of z and y_i.

Squaring the amplitude and summing over polarizations, we obtain the differential cross section

$$
\begin{aligned}
\mathrm{d}\sigma = \frac{4}{9\pi^2}\frac{\alpha^2\alpha_s^2}{Q^4}\frac{\bar{z}}{z}\mathrm{d}z\ \mathrm{d}y_1\ \mathrm{d}\cos\theta\ \mathrm{d}\phi \\
\times\Bigg\{ \frac{\bar{z}}{2}(1+\cos^2\theta) \\
\Big(\Big[q_s B - q_u\big(\bar{B}+z\bar{A}(z)\big)\frac{y_2}{y_1}\Big]^2 + \Big[q_u\bar{B} - q_s\big(B+zA(z)\big)\frac{y_1}{y_2}\Big]^2\Big) \\
+ 2\sin^2\theta\Big[q_s B\sqrt{\frac{y_1}{y_2}} - q_u\bar{B}\sqrt{\frac{y_2}{y_1}}\Big]^2 \\
- 4\sqrt{\bar{z}}\cos\theta\sin\theta\cos\phi \\
\Big[q_s B\sqrt{\frac{y_1}{y_2}} - q_u\bar{B}\sqrt{\frac{y_2}{y_1}}\Big]\Big[q_s\frac{B+y_1 zA(z)}{y_2} - q_u\frac{\bar{B}+y_2 z\bar{A}(z)}{y_1}\Big] \\
+ \bar{z}\sin^2\theta\cos 2\phi\Bigg(\Big[q_s B\sqrt{\frac{y_1}{y_2}} - q_u\bar{B}\sqrt{\frac{y_2}{y_1}}\Big]^2 - z^2 q_u q_s A(z)\bar{A}(z) \\
+ z\Big[q_s B\sqrt{\frac{y_1}{y_2}} - q_u\bar{B}\sqrt{\frac{y_2}{y_1}}\Big]\Big[q_s A(z)\sqrt{\frac{y_1}{y_2}} - q_u\bar{A}(z)\sqrt{\frac{y_2}{y_1}}\Big]\Bigg)\Bigg\}
\end{aligned}
\tag{5.37}
$$

for helicity-zero, and

$$
\mathrm{d}\sigma = \frac{4}{9\pi}\frac{\alpha^2\alpha_s^2}{Q^4}z\bar{z}^2\mathrm{d}z\ \Big[\frac{q_s A(z)}{y_2} - \frac{q_u\bar{A}(z)}{y_1}\Big]^2\mathrm{d}y_1\ (1+\cos^2\theta)\mathrm{d}\cos\theta \tag{5.38}
$$

for helicity-1 mesons; in the latter case, we have integrated out the trivial ϕ-dependence.

To make use of the portion of the cross section proportional to $(1+\cos^2\theta)$, we must be able to discern it above the direct fragmentation contribution of eq. (5.26). We must caution the reader that the results from any approach which neglects hadronization effects are entirely misleading at this juncture. Neglect of hadronization effects leads to the conclusion that, as $z \to 1$, the endpoints $y \to 0, 1$ become experimentally accessible. As a result, the $1/y$ behavior of the cross section of eq. (5.37) was claimed to lead to a substantial signal at large z.

In practice, the reverse holds. As z grows, the small-y growth of the cross section is curtailed not by an experimental cut but through the multiple-scattering process described in Sec. 5.4. Meanwhile, the energy in the hadronizing system decreases, so that our ability to isolate the region where y is not small is lost. To prevent unacceptable contamination of the signal, we must impose the harsh cut of eq. (5.35); as a result, the cross section for large z is controlled by the $\bar{z}$ factor in eq. (5.3), and almost no signal can be measured in the region $z > 0.9$.

Numerically, it happens that the signal is actually cleaner at small z. This is because the signal of eq. (5.37) grows more slowly as $y \to 0$ than the background; thus the ability to reject events with small y is paramount. Since the hadronizing system is more energetic at smaller z, the event shape cuts we use are more effective, and we obtain the best results by integrating over the region $0.5 < z < z_{\max}$. We should choose the upper bound $z_{\max}$ on z to maximize the ratio $S/\sqrt{N}$, where S is the signal of eq. (5.37) and N the noise from eq. (5.24)[50]. Examination of the numerical results (using the symmetric wavefunction, so that our cuts will not depend on a model wavefunction) shows that the ratio $S/\sqrt{N}$ is maximized if we use the upper bound $z_{\max} = 0.8$.

To estimate the reliability of our perturbative methods, it is useful to examine the differential cross section $\mathrm{d}\sigma/\mathrm{d}z\mathrm{d}y_1$, as in Fig. 5.23. For moderate values of z, the hadronizing system is sufficiently energetic to allow excellent rejection of the endpoint region; as z increases, the cross section $\mathrm{d}\sigma/\mathrm{d}z$ comes to be dominated by small momentum transfers $q^2 = zy_{\min}Q^2$. This problem is more severe for neutral mesons with symmetric wavefunctions, as shown in Fig. 5.23(b), where the amplitude in the central region is suppressed by cancellations between couplings to

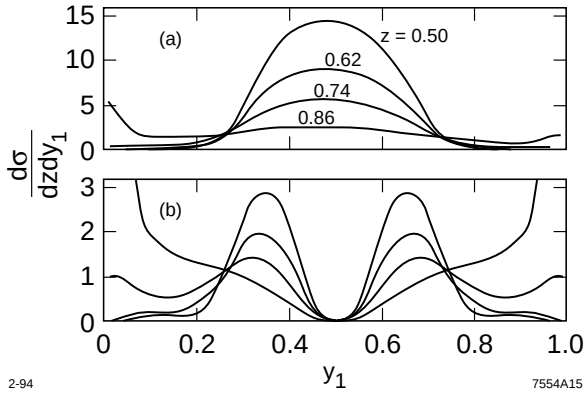

Fig. 5.23. The differential cross section $\mathrm{d}\sigma/\mathrm{d}z\mathrm{d}y_1$ for several values of z, for (a) the ZZC model of the K^- and (b) the asymptotic model of the K^0 (or π^0). As z increases, the cross section comes to be dominated by endpoint contributions, for which perturbative predictions are untrustworthy.

	Distribution	Cross Section $\sigma_{\rm sx}$ (fb)		
Meson	Amplitude	Charged	Neutral	Ratio
K	ZZC	1.46	0.40	3.6
	Toy	0.55	0.23	2.4
	asymptotic	0.62	0.10	5.9
π	ZZC	1.56	0.88	1.8
	asymptotic	0.36	0.15	2.4
$\rho_{_L}$	ZZC	0.87	0.20	4.3
$\rho_{_T}$	ZZC	0.34	0.09	3.9
$K^*_{_L}$	ZZC	0.89	0.19	4.8
ϕ	ZZC	0.42	0.09	4.8

Table 5.2. The semiexclusive production cross sections for each of the model meson distribution amplitudes under consideration.

the two separate quarks. (Naturally, the Dirac form factors of these mesons vanish altogether.)

Table 5.2 shows the total cross sections expected for semiexclusive production, based on the model wavefunctions of Table 5.1. What else can we learn from the cross section of eq. (5.37)? We first consider the term proportional to $\sin^2\theta$:

$$\frac{16}{9\pi}\frac{\alpha^2\alpha_s^2}{Q^4}\frac{\bar{z}}{z}\mathrm{d}z\,\left[q_s B\sqrt{\frac{y_1}{y_2}}-q_u\bar{B}\sqrt{\frac{y_2}{y_1}}\right]^2\mathrm{d}y_1\;\sin^2\theta\mathrm{d}\cos\theta. \tag{5.39}$$

Since this term depends on the distribution amplitude only through the constant B, it will grow more slowly than $\mathrm{d}\sigma_{\rm sx}$ at large z. Also, the y-dependence is less pronounced, so that the integral over y_1 will not gain large contributions from terms like y_1^{-2}.

As a result, this contribution to the total cross section is numerically small, amounting to no more than 30% of the total semiexclusive contribution. Since the angular distribution of background events is not precisely $1+\cos^2\theta$ due to hadronization effects, a clean separation of this term seems unfeasible.

The existence of an energetic meson introduces a preferred axis into the computation, so that there is no reason to expect the backgrounds to have trivial ϕ-dependence. Since the sign of $\cos\phi$ cannot be determined without successfully tagging the primary quark flavors in the two recoil jets, we are left with only the part of eq. (5.37) proportional to $\cos 2\phi$, which is numerically much smaller than the dominant $1+\cos^2\theta$ term. Thus isolation of the ϕ-dependent terms in the cross section appears impossible.

5.7.1. Glueball Production

From the amplitude of eq. (5.11), we obtain the unpolarized differential cross section for semiexclusive production of 0^+ mesons:

$$\mathrm{d}\sigma = \frac{\pi\alpha^2\alpha_s^2 q_i^2}{24Q^4}\,\frac{\bar z}{z}\mathrm{d}z\;\mathrm{d}y_1\;\mathrm{d}\cos\theta\;\mathrm{d}\phi\left\{\frac{4}{y_1y_2}\Big[2\bar z B_{gg}+\frac{zf_{gg}}{2\sqrt{3}}\Big]^2\sin^2\theta + \bar z\Big(\frac{1}{y_1^2}+\frac{1}{y_2^2}\Big)\Big[(2-z)B_{gg}+\frac{f_{gg}}{2\sqrt{3}}\Big]^2(1+\cos^2\theta)\right\},$$

where we have integrated over $\mathrm{d}\phi$. Here q_i^2 is the QED coupling of the recoil quark, which should be summed over all quark flavors. However, we should not make the substitution $3\sum q_i^2 \to R_{e^+e^-}(\bar z Q^2)$, since production of a gg state recoiling against a resonance is suppressed by final-state interactions (see Sec. 5.1.5). Instead, we consider only the light quarks u, d, and s; our events shape cuts will strongly suppress the signal from events like $e^+e^- \to f_0 c\bar c$, where the thrust of the recoil system is unlikely to be large.

The gluons are produced collinearly, and are nominally on shell (up to corrections of order the meson mass). We use the fixed coupling $\alpha_s = 0.4$, reflecting our belief that the small size of the meson will limit the growth of the running coupling.

To estimate the semiexclusive cross section, we first use the asymptotic wavefunction $\phi_{gg}(x) = \sqrt{3} f_{gg} x\bar{x}$. Then $B_{gg} = f_{gg}\sqrt{3}/2$, and the semiexclusive cross section scales as f_{gg}^2. With the cuts of eqs. (7.7) and (7.8), we obtain an observed integrated cross section of $71 f_{gg}^2$ fb GeV^{-2}.

Figure 5.24 shows the resulting differential cross section $\mathrm{d}\sigma/\mathrm{d}z$. It falls off rapidly with increasing z, reflecting the fact that glueball production is forbidden at leading twist in the exclusive limit. The behavior of $\mathrm{d}\sigma/\mathrm{d}z$ is well approximated by $\exp(-7z)$ for scalar or longitudinally polarized states and by $\exp(-10.5z)$ for transversely polarized states.

The angular distribution arising from our *ansatz* for the two-gluon distribution amplitude is also noteworthy. The observed distribution, after implementation of our acceptance cuts, is very closely approximated by

$$\frac{\mathrm{d}\sigma_{\mathrm{sx}}}{\mathrm{d}\cos\theta} \propto 1 - 0.19\cos^2\theta$$

over the entire region $0.5 < z < 0.8$. This seems to be a numerical peculiarity of the asymptotic distribution amplitude; using instead the 'double-humped' distribution amplitude

$$\phi(x) \propto x\bar{x}(x-\bar{x})^2$$

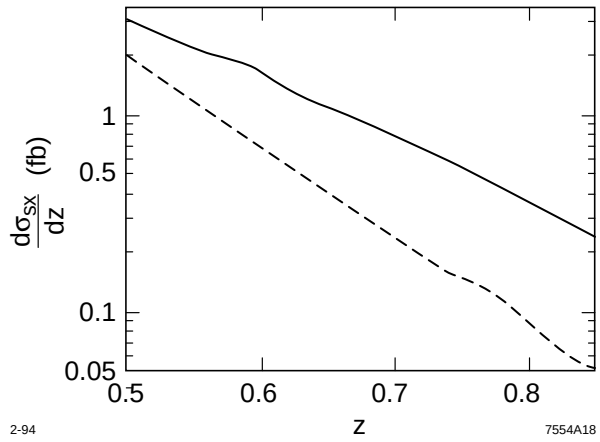

Fig. 5.24. The differential cross section $\mathrm{d}\sigma/\mathrm{d}z$ for semiexclusive production of gg states with $J_z = 0$ (solid line) and $J_z = 2$ (dashed line). We have used the *ansatz* that the gluon distribution is proportional to $x\bar{x}$, normalized to $f_{\mathrm{gg}} = 100$ MeV. The latter is probably somewhat optimistic.

predicts an angular distribution which varies from $1 - 0.20\cos^2\theta$ at $z = 0.5$ to $1 - 0.08\cos^2\theta$ at $z = 0.8$, as well as increasing the total cross section to 160 f_{gg}^2 fb GeV^{-2}.

Note that f_{gg} will not be larger than about 100 MeV, so these cross sections are commensurate with our predictions for $q\bar{q}$ mesons. However, they have the advantage of being peaked at smaller values of z, where the hadronizing system is more energetic and pQCD predictions less subject to soft corrections. The primary theoretical drawback is the α_s^2 dependence of the cross section, which introduces substantial uncertainty into the predicted normalization of the semiexclusive cross section.

We can similarly compute the total cross section for production of 2^+ mesons. With the additional assumption that $\phi_{gg/L} = \phi_{gg/T}$, we obtain after all experimental cuts the result $\mathrm{d}\sigma_{\mathrm{sx}} = 103 f_{gg}^2 \mathrm{fb}/\ \mathrm{GeV}^{-2}$, again using the asymptotic form of the distribution.

5.7.2. Direct Photon Production

Using the kinematics of Sec. 5.1, we can easily compute the amplitude for direct-photon production. The result is

$$\mathcal{M}^{(++)} = \frac{C_F e^3 q_e q_i}{z}\ \left(c\sqrt{y_2} + se^{i\phi}\sqrt{\bar{z}y_1}\right)^2\ \left[\frac{q_i}{\sqrt{y_1 y_2}} + \frac{q_e}{\sqrt{\bar{z}}sce^{i\phi}}\right]$$

when the photon, electron, and antiquark share the same helicity; the results for other helicities are obtained by $s \leftrightarrow c$ and $y_1 \leftrightarrow y_2$. In this case the color factor $C_F = \sqrt{3}$.

The direct photon production cross section is much less well behaved at the endpoints, since the mechanisms described in Sec. 5.5 do not affect its collinear

divergences. Thus our methods do not suffice to accurately estimate the cross section for direct photon production in these regions. To gain some feel for the comparative size of these cross sections, however, we may consider the ratio of amplitudes away from the collinear region.

We must consider the possibility that γ-K^0 or γ-π^0 misidentification could represent a substantial background to the semiexclusive signal. We find that at $\sqrt{s} =$ 10 GeV, direct photon cross sections are typically 20–50 times the semiexclusive cross sections in which we are interested, so that γ rejection must be complete to less than 1% in order to allow clean extraction of the semiexclusive signal. At these energies, semiexclusive events do not constitute a significant background to direct photon production; however, at lower energies where the Q^{-2} suppression is less drastic, they must be considered.

5.7.3. Z^0 Decays

The program implemented to search for semiexclusive events in Z decays is similar to that above. The experimental cut changes in appearance but not in substance, as described in Sec. 5.6.3.

The simple substitutions $q_i \to \mathbf{Q}_i$, $e \to g$, and $Q^4 \to m_Z^2\Gamma_Z^2$ enable us to compute the cross sections at the Z peak without further ado. In this case, the wide acceptance allowed by eq. (5.36) serves to offset the strong f_h/m_Z suppression of the amplitude. On the other hand, the considerations of Sec. 5.1.3 show that the D and B wavefunctions probed at $Q = m_Z$ will not be very strongly peaked, so that the hard-scattering amplitudes themselves will not see the wavefunction enhancement we would expect at lower momentum transfers. For light mesons, the consequences of

	Distribution	Branching Ratio Γ_{sx} ($\times 10^{-6}$)		
Meson	Amplitude	Charged	Neutral	Ratio
K	ZZC	1.53	0.76	2.0
	Toy	0.98	0.49	2.0
	asymptotic	0.91	0.41	2.2
π	ZZC	1.16	0.32	3.7
	asymptotic	0.56	0.14	4.1
ρ_L	ZZC	0.70	0.18	3.9
ρ_T	ZZC	0.44	0.11	4.0
K^*_L	ZZC	1.00	0.46	2.2
ϕ	ZZC	1.26	0.39	3.2

Table 5.3. Semiexclusive cross sections at the Z peak. Note that the differences arising from the choice of distribution amplitude are less pronounced due to the smoothing effects of the evolution with Q^2.

evolution are even more pronounced, and it will be impossible to extract information about the distribution amplitude at such high energies; see Fig. 5.5.

We again follow the same program of computing the acceptance, then integrating the cross section over $\mathrm{d}y_1\mathrm{d}z$ to obtain observable quantities. The acceptance is shown in Fig. 5.20 and the resulting cross sections in Table 5.3.

5.7.4. Heavy-quark Mesons

The analysis of semiexclusive reactions is particularly rewarding in the study of heavy-quark mesons. This is largely due to the sensitivity of the production cross section to the extent to which the distribution amplitude is peaked at large momentum fraction x, which is closely related to the moment $\langle x \rangle$ of the distribution amplitude. These moments have been the subject of substantial theoretical interest [51-52], but precise experimental determinations have so far been unavailable.

We wish to extract a relation between the moment $\langle x \rangle$ and the integrated semiexclusive production cross section $\sigma_{\rm sx}$. Both of these quantities depend on some complicated distribution amplitude, which will introduce model-dependence into the relationship. We estimate this dependence by using three simple models for the distribution amplitudes of heavy-light mesons.

The first is the toy model of Ref. [3],

$$\phi(x) = f_h \sqrt{3} \frac{(1-x)(x-x_0)}{(1-x_0)^3} \qquad \text{with} \quad x_0 = 2\langle x \rangle - 1.$$

Because this distribution is symmetric about $\langle x \rangle$ and has no small-x 'tail,' it is less concentrated at very large x than we would expect for a realistic wavefunction, and will thus lead to somewhat lower estimates of $\sigma_{\rm sx}$.

The second model is simply

$$\phi(x) = \frac{(n+1)(n+2)}{2\sqrt{3}} f_h x^n \bar{x} \qquad \text{with} \quad n = \frac{2}{\langle 1-x \rangle} - 3.$$

This yields a distribution which is very strongly peaked at x near 1, and which thus provides an estimate of $\sigma_{\rm sx}$ for given $\langle x \rangle$ which may be unrealistically large. However, it is more realistic than the toy distribution from Ref. [3] used above.

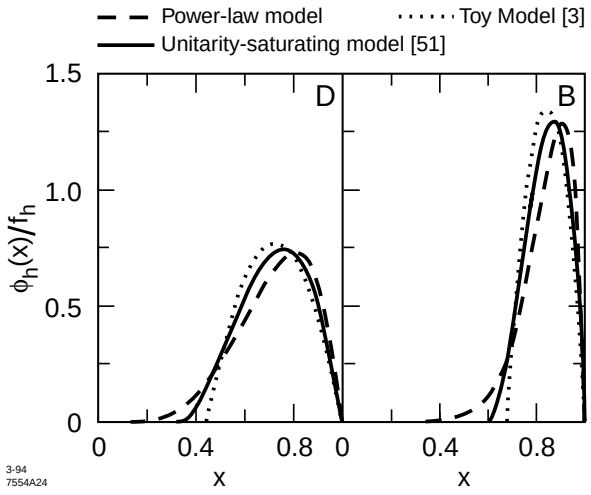

Fig. 5.25. Three models of the distribution amplitudes of the B and D mesons, parametrized to yield $\langle x_c \rangle = 0.72$ and $\langle x_b \rangle = 0.84$. We assume $f_B = f_D = 190$ MeV.

The final model wavefunction is derived from the wavefunction given in Ref. [51], which is chosen to maximize $\langle x \rangle$ subject to the constraints of unitarity and of the values of the decay constant and quark and meson masses. Integrating the wavefunction described in Ref. [51] over all $k_\perp$, we obtain the distribution amplitude

$$\phi(x) = \frac{3\sqrt{3}}{2} f_h (1-x) \Big[x(1+2x_0) \ln\Big(\frac{1+2x}{1+2x_0}\Big) - 2x_0(x-x_0) \Big] \tag{5.40}$$

with

$$\begin{aligned} \langle x \rangle &= \frac{81}{64} \frac{1+2x_0}{(1-x_0)^4} \ln\Big(\frac{3}{1+2x_0}\Big) - \frac{(2+x_0)(13+40x_0-38x_0^2+12x_0^3)}{32(1-x_0)^3} \\ &\simeq \frac{3+2x_0}{5} - 0.0138(1-x_0)^2 + \cdots \end{aligned}$$

Under the assumption that the wavefunction $\psi_{D \to c\bar{q}}$ is purely real and positive, the methods of Ref. [51] can be used to obtain the upper bound $\langle x \rangle < 0.73$, in contrast to the estimate $\langle x \rangle = 0.79$ of Ref. [15]. The unitarity-saturating wavefunction of eq. (5.40) is more strongly peaked toward $x = 1$ than the toy model, and is still extremely asymmetric; thus it should not substantially underestimate the rate of semiexclusive production when compared to realistic models. The three model distribution amplitudes are shown in Fig. (5.40) for $\langle x \rangle = 0.72$ and 0.84, which are the unitarity bounds of Ref. [51] for the D and B mesons respectively.

With the acceptance functions described in Sec. 5.6.4, it is now a simple matter to compute the cross sections for semiexclusive production at the Υ_{4s} resonance. The dependence of the total cross section on $\langle x \rangle$ is displayed in Fig. 5.26. The error bars shown do *not* represent data, but serve to indicate the degree of model dependence in the prediction. The uncertainty in $\langle x \rangle$ due to model dependence is on the order of 0.03, which is roughly equal to the uncertainty introduced by a 60%

error in the measurement of $\sigma_{\rm sx}$. Since both the charged and neutral channels can be used in this measurement, the model dependence will probably be the dominant source of error. If constraints on the limiting behavior of $\phi(x)$ as $x \to 1$ can be obtained independently, they would serve to eliminate the source of most of this model dependence.

At the Z^0 peak, the prospects for probing D meson structure are exceedingly dim, largely due to the erosion of nonperturbative wavefunction information during the evolution to the large momentum scales in question. However, there is now sufficient energy to produce B mesons in perturbative processes, and we can ask the same questions about their distribution.

The apparent conflict between QCD sum rules[15,53], which provide the estimate $\langle x \rangle = 0.90$, and unitarity constraints which suggest $\langle x \rangle < 0.84$, exists in this case as well. Though both of the above arguments are predicated on small momentum transfer, it is still of interest to measure the moment $\langle x_b \rangle$ in semiexclusive production at the Z, though one must bear in mind the remarks of Sec. 5.1.3.

The expected cross sections for semiexclusive B production at the Z are shown in Fig. 5.27. Again, the model dependence is substantial, leading to an uncertainty of about 0.03 in the extraction of $\langle x \rangle$. However, the branching fractions are sufficiently large that at least an approximate measurement may be possible in the current LEP experiments [54]. This measurement will provide crude but essential information about the structure of the B meson.

Note that the abcissa of Fig. 5.27 is $\langle x \rangle + 0.24 \ln(f_B/190 \text{ MeV})$, to compensate for the f_B-dependence of the cross section. Since the cross section does not rise precisely exponentially with $\langle x \rangle$, this introduces some imprecision; however, the resulting errors are negligible. Over the region of phenomenological interest,

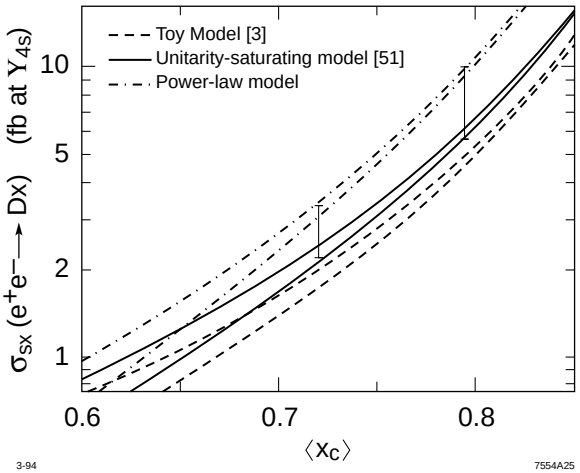

Fig. 5.26. The semiexclusive D production cross section at Υ_{4s} energies as a function of $\langle x \rangle$, for the three models shown in Fig. 5.25. The error bars shown serve to indicate the extent of model dependence. The upper curves describe charged D production; the lower, neutral.

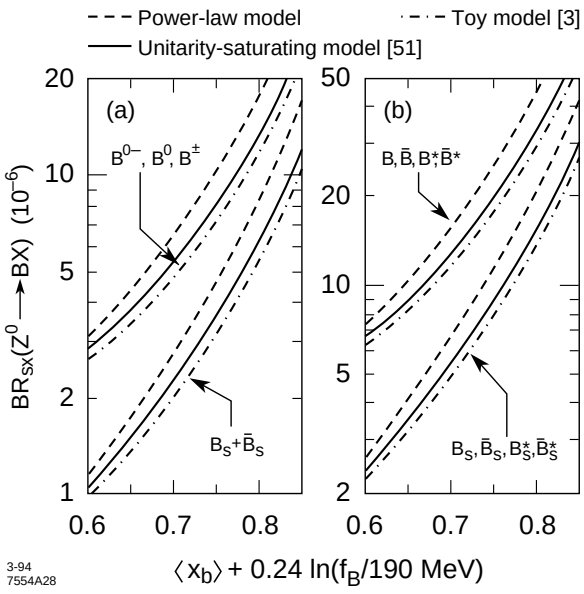

Fig. 5.27. Semiexclusive branching ratios for B mesons produced in Z decay. In (a), the upper curve sums contributions from B^0, $\bar{B}^0$, B^+ and B^- mesons while the lower curve gives the branching fraction to B_s and $\bar{B}_s$ mesons. The parameters $\langle x \rangle$ and f_B need not be the same in the two cases. In (b), we have included the contributions from the first excited states B^*, summed over polarizations, so that $\langle x \rangle$ is not precisely defined; we assume $f_{B^*} = f_B$.

$150 < f_B < 250$ MeV and $0.6 < \langle x \rangle < 0.8$, they introduce an error of less than 0.005 into the measurement of $\langle x \rangle$.

The average momentum fraction $\langle z \rangle$ is very mildly dependent on $\langle x \rangle$: $\mathrm{d}\langle z \rangle / \mathrm{d}\langle x \rangle \simeq 0.1$. Since it is unrealistic to expect that enough events can be gathered to evaluate $\langle z \rangle$ with any precision, this does not provide us with an independent determination of $\langle x \rangle$.

Figure 5.28 shows the dependence on $\langle x \rangle$ of the ratio of semiexclusive neutral to charged B production. Although this is a very difficult measurement from an experimental standpoint, its relative model-independence is striking.

In examining Figs. 5.27-5.28, one must bear in mind that the moment $\langle x \rangle$ being measured does not correspond directly to that computed in either of Refs. [15,51,53] due to the effects of evolution. Also, the total cross sections shown in Fig. 5.27 are proportional to f_B^2, which is itself subject to substantial uncertainty.

5.7.5. Extraction of Moments of the Distribution Amplitude

To test the validity of the approach of Ref. [13], in which the moments $\int (x - \bar{x})^n \phi(x) \mathrm{d}x$ of the distribution amplitude ϕ are extracted from QCD sum rules, we wish to obtain the same quantities directly from experiment. As we have shown, the experimentally observable quantities are entirely determined by the integrals $A, \bar{A}, C$, and $\bar{C}$ of eq. (5.5). Thus, to reconstruct the moments from experiment without recourse to model calculations, we must be able to fit the integrand $(x - \bar{x})^n$ which enters into the computation of moments to a sum of the integrands

$$\frac{1}{\bar{x}(1 - zx)} \qquad \text{and} \qquad \frac{1}{x(1 - z\bar{x})}$$

which determine $A(z)$ and $\bar{A}(z)$.

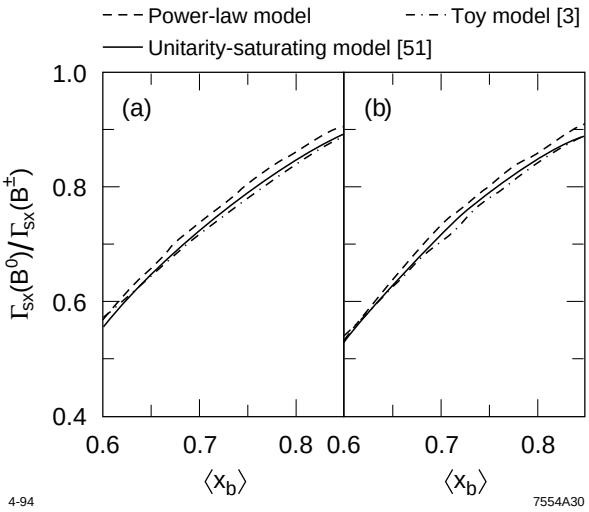

Fig. 5.28. The ratio of neutral to charged B production as a function of $\langle x \rangle$. In (a), only the pseudoscalar B states are considered; in (b), we sum contributions from B and B^* production.

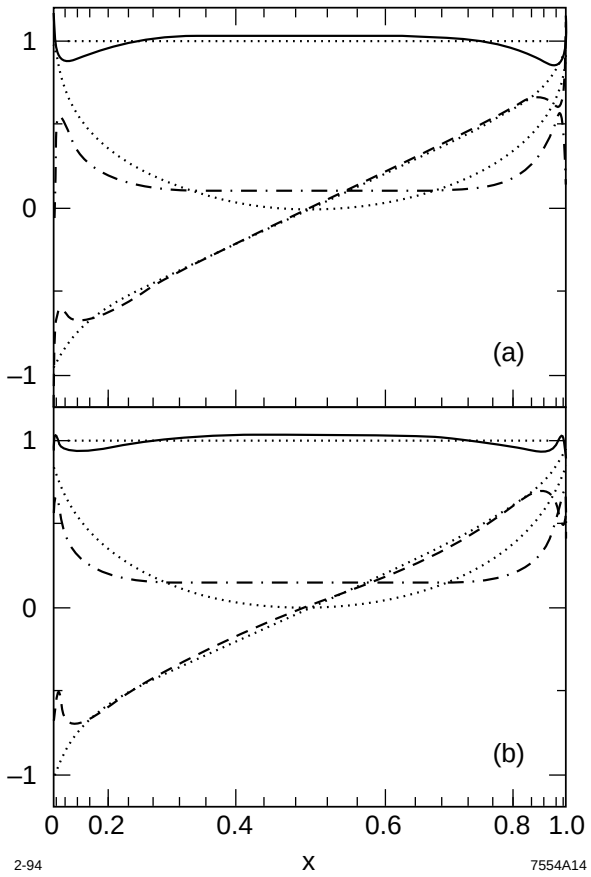

Fig. 5.29. Reconstruction of the integrands $(x - \bar{x})^n$, required for calculation of moments of the distribution amplitude, from the integrands in the transforms $A(z)$ and $\bar{A}(z)$. The fitted curves sum contributions from $A(z)$ and $\bar{A}(z)$ at (a) eight points; (b) 20 points. Note that the scale of x is distorted to show the metric of integration.

Figure 5.29(a) shows the results of such an attempt. Here we have assumed that $A(z)$ and $\bar{A}(z)$ may be measured in eight bins evenly spaced from $z = 0.5$ to $z = 1$, and that B and $\bar{B}$ are known. We used MINUIT to minimize the difference of the moment and fit integrands under the $\mathcal{L}^2$ metric with weight $x\bar{x}$ [55]. Figure 5.29(a) shows the moment integrands and the best fits to them: for example, when attempting to reconstruct the 0^{th} moment (the decay constant) from the measured values of A and $\bar{A}$, we end up integrating not $\phi(x)$, but $\phi(x)$ multiplied by the function shown as a solid line in Fig. 5.29(a). One could say that the line represents the best available approximation to 1.

For $n = 0$ or 1, the fit is tolerably good. However, the fit for $n = 2$ is unacceptable; this situation persists even if we increase the number of bins to 20 (Fig. 5.29(b)). Thus we are forced to conclude that only the first moment can be measured model-independently with any accuracy in semiexclusive processes.

5.7.6. Conclusions

We have analyzed semiexclusive meson production in some detail, noting the obstacles to unambiguous theoretical calculations and to clean experimental results. The most difficult remaining obstacle is the poorly understood behavior of the recoil system during hadronization, which will make it difficult to accurately predict the rate of background events for a given choice of experimental cuts.

Some progress can be made by appealing to the expectation [22] that the soft backgrounds should scale as $\exp\{-2\Delta Y\}$, or equivalently as $\exp\{2Y_{\text{max}}\}$. Since the semiexclusive events we wish to observe are intrinsically hard, the cross section $\mathrm{d}\sigma_{\text{sx}}/\mathrm{d}Y_{\text{max}}$ should decrease less rapidly with decreasing Y_{max} than the soft background rate; thus it should be possible to fit separate curves to the background

and signal rates. At the values of $Y_{\max}$ proposed here, we find that the behavior of the semiexclusive signal is well approximated by $\exp\{1.6\ Y_{\max}\}$.

The intrinsic hardness of any process producing a strongly isolated meson is a double-edged sword. On the one hand, it places us in a region in which Monte Carlo predictions of the expected background are extremely unreliable; however, it also tells us that the scattering producing the meson is dominated by short-distance physics. Thus we have good reason to believe that the mechanism we have considered will account for the bulk of the observed cross section. We have obtained several wavefunction-independent predictions, such as the $Y_{\max}$ dependence of the observed signal, which can be used to test the consistency of this view.

ϕ_K. In each case, the upper line shows the rate Figure 5.30 shows the differential semiexclusive production cross section for K mesons as a function of z, for our three models of the kaon distribution amplitude. Besides the absolute normalization, which indicates the extent to which the distribution is concentrated near the endpoints, there are two noteworthy features of Fig. 5.30.

First, the ratio between charged and neutral production cross sections is a sensitive test of the asymmetry ϕ_K. A symmetric distribution leads to efficient cancellation between the q_s- and q_d-dependent parts of the amplitude for K^0 production, and hence to a very large predominance of charged kaons. The extremely asymmetric toy distribution yields a comparatively small ratio. This ratio is largely immune to effects from our treatment of soft physics, and provides a sensitive test of models for ϕ_K. Predictions from each model distribution are included in Table 5.2.

Second, contrary to the conclusions of Ref. [3], we find that the shape of the cross section depends only weakly on the distribution amplitude chosen. Thus comparison with the observed differential cross section will serve more to test the

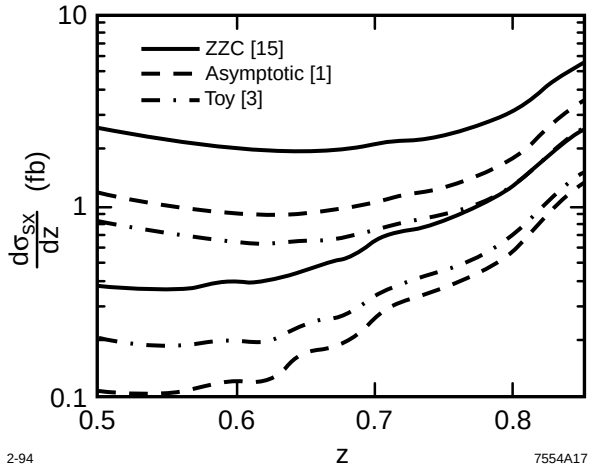

Fig. 5.30. The differential cross section $\mathrm{d}\sigma_{\mathrm{sx}}/\mathrm{d}z$ for semiexclusive K production, for three models of ϕ_K. In each case, the upper line shows the rate for K^-, the lower for K^0. The unevenness in the lines arises from statistical fluctuations in our Monte Carlo calculations of the acceptance $P(z, y_1)$ near the endpoints. It is more pronounced for neutral than for charged production; see Fig. 5.23.

validity of our picture of semiexclusive production than to place constraints on models of the hadron. If we define the expectation value $\langle z \rangle_{0.5}^{0.8}$ of z for all mesons with $0.5 < z < 0.8$, we obtain $\langle z \rangle_{0.5}^{0.8} = 0.66 - 0.67$ for all three distributions under consideration.

Finally, we have noted that the rate of semiexclusive production provides a sensitive measurement of the first moment $\langle x \rangle$ of the distribution amplitudes of heavy-light mesons. This will provide welcome experimental input to a field where comparisons between theory and experiment are often elusive.

We conclude that at integrated luminosities between 10 and 100 fb^{-1}, the analysis of semiexclusive production has limited but significant applicability to the study of mesonic structure. If still larger event samples can be obtained, several new avenues of exploration will open within the same framework. Most of these have been touched upon here. For example, discrimination between the asymptotic and ZZC models of ϕ_K through a precise measurement of $\langle z \rangle_{0.5}^{0.8}$ would require a clean sample of a few hundred semiexclusive events, as would a model-independent reconstruction of the first moment of the distribution amplitude or a precise measurement of the angular dependence of $\mathrm{d}\sigma/\mathrm{d}\Omega$.

APPENDIX 5.A: Computation of Hard-scattering Amplitudes

Section 5.1 defines our frame of reference; for definiteness, we will let l_1 and l_2 refer to the momenta of the outgoing quark and antiquark of the recoil system, respectively.

The method of Ref. [11] takes advantage of the fact that in the chiral representation of the Dirac algebra, each of the matrices γ^μ has block-diagonal entries of zero. Thus we can work with effective two-component matrices

$\gamma_+^\mu = (1, \vec{\sigma})^\mu$ and $\gamma_-^\mu = (1, -\vec{\sigma})^\mu$, and corresponding two-element spinors satisfying $\not{p}_\pm u_\mp(p) = 0$ and $u_\pm(p) u^\dagger{}_\pm(p) = \not{p}_\pm(p)$.

Spinor amplitudes are constructed like ordinary four-component amplitudes, with the simplifying rules $\gamma_\pm^\mu \gamma_\pm^\nu \equiv 0$ and $\gamma_\pm^\mu u_\pm(p) \equiv 0$ serving to enforce helicity conservation along fermion lines. Since $u_+(p)$ is the correct spinor for a fermion with positive helicity, or an antifermion with negative helicity, this method serves admirably for the construction of individual helicity amplitudes.

The algebra is greatly simplified by the Fierz relation

$$g_{\mu\nu} (\gamma_\pm^\mu)_j^i (\gamma_\mp^\nu)_l^k = \delta_l^i \delta_j^k,$$

so that all internal Lorentz indices may be effortlessly contracted. Subscripts may be flipped by use of the relation

$$u^\dagger{}_\pm(p) \gamma_\mp^\mu \cdots u_\pm(q) = \tilde{u}^\dagger \pm (q) \cdots \gamma_\pm^\mu \tilde{u}_\pm(p),$$

where $\tilde{u}_\mp \equiv i\sigma^2 u_\pm^*$. It is convenient, though not necessary, to define spinors to satisfy the additional relationship $\tilde{u}_\pm = \pm u_\pm$.

As in Sec. 5.1, we define $E \equiv E_{\rm beam}$, $s \equiv \sin(\theta/2)$, and $c \equiv \cos(\theta/2)$. With these definitions, the explicit momenta are:

$$\begin{aligned}
k &= E(1, 2sc\cos\phi, 2sc\sin\phi, c^2 - s^2) && \text{for the incoming electron or photon;} \\
k' &= E(1, -2sc\cos\phi, -2sc\sin\phi, s^2 - c^2) && \text{for the incoming positron or photon;} \\
p &= E(z, 0, 0, z) && \text{for the directly produced meson;} \\
l_1 &= E(y_1 + \bar{z}y_2, 2\sqrt{\bar{z}y_1 y_2}, 0, \bar{z}y_2 - y_1) && \text{for the outgoing quark; and} \\
l_2 &= E(y_2 + \bar{z}y_1, -2\sqrt{\bar{z}y_1 y_2}, 0, \bar{z}y_1 - y_2) && \text{for the outgoing antiquark.}
\end{aligned}$$

The corresponding matrices and spinors are:

$$
\begin{aligned}
\not{k}_+ &= 2E \begin{pmatrix} c^2 & sce^{-i\phi} \\ sce^{i\phi} & s^2 \end{pmatrix}, & u_+(k) &= \sqrt{2E} \begin{pmatrix} c \\ se^{i\phi} \end{pmatrix}; \\
\not{k}_- &= 2E \begin{pmatrix} s^2 & -sce^{-i\phi} \\ -sce^{i\phi} & c^2 \end{pmatrix}, & u_-(k) &= \sqrt{2E} \begin{pmatrix} -se^{i\phi} \\ c \end{pmatrix}; \\
\not{k}'_+ &= 2E \begin{pmatrix} s^2 & -sce^{-i\phi} \\ -sce^{i\phi} & c^2 \end{pmatrix}, & u_+(k') &= \sqrt{2E} \begin{pmatrix} se^{-i\phi} \\ -c \end{pmatrix}; \\
\not{k}'_- &= 2E \begin{pmatrix} s^2 & sce^{-i\phi} \\ sce^{i\phi} & s^2 \end{pmatrix}, & u_-(k') &= \sqrt{2E} \begin{pmatrix} c \\ se^{-i\phi} \end{pmatrix}; \\
\not{p}_+ &= 2E \begin{pmatrix} z & 0 \\ 0 & 0 \end{pmatrix}, & u_+(p) &= \sqrt{2E} \begin{pmatrix} \sqrt{z} \\ 0 \end{pmatrix}; \\
\not{p}_- &= 2E \begin{pmatrix} 0 & 0 \\ 0 & z \end{pmatrix}, & u_-(p) &= \sqrt{2E} \begin{pmatrix} 0 \\ \sqrt{z} \end{pmatrix}; \\
\not{l}_{1+} &= 2E \begin{pmatrix} \bar{z}y_2 & \sqrt{\bar{z}y_1y_2} \\ \sqrt{\bar{z}y_1y_2} & y_1 \end{pmatrix}, & u_+(l_1) &= \sqrt{2E} \begin{pmatrix} \sqrt{\bar{z}y_2} \\ \sqrt{y_1} \end{pmatrix}; \\
\not{l}_{1-} &= 2E \begin{pmatrix} y_1 & -\sqrt{\bar{z}y_1y_2} \\ -\sqrt{\bar{z}y_1y_2} & \bar{z}y_2 \end{pmatrix}, & u_-(l_1) &= \sqrt{2E} \begin{pmatrix} -\sqrt{y_1} \\ \sqrt{\bar{z}y_2} \end{pmatrix}; \\
\not{l}_{2+} &= 2E \begin{pmatrix} \bar{z}y_1 & -\sqrt{\bar{z}y_1y_2} \\ -\sqrt{\bar{z}y_1y_2} & y_2 \end{pmatrix}, & u_+(l_2) &= \sqrt{2E} \begin{pmatrix} \sqrt{\bar{z}y_1} \\ -\sqrt{y_1} \end{pmatrix}; \\
\not{l}_{2-} &= 2E \begin{pmatrix} y_2 & \sqrt{\bar{z}y_1y_2} \\ \sqrt{\bar{z}y_1y_2} & \bar{z}y_1 \end{pmatrix}, & u_-(l_2) &= \sqrt{2E} \begin{pmatrix} \sqrt{y_2} \\ \sqrt{\bar{z}y_1} \end{pmatrix}.
\end{aligned}
$$

One useful fact is that amplitudes for negative-helicity electrons, which contain a factor $u^\dagger{}_-(k')\gamma_+^\mu u_-(k) = \tilde{u}_+^\dagger(k)\gamma_-^\mu \tilde{u}_+(k')$, can be changed into their positive-helicity counterparts by the substitutions $se^{-i\phi} \to c$ and $c \to se^{i\phi}$. Alternatively, we can multiply the amplitudes with positive e^- helicity by a phase factor $e^{-2i\phi}$, so that the positive-helicity amplitudes are obtained from their negative-helicity counterparts by the substitution $c \leftrightarrow s$.

The hard-scattering amplitudes for the e^+e^- annihilation processes considered in this chapter are given in the text for positive-helicity electrons; we do not present the results for negative-helicity electrons, which can be derived trivially by applying the above observation.

APPENDIX 5.B: Photon-photon collisions

For the calculation of two-photon amplitudes, we must also find a representation of the polarization vectors. This is most easily accomplished in axial gauge with reference vector parallel to p^μ, so that

$$\not{\epsilon}(k,\uparrow) = \frac{|k_+\rangle\langle p_+| + |p_-\rangle\langle k_-|}{\langle k_-|p_+\rangle}, \quad \text{and}$$
$$\not{\epsilon}(k,\downarrow) = \frac{|p_+\rangle\langle k_+| + |k_-\rangle\langle p_-|}{\langle p_-|k_+\rangle}.$$

The amplitudes for these processes are generally quite complicated. However, for $\gamma_\uparrow\gamma_\uparrow \to K^-\bar{s}_-u_+$, the amplitude factors to

$$T_H = \frac{1}{sc}\frac{z}{x}\sqrt{\frac{y_1}{y_2}}\left[\frac{q_s\sqrt{y_1}}{\bar{u}_-(l_1)u_+(k)} - \frac{q_u\sqrt{y_2}}{\bar{u}_-(l_2)u_+(k)}\right]\left[\frac{q_s\sqrt{y_1}}{\bar{u}_-(l_1)u_+(k')} - \frac{q_u\sqrt{y_2}}{\bar{u}_-(l_2)u_+(k')}\right]; \tag{5.41}$$

the amplitude for $\gamma_\downarrow\gamma_\downarrow$ is obtained by the replacements $x \to \bar{x}$, $T_H \to T_H^*$, $y_1 \leftrightarrow y_2$.

We are unable to obtain such a simplification for the case in which the photons have opposite helicity. The hard-scattering amplitude for semiexclusive K production from a $\gamma_\uparrow\gamma_\downarrow$ initial state is

$$
\begin{aligned}
T_H = \frac{q_s^2}{zy_2}\Bigg[&\frac{se^{-i\phi}z\sqrt{y_1}\big((1-zx)c\sqrt{y_2}+se^{-i\phi}\sqrt{\bar{z}y_1}\big)}{x\bar{x}(1-zx)}\\
&+\frac{z(c\sqrt{\bar{z}y_2}+se^{-i\phi}\sqrt{y_1})(c^2-y_1)}{x(c\sqrt{\bar{z}y_2}+se^{i\phi}\sqrt{y_1})}-\frac{z\sqrt{y_1y_2}(c\sqrt{\bar{z}y_2}+se^{-i\phi}\sqrt{y_1})}{\bar{x}(c\sqrt{y_2}-se^{-i\phi}\sqrt{\bar{z}y_1})}\Bigg]\\
&+\frac{zq_uq_s(y_2-s^2)^2}{\big(z\bar{x}(y_2-s^2)-|c\sqrt{y_2}-se^{i\phi}\sqrt{\bar{z}y_1}|^2\big)(c\sqrt{\bar{z}y_2}+se^{i\phi}\sqrt{y_1})(c\sqrt{y_2}+se^{i\phi}\sqrt{\bar{z}y_1})}\\
&+\frac{q_uq_s}{zx(y_1-s^2)-|c\sqrt{y_1}-se^{i\phi}\sqrt{\bar{z}y_2}|^2}\Bigg[\frac{z^2y_1y_2}{(c\sqrt{\bar{z}y_1}-se^{i\phi}\sqrt{y_2})(c\sqrt{y_1}-se^{i\phi}\sqrt{\bar{z}y_2})}\\
&+\frac{z\sqrt{y_1y_2}(c\sqrt{\bar{z}y_2}+se^{-i\phi}\sqrt{y_1})}{\bar{x}(c\sqrt{y_1}-se^{i\phi}\sqrt{\bar{z}y_2})}-\frac{z\sqrt{y_1y_2}(c\sqrt{y_2}+se^{-i\phi}\sqrt{\bar{z}y_1})}{x(c\sqrt{\bar{z}y_1}-se^{i\phi}\sqrt{y_2})}\\
&-\frac{(c\sqrt{y_2}+se^{-i\phi}\sqrt{\bar{z}y_1})(c\sqrt{\bar{z}y_2}+se^{-i\phi}\sqrt{y_1})}{x\bar{x}}\Bigg]\\
&+\frac{q_u^2}{zy_1}\Bigg[\frac{cz\sqrt{y_2}\big(c\sqrt{\bar{z}y_2}+(1-z\bar{x})se^{-i\phi}\sqrt{y_1}\big)}{x\bar{x}(1-z\bar{x})}\\
&+\frac{z(c\sqrt{\bar{z}y_2}+se^{-i\phi}\sqrt{y_1})(s^2-y_2)}{\bar{x}(c\sqrt{y_2}+se^{i\phi}\sqrt{\bar{z}y_1})}-\frac{z\sqrt{y_1y_2}c\sqrt{y_2}+se^{-i\phi}\sqrt{\bar{z}y_1})}{xc\sqrt{\bar{z}y_1}-se^{i\phi}\sqrt{y_2})}\Bigg].
\end{aligned}
$$

We also consider the semiexclusive production of vector mesons. The amplitude for $\gamma_\uparrow\gamma_\uparrow \to K^*_\uparrow \bar{s}_- u_-$ is

$$
T_H = \frac{1}{sc}\frac{\bar{z}\sqrt{y_1y_2}}{x\bar{x}}\left[\frac{q_s\sqrt{y_1}}{\bar{u}_-(l_1)u_+(k)}-\frac{q_u\sqrt{y_2}}{\bar{u}_-(l_2)u_+(k)}\right]\left[\frac{q_s\sqrt{y_1}}{\bar{u}_-(l_1)u_+(k')}-\frac{q_u\sqrt{y_2}}{\bar{u}_-(l_2)u_+(k')}\right].
$$

The corresponding amplitude for $\gamma_\downarrow\gamma_\downarrow$ vanishes.

Again, we are unable to find a simple form for the case of opposite photon helicities. The semiexclusive hard-scattering amplitude for $\gamma_\uparrow\gamma_\downarrow \to K^*_\uparrow \bar{s}_- u_-$ is extremely awkward, and to present it here would serve no purpose.

In the same-helicity case, however, note that the x-dependence of T_H is subsumed into an overall constant [56]; the interplay between the internal momentum fraction x and the kinematic observables y_i and z, which is the

major motivation for studying semiexclusive processes, is absent. As a result, the semiexclusive cross section is no more valuable than the form factor in studying the meson wavefunction; we can predict only an absolute normalization, which experience teaches us is the least reliable and least valuable type of prediction. Since the normalization also suffers from additional uncertainties arising from the case $\vec{l}_i \parallel \vec{k}$, where pQCD is less important than vector-meson dominance, we must conclude that two-photon semiexclusive processes promise no insight into the structure of hadrons.

References for Chapter 5

[1] G.P. Lepage and S.J. Brodsky, *Phys. Rev.* **D22**, 2157 (1980).

[2] See Chapter 4 of this thesis, and references therein.

[3] V.N. Baier and A.G. Grozin, *Phys. Lett.* **96B**, 181 (1980); A.G. Grozin. *Sov. J. Nucl. Phys.* **37**, 255 (1983); V.N. Baier and A.G. Grozin, *Sov. J. Part. Nucl.* **16**, 1 (1985); see also A.G. Grozin, *Z. Phys.* **C34**, 531 (1987).

[4] S.J. Brodsky and G.R. Farrar, *Phys. Rev.* **D11**, 1309 (1975). See also P.V. Landshoff, *Phys. Rev.* **D10**, 1024 (1974), and A.H. Mueller, *Phys. Rept.* **73**, 237 (1981).

[5] Semiexclusive production of baryons is studied in A. Grozin, *Z. Phys.* **C34**, 531 (1987).

[6] D. Millers and J.F. Gunion, *Phys. Rev.* **D34**, 2657 (1986); A.S. Kronfeld and B. Nižić, *Phys. Rev.* **D44**, 3445 (1991).

[7] T. Hyer, *Phys. Rev.* **D47**, 3875 (1993).

[8] This naive definition ignores complications due to renormalization. However, the resulting formalism is still correct to leading twist; see Ref. [1].

[9] S. Gupta, *Phys. Rev.* **D24**, 1169 (1981). Baier and Grozin [3] have argued that Gupta's calculated amplitudes are incorrect; we do not use those results, only the proof of factorizability.

[10] Note that ϕ is not the azimuthal angle of the hadron; the latter does not enter into the amplitude.

[11] G.R. Farrar and F. Neri, *Phys. Lett.* **130B**, 109 (1983), *Phys. Lett.* **152B**, 443 (1984); see also M.L. Mangano and S.J. Parke, *Phys. Rept.* **200**, 301 (1991).

[12] E.D. Bloom and F.J. Gilman, *Phys. Rev. Lett.* **25**, 1140 (1970); *Phys. Rev.* **D4**, 2901 (1971).

[13] M.A. Shifman, A.I. Vaĭnshteĭn, and V.I. Zakharov, *Nucl. Phys.* **B147**, 385 (1979).

[14] V.L. Chernyak, A.R. Zhitnitsky, and I.R. Zhitnitsky, *Nucl. Phys.* **B204**, 477 (1982).

[15] A.R. Zhitnitskiĭ, I.R. Zhitnitskiĭ and V.L. Chernyak, *Sov. J. Nucl. Phys.* **38**, 775 (1983).

[16] V.L. Chernyak and A.R. Zhitnitsky, *Nucl. Phys.* **B246**, 52 (1984); I.D. King and C.T. Sachrajda, *Nucl. Phys.* **B297**, 785 (1987); V.L. Chernyak, A.A. Ogloblin, and I.R. Zhitnitskiĭ, *Sov. J. Nucl. Phys.* **48**, 536 (1988) [*Yad. Fiz.* **48**, 841 (1988)].

[17] V.L. Chernyak, A.A. Ogloblin, and I.R. Zhitnitskiì, *Z. Phys.* **C42**, 583 (1989); A.N. Kronfeld and B. Nižić, *Phys. Rev.* **D44**, 3445 (1991).

[18] The Gegenbauer polynomials C_i are customarily defined to be orthonormal over the interval $[-1,1]$ with measure $w(x) = (1-x^2)/4$ [1]. These are related to the functions P_i which we will use by $P_i(x) = \sqrt{2}C_i^{3/2}(x-\bar{x})$. We will continue to refer to the P_i as Gegenbauer polynomials.

[19] The derivation in Ref. [14] neglects the breaking of $SU(3)$ symmetry by the strange quark mass. No estimate of the symmetry-breaking quantities a_1 and a_3 is made.

[20] We are indebted to S. Brodsky for discussions of this point.

[21] S.J. Brodsky and G.P. Lepage, *Phys. Rev.* **D24**, 2848 (1981).

[22] E. Berger, *Z. Phys.* **C4**, 289 (1980).

[23] J.D. Bjorken, *Phys. Rev.* **D47**, 101 (1993); J. Randa, *Phys. Rev.* **D21**, 1795 (1980).

[24] J.D. Bjorken, S.J. Brodsky, and H. Lu, *Phys. Lett.* **B286**, 153 (1993).

[25] Indeed, we may argue that such a 'background' event is itself intrinsically hard, so that any events containing such a gap are *ipso facto* semiexclusive. This is the viewpoint adopted by Baier and Grozin [3].

[26] This also allows for the possibility of the production of the meson in a Fock state with nonzero orbital angular momentum. As with helicity-flip terms, this will again contribute to the cross section at order $k_\perp^2/Q^2$.

[27] V.V. Sudakov, *Sov. Phys. – JETP* **3**, 65 (1956); A.H. Mueller, *Phys. Rept.* **73**, 237 (1981).

[28] There are indeed strong peaks in the inclusive cross section $\sigma_{\rm tot}(e^+e^- \to$ hadrons) above 2 GeV; however, they arise from heavy-quark resonances.

[29] J. Botts and G. Sterman, *Nucl. Phys.* **B325**, 62 (1989).

[30] A.R. Zhitnitskiĭ, I.R. Zhitnitskiĭ, and V.L. Chernyak, *Sov. J. Nucl. Phys.* **41**, 284 (1985) [*Yad. Fiz.* **41**, 445 (1985)].

[31] There is also a distribution $\phi_{3\rho}^A$, but it does not contribute to the process in which we are interested, in which the recoil q and $\bar{q}$ have opposite helicity.

[32] A.C. Mattingly and P.M. Stevenson, DE-FG05-92ER40717-7.

[33] S.J. Brodsky, G.P. Lepage, and P.B. Mackenzie, *Phys. Rev.* **D28**, 228 (1983).

[34] V.L. Chernyak and A.R. Zhitnitskiĭ, *Phys. Rept.* **112**, 173 (1984).

[35] Fermilab E665 Collaboration (M.R. Adams *et al.*), *Phys. Lett.* **287B**, 375 (1992).

[36] J. Botts, *Phys. Rev.* **D44**, 2768 (1992).

[37] See *e.g.* G. Farrar, E. Maina, and F. Neri, *Nucl. Phys.* **B259**, 702 (1985), *Nucl. Phys.* **B263**, 746 (1986).

[38] Reference [32] also displays an optimized third-order result for the coupling constant. However, we were unable to obtain numerical values or a parametric fit of this result, so we are compelled to use only the simpler form of eq. (5.22).

[39] This conclusion actually holds only at leading logarithmic order; beyond that, corrections begin to depend on the details of the hard-scattering process from which the $q\bar{q}$ pair originates. However, such subleading corrections are outside the intended scope of this work.

[40] L.R. Surguladze and M.A. Samuel, *Phys. Rev. Lett.* **66**, 560 (1991); S.G. Gorishny, A.L. Kataev, and S.A. Larin, *Phys. Lett.* **259B**, 144 (1991).

[41] P.M. Stevenson, *Phys. Lett.* **100B**, 61 (1981).

[42] EMC Collaboration (M. Arneodo *et al.*), *Nucl. Phys.* **B321**, 541 (1989).

[43] We note that tidal interactions proportional to $1/r^3$ are possible. However, they depend on the meson's having a nonzero average color dipole moment. Since we are attempting to determine the region in which multiple scattering is unimportant and the tree-level calculation of eqs. (5.6)-(5.11) are trustworthy, we take at face value their implication that no color dipole moment is induced in the direct production process.

[44] G. Sterman and H. Li, *Nucl. Phys.* **B381**, 129 (1992); H. Li, ITP–SB–92–25.

[45] In fact, the cross section has the potential to exhibit a power-law dependence on $\Lambda_{\rm QCD}$, arising from the infrared behavior of $\alpha_{\rm eff}$. However, this threat never materializes. At moderate Q^2 ($Q \sim 10$ GeV), the suppression of $\alpha_{\rm eff}$ sets in before y becomes extremely small, while at large Q^2 (*e.g.* $Q = m_Z$) the jets inherit the parton momenta, and the small-y region will be excluded by experimental cuts. The insensitivity to $\Lambda_{\rm QCD}$ is demonstrated in our calculated cross sections, as described in Sec. 5.3.

[46] Intrinsically hard processes, such as direct production itself, are not expected to be well predicted by the Lund code. However, the hadronizing recoil system in which we are interested contains no such anomalies, so that our use of a Monte Carlo is justified.

[47] This idea was suggested to the author by J.D. Bjorken.

[48] Of course, this is equivalent to the requirement of a rapidity gap; the difference is one of notation, not of substance.

[49] The thrust actually lacks the transformation properties of a vector; nonetheless, we will persist in this notation.

[50] The behavior of the events from eqs. (5.37) and (5.24) passing our cuts is similar, so that the value of $z_{\max}$ obtained in this way exhibits little dependence on the wavefunction.

[51] T. Hyer, SLAC-PUB-6383.

[52] M. A. Shifman, in *Aachen QCD Workshop 1992*, and references therein.

[53] M. A. Shifman and A. Voloshin, *Sov. J. Nucl. Phys.* **45**, 242 (1987) [*Yad. Fiz.* **45,** 463 (1987)].

[54] B. Jacobson, private communication.

[55] The integrands in A and $\bar{A}$ diverge at $x \to 0$ or 1, so that this metric does not yield a finite result unless the coefficients are constrained to yield a sum which is finite at the endpoints (though it may fluctuate substantially near the limit).

[56] One might hope to compare the term $B = \int \phi(x)/x \, \mathrm{d}x$ from eq. (5.41), which controls the process $\gamma_\uparrow\gamma_\uparrow \to K^- \bar{s}_- u_+$, with the corresponding $\bar{B} = \int \phi(x)/\bar{x} \, \mathrm{d}x$ which enters into the amplitude for $\gamma_\uparrow\gamma_\uparrow \to K^- \bar{s}_+ u_-$. However, in the region in which the assumption of duality is valid, it is *de facto* impossible to extract the spins of the hadronizing quarks; thus the only nonperturbative parameter which can be observed experimentally is the unpolarized sum $B^2 + \bar{B}^2$, which determines the absolute normalization.

5. CONCLUSIONS AND OUTLOOK

The framework of light-cone quantization is probably the most promising tool with which a general and quantitative understanding of hadronic bound states can be achieved. In this thesis, we have shown that both theoretical and experimental constraints on the nature of light-cone wavefunctions can be obtained with current or near-future data.

The outstanding problem confronting light-cone theorists is the understanding of cutoff dependence, which on the light cone entails a thorough understanding of the consequences of violation of Lorentz invariance. It is our belief that most of the ingredients needed to undertake a program of high-precision model-independent computation of hadronic currents and observables at moderate energy (*i.e.*, $Q \lesssim m_b$) are currently available. The results given here will aid in the understanding of the wavefunctions of both light and heavy mesons in the valence Fock state; this represents a step toward the computation of reliable predictions of rare B decay rates, for example.

The major challenge in this program is the construction of accurate cutoff-dependent effective Hamiltonians. The results of our first chapter will provide a check of the rotational invariance of such approximations, and thus will help to constrain the form of the effective theory.

The next hurdle for light-cone quantization is the thorough understanding of vacuum structure, which will be necessary to produce the high-precision information about the proton structure which will be required by the next generation of hadron colliders. There is good reason to believe that this problem is intimately commingled with the loss of manifest rotational invariance.

The above theoretical program must be continually tempered by quantitative phenomenological comparison with experiment. Nagging complications from soft contributions require a substantial degree of sophistication in the examination even of nominally hard processes; it is our hope that Chapters 4 and 5 of this thesis will serve to advance the reliability of confrontations between theory and experiment.